Optimization of the capacity factor of energy ships for far-offshore wind energy conversion using weather-routing

Roshamida Binti Abd Jamil

THESE DE DOCTORAT DE

L'ÉCOLE CENTRALE DE NANTES

ECOLE DOCTORALE N° 602
Sciences pour l'Ingénieur
Spécialité : Mécanique des milieux fluides

Par
Roshamida BINTI ABD JAMIL

Optimization of the capacity factor of energy ships for far-offshore wind energy conversion using weather-routing

Thèse présentée et soutenue à l'École Centrale de Nantes, le 17/01/2022
Unité de recherche : UMR 6598 Laboratoire de recherche en hydrodynamique, énergetique et environnement atmospherique (LHEEA)

Rapporteurs avant soutenance :

Irene PENESIS **Professeure**, University of Tasmania, Australia
John RINGWOOD **Professeur**, Maynooth University, Ireland

Composition du Jury :

Président : **Jean-Luc ACHARD** **Directeur de recherche émérite, CNRS, INP Grenoble**
Examinateur : **Zulkifly BIN MAT RADZI** **Professeur, Université Nationale de Défense de Malaisie**

Dir. de thèse : **Aurélien BABARIT** **Ingénieur de recherche HDR,** École Centrale de Nantes
Co-encadrant : **Jean-Christophe GILLOTEAUX** **Ingénieur de recherche,** École Centrale de Nantes

Invité :
Salvy BOURGUET Maître de conférences - HDR, Université de Nantes

TABLE OF CONTENTS

LIST OF FIGURES

LIST OF TABLES

ACKNOWLEDGEMENT

First and foremost, I would like to praise and thank God, the almighty, who has granted countless blessing, knowledge, and opportunity to the writer, so that I have been finally able to accomplish the thesis.

This thesis would not have been possible without the inspiration, encouragement, guidelines and support of several individuals. I take this opportunity to give special thanks to the following people.

I would like to express my sincere gratitude to my main supervisor, Aurelien Babarit, for giving me the chance to join his research group and for his continuous guidance, inspiration, encouragement, and support. He has been a thoughtful and wonderful supervisor, and without him, this thesis would not have been completed or written. "Aurelien, thank you for valuable discussions and incredible feedback on my work. I have learned quite a lot on renewable energy from you."

I would also like to extend my appreciation to my co-supervisor, Jean-Christophe Gilloteaux, for exciting and fruitful discussions, especially in wind turbines technologies. I am grateful for his unlimited support, especially when I desire a piece of advice on wind turbines. He was always open to me whenever I needed his advice on research or other issues.

My deep gratitude also goes to all colleagues at the EMO research team and the LHEEA for the friendly and pleasant working atmosphere. In particular, I am grateful to be part of the LHEEA team and system administrators.

I would like to say a heartfelt thank you to my parents, Mr. Abd Jamil and Mrs. Rodziah, my parents' in-law, Mr. Chin and Mrs. Selamah, for always believing in me and for their unconditional support, encouragement, sacrifice and prayers. Without their support and prayers, this work would not have been possible. I am also grateful to my sibling and sibling-in-law for their steady support and prayers.

Last but not least, my deep and special appreciation goes to my beloved husband, Mohammad Zulkhairy, who has given me strength, support, encouragement, and inspiration. Thank you for your unconditional love and everything that comes to my life with you. I will never forget the patience, sacrifices, and suffering you endured in caring for our children, mainly when I focus entirely on my work. I also want to acknowledge my daughters, Aisyah Sofea, Ainul Mardhiah and my son, Az-Zubayr.

Finally, I would like to thank everybody who has contributed either directly or indirectly to this thesis and express my apology that I could not mention personally one by one.

Sincerely,

Roshamida ABD JAMIL

DEDICATION

"This thesis is specially dedicated;

To my Husband, Mohammad Zulkhairy Chin

To my beloved daughters & son, Aisyah Sofea, Ainul Mardhiah & Az-Zubayr

To my parents, Abd Jamil & Rodziah

To my parents-in-law, Chin & Selamah

To my family & family-in-law

also

To the memory of my late brother-in-law, Mohd Shukor Bin Chin,

who always believed in my ability to succeed in the academic arena.

You are gone, but your belief & love has made this journey possible.

May this success accomplish your unfinished Master thesis and fulfil your dreams;

And to my late sister-in-law, Rosita Binti Chin

Your strong-willed character always guides me to be strong and hold tight in anything I am doing.

We lose both of you, but you'll always live inside of us."

CHAPTER 1

INTRODUCTION

1.1. Motivation and Problem Studied

1.1.1. State of The Art in Wind Energy

The Covid-19 pandemic had a significant impact on energy consumption worldwide, with global energy and electricity consumption falling respectively by 4% (Figure 1) and 0.9% (Figure 3) in 2020 [2].

However, people across the world are putting in their best efforts to combat this pandemic. As a result, the global economy is expected to improve in 2021. In particular, global energy consumption is expected to rebound by 4.6% relatively to 2020, and global electricity consumption is expected to increase by over 1000 TWh (4.5% increase) [2].

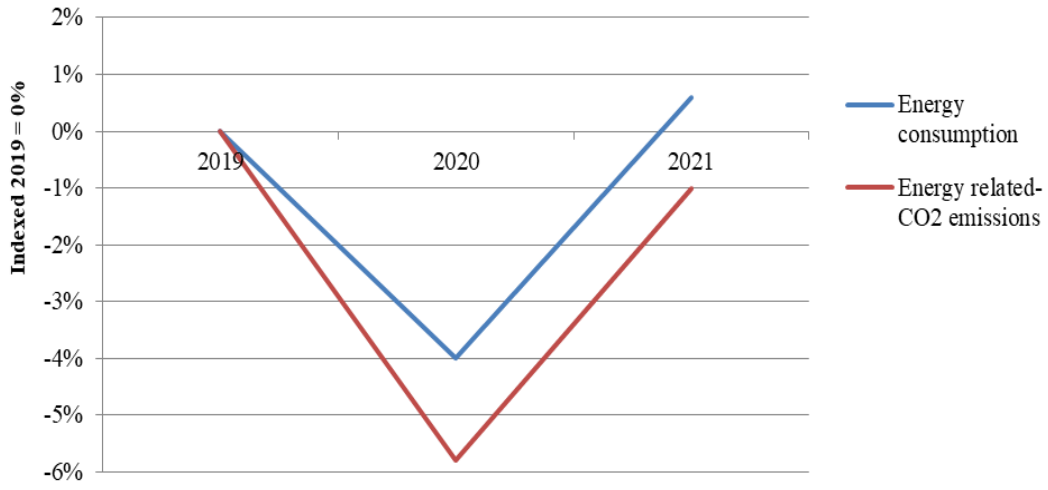

Figure 1 Evolution of total primary energy consumption and energy-related CO2 emissions, relative to 2019 [Source: IEA (2021)[2]]

Despite the decrease of global energy consumption due to the Covid-19 crisis, renewable energy demand has remained robust. Renewable energy production capacity grew by 10.3% (261 GW) in 2020 [2][36] and is expected to grow by a further 8% in 2021.

Figure 2 show the share of renewable and power capacity expansion between 2001 and 2019. The share of renewables in global electricity generation capacity increased to 28.6% in 2020, up from 26.9% in 2019 [55]. In 2021, it is expected to reach 8300TWh in 2021 (29.6%)[2].

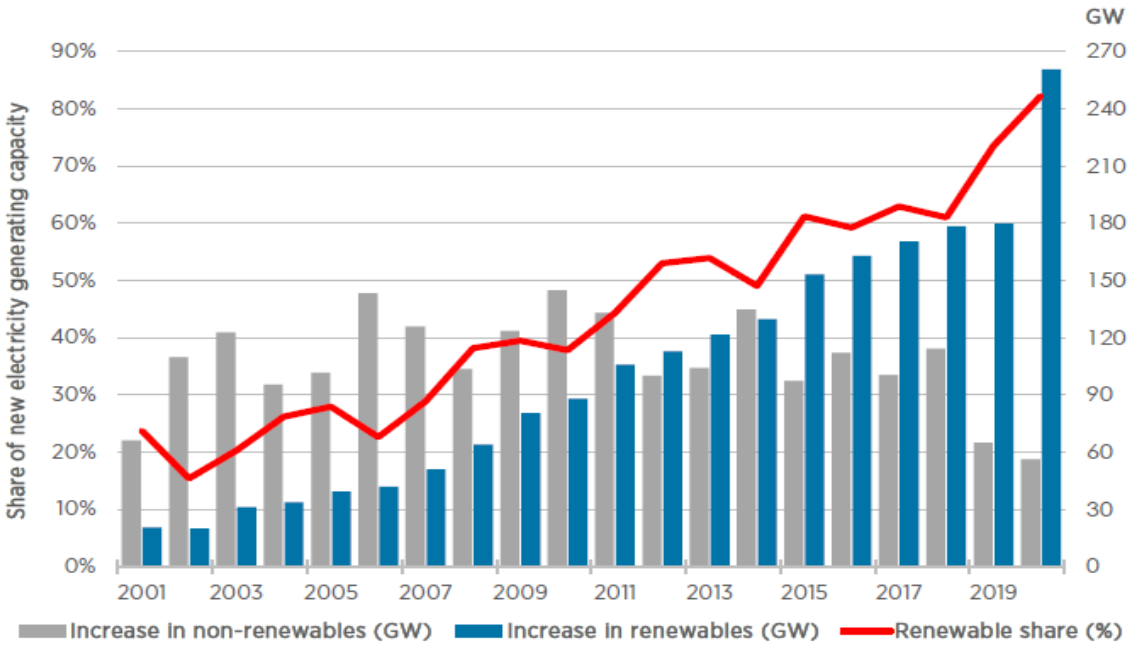

Figure 2 Renewable share of annual power capacity expansion [Souce: IRENA Renewable energy statistics (2021) [55]]

Nowadays, renewable energy is developed for climate and energy supply security. The largest sources of greenhouse gas (GHG) emissions from human activities are transportation and burning fossil fuels for electricity generation [1]. Therefore, to limit global warming, the reduction of the global greenhouse gas emission is vital. Renewable energy is typically local energy, exposed to seasonal and time-to-day changes (weather). Solar PV and wind energy are the most promising resources in the sector of renewable energy, and most importantly their lifecycle greenhouse-gases emissions intensity is an order of magnitude smaller than fossil fuels in terms of grams of CO2-equivalent emissions per kilowatt-hour (CO2-eq/kWh) [1].

Solar PV and wind are expected to put up two-thirds of renewables' growth. Renewable electricity generation (see Figure 4) from wind uniquely is set to grow by 275 TWh (17% year-on-year growth) in 2021, up from 175 TWh (12% year-on-year growth) in 2020 [2]. Meanwhile, electricity generation from solar PV increased by 145 TWh (18% year-on-year growth) in 2021 (153 TWh (23% year-on-year growth) in 2020) [2].

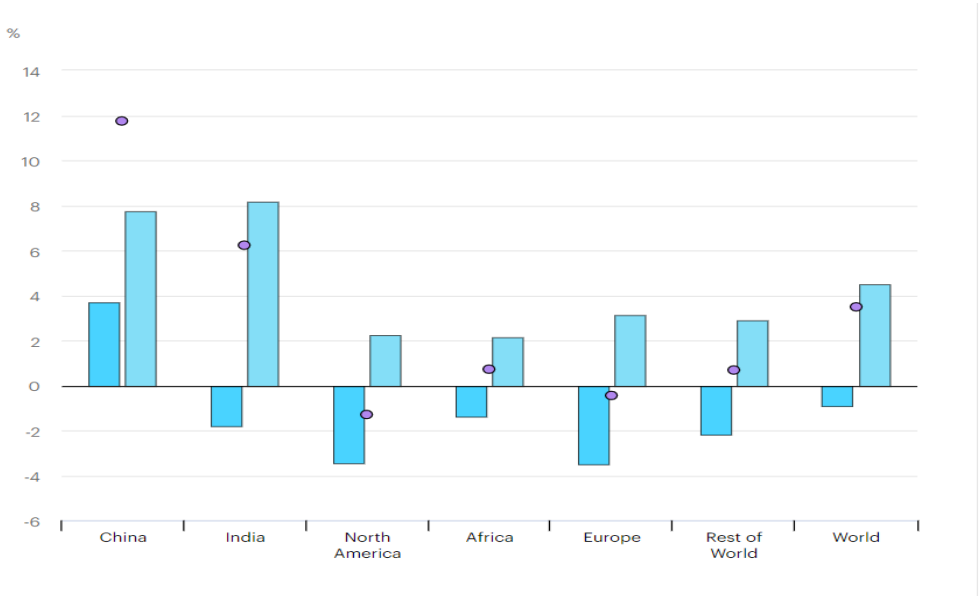

Figure 3 Change in electricity consumption in 2020 and 2021 [Source: Global Energy Review 2021, IEA (2021) [2]]

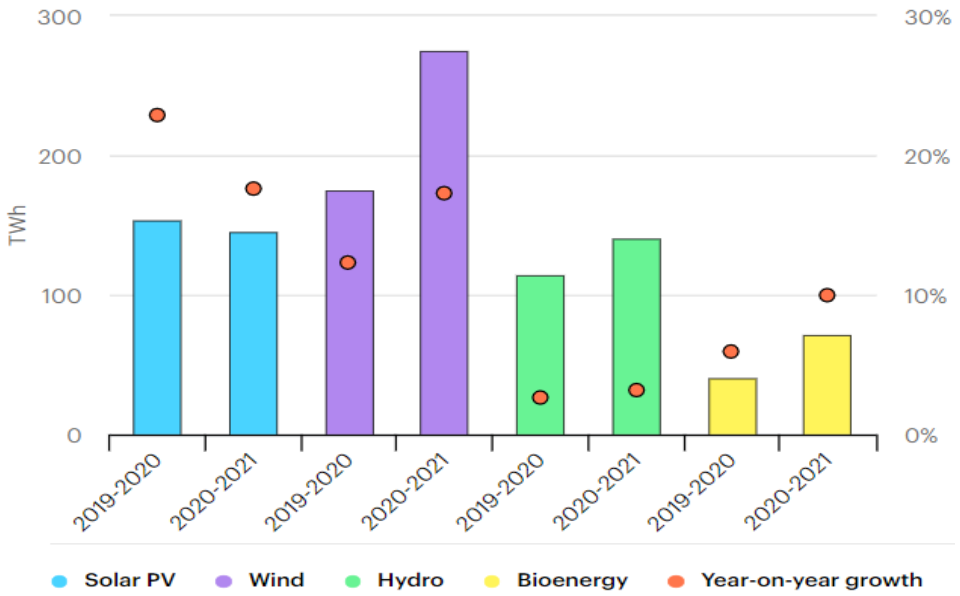

Figure 4 Renewable electricity generation growth by technology, 2019-2020 and 2020-2021 [Source: Global Energy Review 2021, IEA (2021) [2]]

The global wind generating capacity has snowballed in Europe, Asia, and North America since the beginning of the twenty-first century. Table 1 shows the total wind energy capacity, offshore wind energy capacity and solar PV capacity for the year 2019 and 2020 worldwide, in Europe, in Asia and in the North America. Indicatively, global wind energy and solar PV is on track to record a significant increase in its capacity in 2020 from 2019 [37].

Table 1 Total global energy capacity (Source: IRENA Energy Statistics 2021 [55])

	Wind Energy Capacity (MW)		Offshore Wind Energy Capacity (MW)		Solar Photovoltaic (PV) Capacity (MW)	
	2019	2020	2019	2020	2019	2020
World	622 249	733 276	28 355	34 367	580 760	707 495
Europe	196 311	207 743	22 031	24 920	140 320	161 145
Asia	257 520	332 088	6 295	9 418	328 553	406 283
North America	123 575	139 448	29	29	66 660	82 768

1.1.2. Offshore wind energy resource: Capacity factor of wind turbines in the far-offshore

As already mentioned, wind energy is a rapidly growing power generation source. At present, electricity is produced from wind energy using wind turbines. Even though wind farms may be costly to build, the cost of energy is highly competitive (because wind energy is massively available and free). Wind farms are also climate-friendly as the global lifecycle greenhouse-gases emissions produced by wind turbines is typically 11 - 12 g CO2-eq per kWh of electricity [38], here as fossil fuels produce approximately 600 g CO2-eq per kWh for oil-based power generation and 1000 g CO2-eq per kWh for coal-based power generation [38].

Offshore wind represents a significant energy resource. The estimate of mean global ocean wind power is 731 Wm^{-2} [4], whereas it is 250 - 320 Wm^{-2} onshore [11][42]. This is due to the very low surface roughness at sea. This advantage results in higher wind speed and greater wind power yield [6]. The global offshore wind power was potentially generate more than 420 000 TWh per year [65]. Also, offshore wind is less concerned by space constraints and conflicts of uses that could limit the deployment of onshore wind farms [5]. The UK has an enormous amount of offshore wind capacity in Europe, with 45% of all installations. Germany is second with 34%, followed by Denmark (8%), Belgium (7%) and the Netherlands (5%) [9]. In France, despite that offshore wind energy development started 15 years ago, the first French offshore wind farm will only start producing by 2022. The French offshore wind farm capacity is expected to reach 3.5GW in the next 5 years. [8].

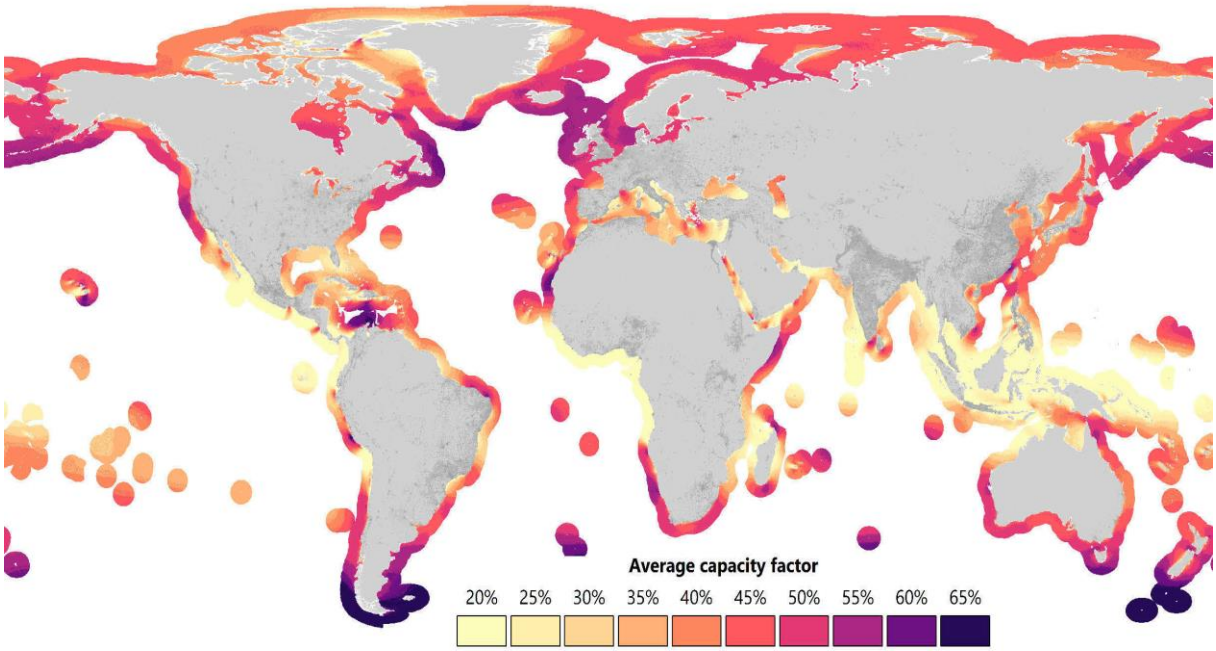

Figure 5 Average simulated capacity factors reflect the availability of the global offshore wind resources (Source: IEA, World Energy Outlook 2019 [65])

The capacity factor (CF, in %) is a key metric to quantify the energy performance of a power generation source. It is defined as the ratio between the effective average power over a given period and the nominal power. In terms of energy, this corresponds to the ratio of the actual electrical energy produced by a system over a given period of time to the energy it would have produced if it had operated at its nominal power during the same period.

The capacity factor of offshore wind farm is in the range 39% to 60% [7][10] to [15], with a global fleet-wide average of 37% for operating wind farms [13]. According to [3], the capacity factor of offshore wind will increase in the future, ranging from 36% to 58% in 2030 and 43% to 60% in 2050. As can be seen in Figure 5, capacity factors in the order of 60% may be achieved along the Atlantic coast from Western France to Estonia and in the Pacific (West Coast) [10][16]. To date, most offshore wind farms are bottom-fixed. This technology limits the deployment to shallow water. In order to address this issue, floating wind turbines have been developed and the first commercial floating wind farms have been installed. Hywind Scotland (56% CF) [68][85] and Kincardine are the biggest floating wind farms in the world. Hywind Scotland (see Figure 6) is sited 25 km far from shore, with 108 m water depth using SPAR buoy-type foundation technology.

The wind farm consists of five 6MW Siemens Wind Turbines with a total installed capacity of 30MW [68].

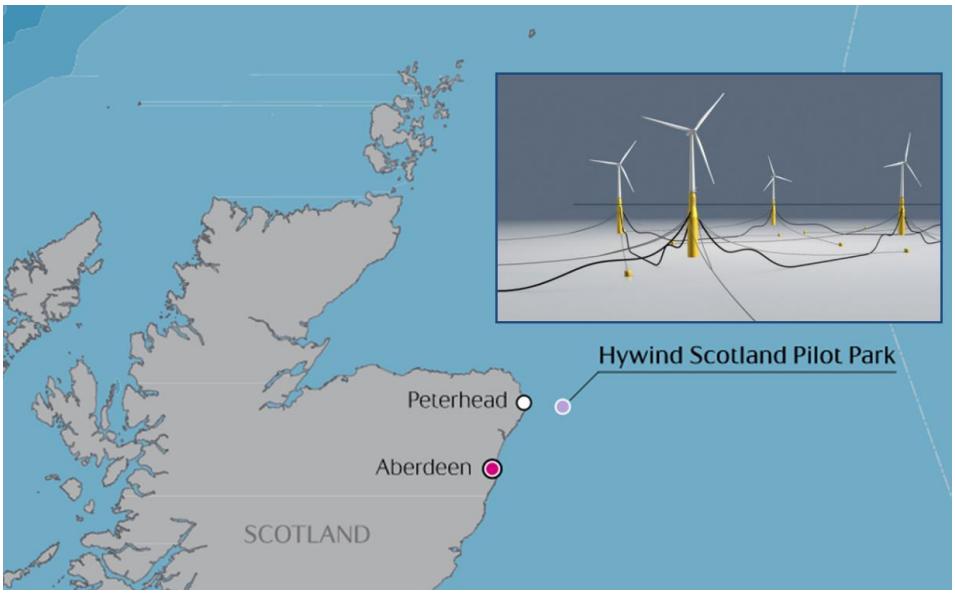

Figure 6 Hywind Scotland floating offshore wind farm (Source: https://www.equinor.com/en/what-we-do/floating-wind/hywind-scotland.html)

The Kincardine (see Figure 7) wind farm is sited 15 km from shore at water depth ranging 60m to 80m using a semi-submersible foundation. The wind farm consists of one operating 2MW wind turbine and an additional five 9.5MW MHI Vestas (expected commissioning in 2021) with a total installed capacity of 50MW [9]. In the future, beating the records of Hywind Scotland and Kincardine wind farms (in the UK), Hywind Tampen (in Norway, commissioning in 2022) will have a total capacity of 88MW [9][69].

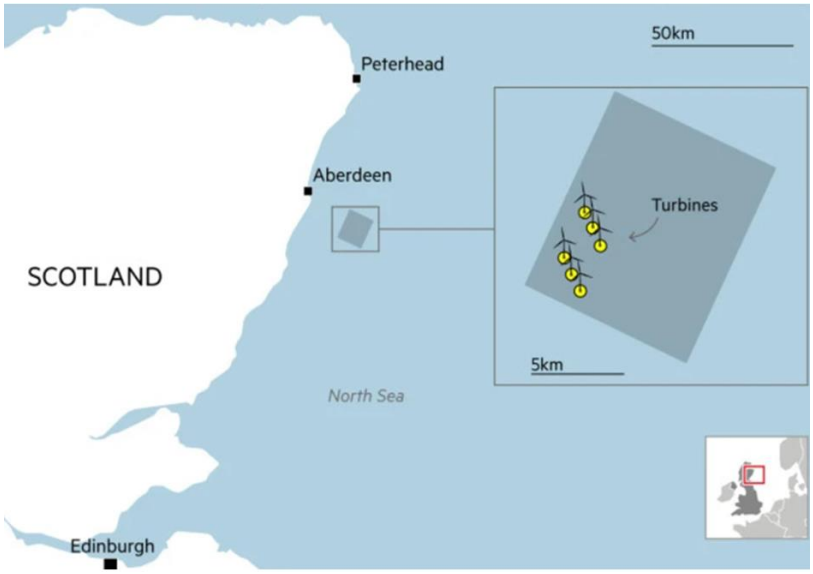

Figure 7 Kincardine floating offshore wind farm (Source: https://www.ft.com/content/49085cd7-fe54-4b2d-a24f-29448f0c784f)

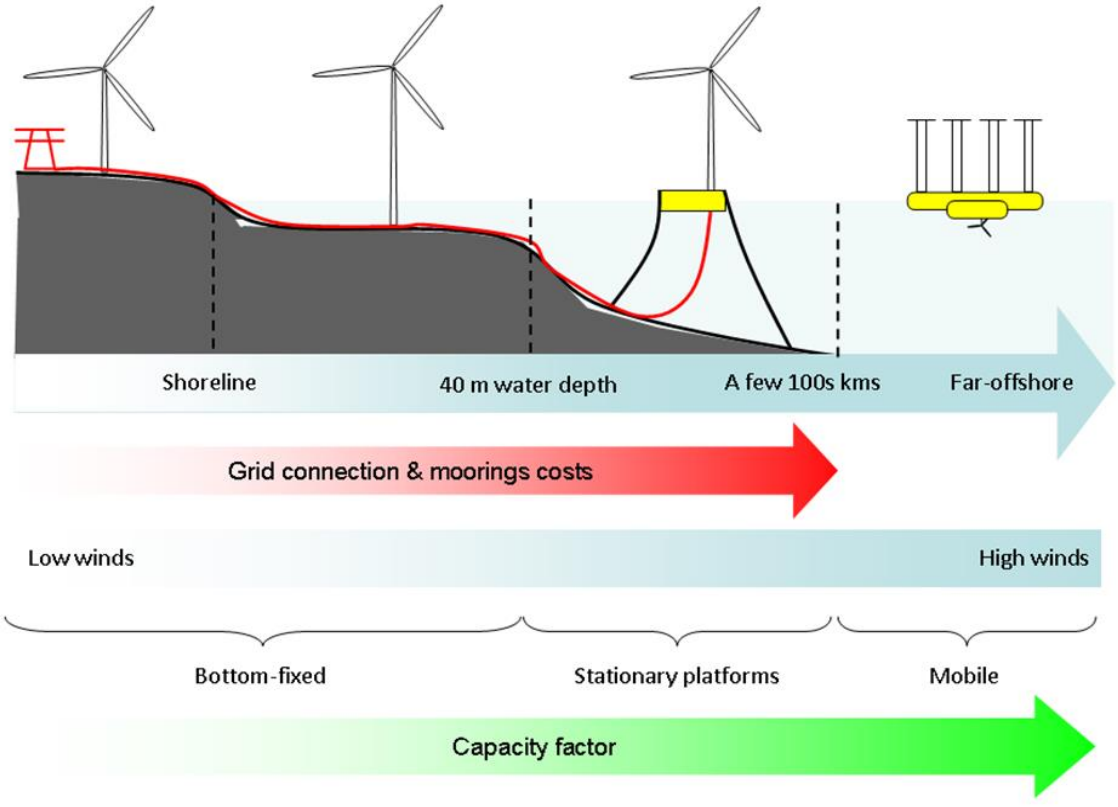

Figure 8 Evolution of capacity factor, grid connection and moorings cost offshore

Even with floating offshore wind turbines, only the nearshore offshore wind energy potential can be harvested [7][10][13][17][26]. Indeed, grid-connection cost, moorings and installation cost and maintenance costs increase as the distance to shore and the water depth increases (see Figure 8) [17][25]. Furthermore, failures of offshore submarine power cables have lowered system availability. Despite the development of offshore wind farms, the number and cost of these incidents do not appear to be decreasing [18]. Therefore, stationary grid-connected offshore wind turbines deployment is likely to be limited to nearshore. Mobile off-grid offshore wind energy conversion technologies are thus required to enable the exploitation of the far-offshore wind energy resource.

The energy ship is an example of such technology [22]. In energy ships, electricity is produced by a water turbine attached underneath the hull of a ship propelled by the wind using sails. Since they are not grid-connected, energy ships must include an onboard energy storage system. It can be based on batteries, hydrogen, methanol, or others [22].

A key advantage of energy ships is that being mobile, they may sail to the resource instead of having to wait for it [21]- [23].

Furthermore, their route schedules can be dynamically optimized [19] taking into account weather forecast to maximize their capacity factor. Although the concept is obvious, to the best of our knowledge, this thesis is the first investigation of the capacity factor of weather-routed energy ships in the far offshore.

Furthermore, in 2015, France enacted a law aiming at the self-sufficiency of its overseas territories for electricity supply by 2030 [24]. At first glance, offshore wind may appear as an appealing solution for the decarbonization of power generation for these islands. However, taking into account that the energy needs in islands are limited, “conventional” grid-connected offshore wind turbines may be challenging from an economic perspective because of infrastructure cost and the lack of economies of scale. Thus, energy ships may be a competitive alternative to offshore wind turbines for the power supply of islands. A study is needed to determine what capacity factor can be achieved for energy ship deployed near small islands.

For those reasons, in this thesis, the capacity factor of weather routed energy ship is investigated in the far offshore and near small islands. A sensitivity study also has been performed in order to investigate the sensitivity of the optimized capacity factor to the two main parameters;

energy ship's sailing capability as function of the storage capacity aboard and unloading time; and weather routing optimization parameters.

1.2. Energy ship concept

The concept of an energy ship was first proposed in 1982 [32]. Since then, there have been several other design proposals (see Figure 9) [20][21][22][29][30][32]-[35]. They differ by the choices of the used technologies and by the architecture of the ship. For wind propulsion for example (see Figure 9), it has been proposed to use kite wings (Kim & Park [20]), rigid sails (see Ouchi & Henzie [33] and Meller [35]) and Flettner rotors (see Babarit et al. [22]).

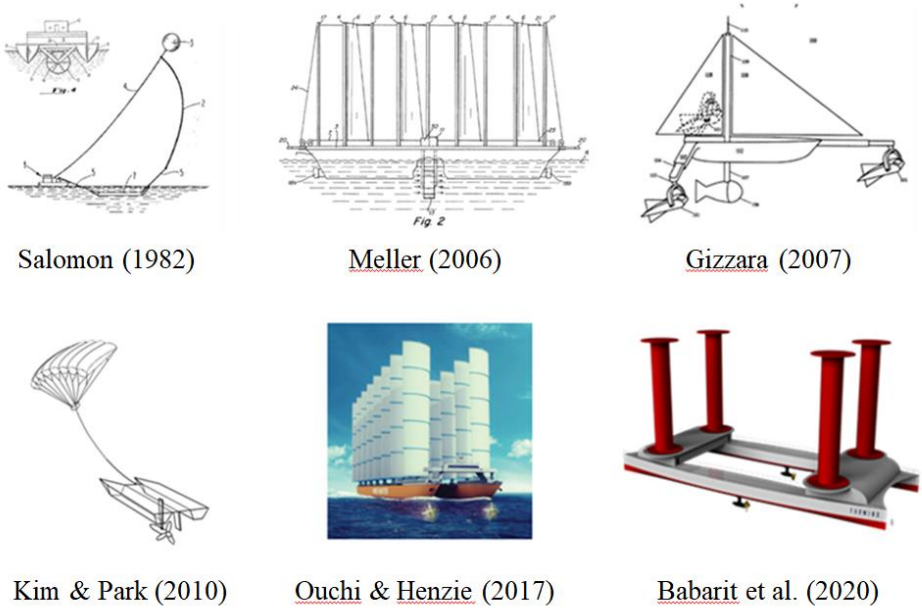

Figure 9 Picture of energy ship proposals

1.2.1. Design and mode of operation of the energy ship considered in this study

The energy ship design considered in this study is derived from that presented in [22]. It consists of an 80 m long catamaran with four 30 m tall Flettner rotors, and two water turbines, at rated power 900 kW each. Figure 10 shows an artist impression of the proposed design. Its main characteristics are given in Table 2.

Figure 10 Artist's view of the considered energy ship design [22]

Flettner rotors were selected against other wind propulsion options (soft sails, rigid sails, kites) because of their commercial availability, high lift capability and controllability (not an exhaustive list) [23]. By using the Flettner rotors, the energy ship utilizes the Magnus Effect from the wind for the ship propulsion. The water turbines convert the kinetic energy of the ship into electricity, which is then stored in the onboard energy storage system for example the li-ion battery or convert into hydrogen or methanol form for storage.

A mathematical model of the energy ship has been developed in order to assess the performance of the energy ship (Velocity and Power Performance Program: VPPP) in previous study [21][22]. The Flettner rotors are modelled through aerodynamic coefficients. The water turbine has been modelled using momentum theory. Ship resistance coefficients were obtained using the REVA software.

Table 2 Main characteristics of the considered energy ship (Design #01)

	Unit	Value
Hull		
Length	m	80
Breadth	m	31.7
Draught	m	1.6
Displacement	t	660
Wind propulsion		
Type	-	Flettner rotors
Number	-	4
Rotor height	m	30

Rotor diameter	m	5
Water turbine		
Number	-	2
Turbine diameter	m	4
Rated power	kW	900
Auxiliaries subsystems		
Power consumption	kW	50
Energy storage system		
Type		Hydrogen /Li-ion batteries
Storage capacity	h	6 – 48

1.2.2. Case studies

Two case studies are considered for the assessment of the annual energy production and average capacity factor of the proposed energy ship design. They have different mode of operations which are described in what follows.

In the first case study, the energy ship is deployed far-offshore in the North Atlantic ocean. In this case, the energy ship is an autonomous wind energy converter that moves in fleets, Figure 11. Those fleets are escorted by tankers that would regularly collect the produced fuel (e.g. Hydrogen). When their tanks are full, tankers are replaced by other empty tankers in order to ensure continuous operations. The full tanker sails to an on-shore terminal where the fuel is unloaded, stored and distributed. Once unloaded, the tanker sails back to the off-shore ocean to meet a fleet to replace an almost full tanker. The tanker would also act as a surveillance & control support vessel for the energy ship.

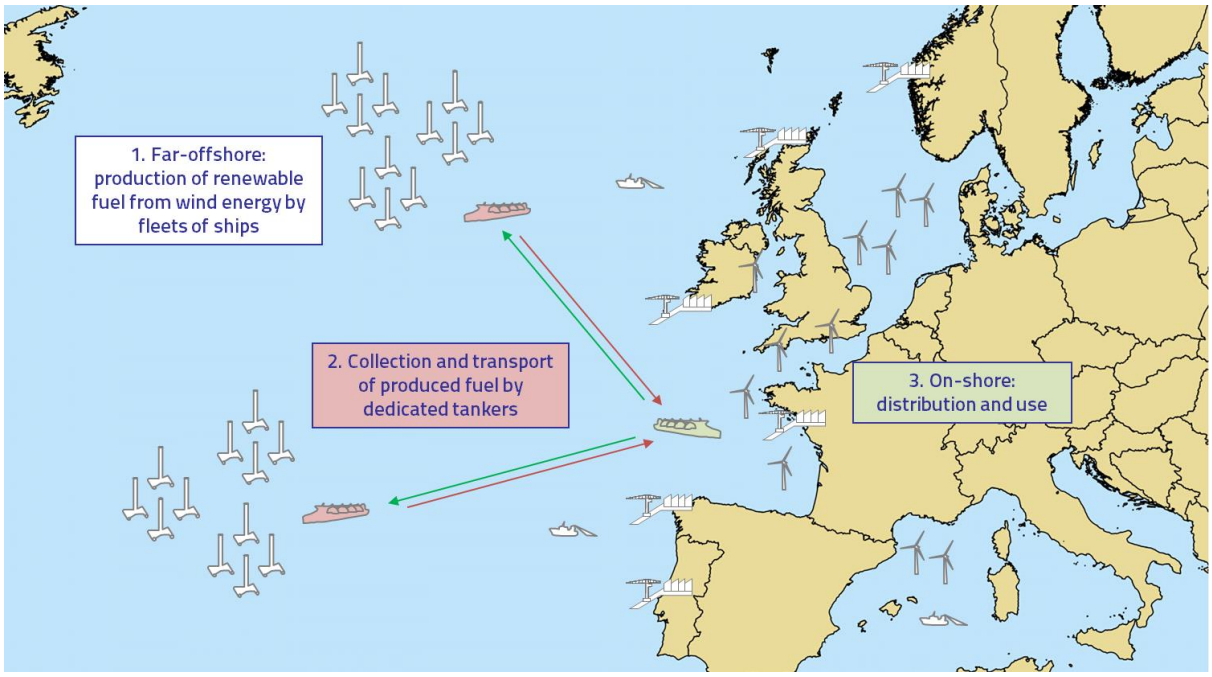

Figure 11 Energy ship's mode of operation for North Atlantic Ocean

In the second case, the energy ship is used for the power supply of islands, see Figure 12. The envisaged mode of operation is as follows. The island grid would be powered by a virtual power plant consisting in several batteries containers. This plant would be located in a port. Once a container would be empty, it would be loaded aboard an energy ship which would then set sail and start a charging cycle. Once the batteries would be charged, the energy ship would come back to the port, unload the filled batteries containers, load empty batteries containers, and start again a new charging cycle.

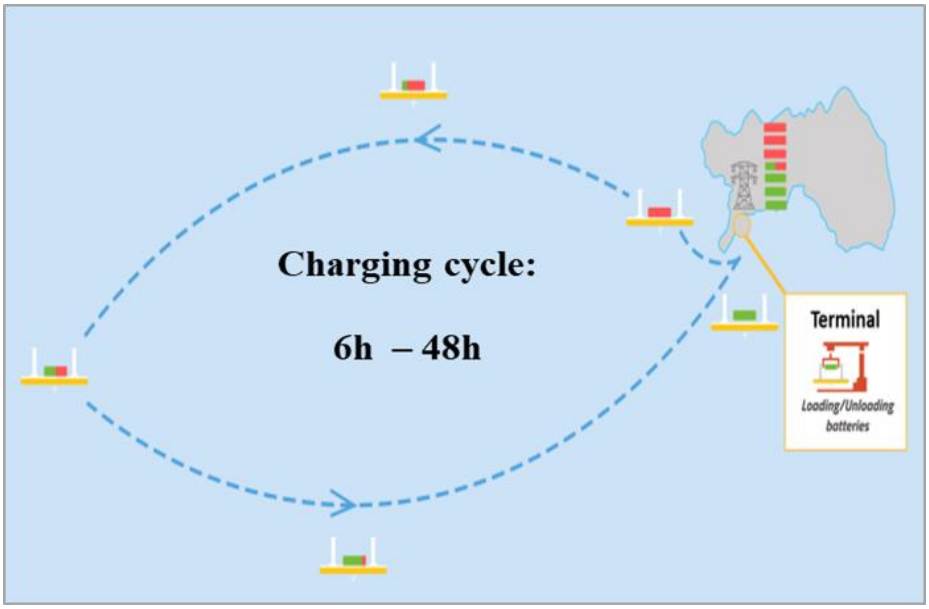

Figure 12 Mode of operation of energy ships for power supply of islands. The 6 - 48 hours indicate the typical duration of the charging cycle for a full charge.

In both cases (fuel production in the far-offshore and power supply of islands), the trajectory of the ships can be optimized using weather-routing (see section 2.4) in order to maximize energy production.

1.3. Research Objectives

There have been various energy ship concept proposed for far offshore wind energy exploitation in the past (see Figure 9) [19][22][32]to [35].The principle of operation is identical, but there are significant differences in the choice of technologies used and in the architecture of the ship. The concept of an energy ship was first proposed in 1982 [32]. The ship uses a wind propulsion system to move around. The ship is equipped with hydro-generators which produce electricity by moving the ship. The electricity is chemically transformed into hydrogen and stored onboard.

An energy ship must include the following sub-systems [22]: the structure and hull of the ship, a wind propulsion system, hydro-generators, that is to say submerged turbines under the ship's hull, a unit of energy storage. On the basis of this study, the diagram of the energy ship is thus proposed in Figure 10 [21] to [23].

To date, there has not yet been a study investigating the capacity factor of weather-routed energy ships in the far offshore or for the power supply of islands. This thesis aims at addressing this knowledge gap by producing optimized capacity factor using weather-routing for the proposed energy ship. The research objectives are thus:

1. Investigate the annual average capacity factor for a given energy ship design deployed in the North Atlantic Ocean; and compare to stationary floating wind turbines. This objective includes the development of a method for the performance assessment of a weather-routed energy ship.
2. Investigate the annual average capacity factor for a given energy ship design deployed in the nearshore; and compare to stationary floating wind turbines.
3. Assess the sensitivity of the capacity factor to the ship characteristics: onboard storage capacity, energy unloading time, velocity and power production polars.
4. Assess the sensitivity of the capacity factor to the parameters of the weather routing algorithm: number of initial optimization waypoints and search step angle.

1.4. Thesis Structure

The thesis is divided into five chapters.

Chapter 1 (this chapter) is the introduction. In a first part, it presents the global energy context. It also highlights the far-offshore wind energy potential. The second part presents the energy ship concept, characteristics, mode of operations and the case studies considered in this research. The rest of Chapter 1 sets out the aims and objectives of the research in this thesis.

Chapter 2 deals with the state of the art of wind energy harvesting (wind turbines). It focuses on their capacity factor depending on their deployment location. It includes the investigation of the capacity factor of 5MW stationary floating wind turbine which would be deployed far-offshore. This chapter also presents an alternative concept for far-offshore wind energy conversion (sailing wind turbine) and its capacity factor.

Chapter 3 deals with the capacity factor optimization of the energy ship in the far-offshore using weather routing. The first part reviews existing ship weather routing methods and tools. This part also presents elaborations on the features and specifications of the QtVlm program. The second part presents the weather routed 1.6MW energy ships' capacity factor investigation. The capacity

factor is compared to the capacity factor of stationary floating wind turbines. In addition, a sensitivity analysis to the two main parameters - the energy ship's sailing capability and numerical optimization parameters - is presented and in this chapter.

Chapter 4 presents the extension work of the weather routed 1.6MW energy ships' capacity factor investigation to the nearshore. This chapter considers two possible deployment locations: the French archipelago of Saint-Pierre-et-Miquelon island and Ile de Sein island. This chapter also includes a statistical analysis of the energy produced by the energy ship, sailed distance, average boat speed, and true wind angle (TWA).

Finally, Chapter 5 is the conclusion of the thesis. It summarizes the key results and outlines perspectives for further research.

CHAPTER 2

CAPACITY FACTOR OF LAND-BASED, NEARSHORE AND FAR-OFFSHORE WIND TURBINES

In this chapter, the state-of-the-art of wind energy harvesting technology (wind turbines) is presented. Its capacity factor is discussed depending on its deployment location.

2.1 State-of-the-art of wind turbines

2.1.1 Wind energy development

Wind-based power is one of the renewable power sources that are expected to play a significant role in global decarbonization. According to previous resource assessments, the available wind energy in the atmosphere could potentially power the entire world [37].

Global wind power capacity grew by 14% between 2019 and 2020 to 743GW with 93GW new added capacity for both onshore and offshore in 2020 [38]. Global capacity is expected to reach 2000 GW global wind energy capacity by 2030, supplying up to 17–19% of global electricity, and reducing CO2 emissions by more than 3 billion tons per year. This projection includes both onshore and offshore wind farms. [38][39]. The expected total installed capacity of offshore wind by the end of 2030 is 64 GW (4.5 GW per year installation rate), providing around 250 TWh per year.

Vestas, GE Renewable Energy, Goldwind, Chinese Envision, Siemens Gamesa, Enercon are the largest wind turbine manufacturers (“OEMs”) in in the world, having supplied 68% of global installed wind power capacity in 2020. Figure 13 shows their respective market share. Vestas was the world's top provider of wind turbines in 2020, covering both onshore and offshore wind [40][46].

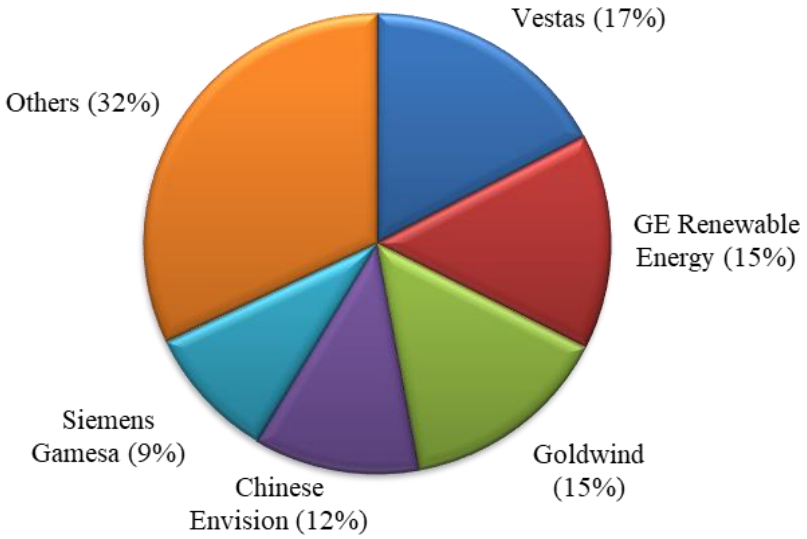

Figure 13 The world's top five rankings for wind turbine original equipment manufacturers ("OEMs") (Source: GWEC (2021[38])

In 2020, the Asia Pacific are takes the lead in global wind power development with 60% new installed capacity in 2020, followed by North America (18%) and Europe (16%) [38].

Looking forward, the wind farm technology in 2030, the development of wind industry technologies may bring up the turbine rating to 13 MW, with rotor diameter of 212 m and hub height of 128 m.

Relative to the capacity factor, in 2030, 46.7% capacity factor was estimated for typical installation site and exceed 50% capacity factor for best sites which discover better wind resources [41].

Figure 14 shows the evolution of wind industry globally between 2001 to 2020. Following the scenario of 12% growth, the install capacity in wind industry could achieved up to 22 TW in 2050.

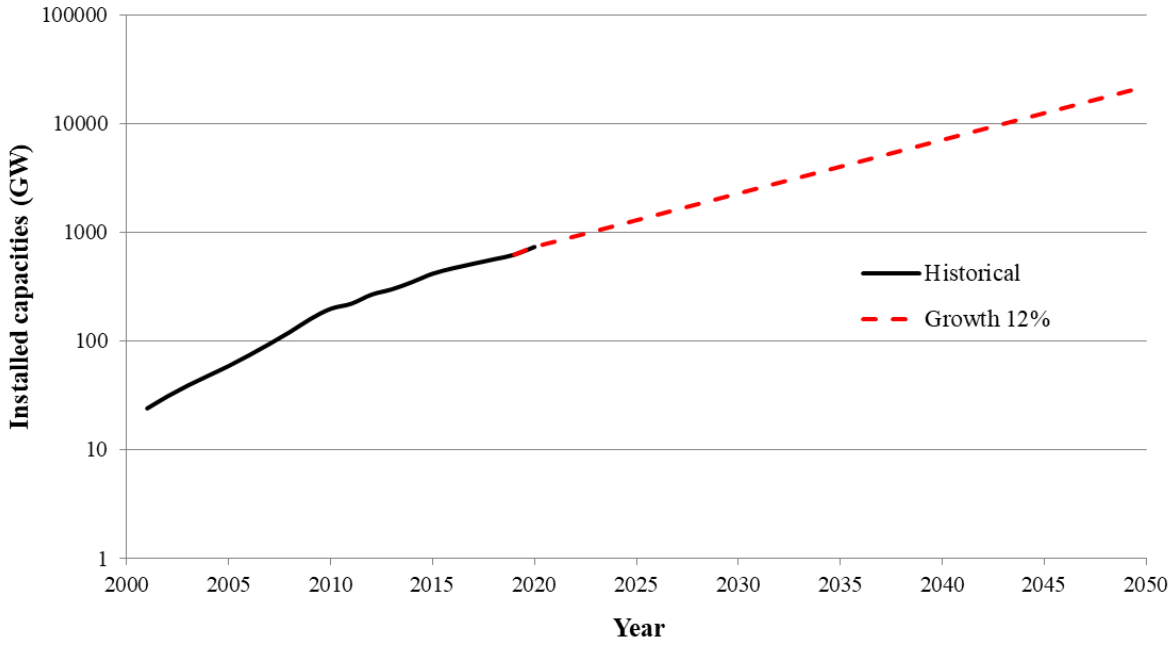

Figure 14 Global wind industry evolution between 2001 to 2020 and expected trends up to 2050 (Source: IEA data and statistics)

2.1.2 Wind turbine technology

Historically, the earliest use of wind energy exists for boat navigation on the Nile River in 5000 BC. In the same era, windmills in China were also used to pump water. Essentially, wind power was utilized to produce mechanical power to pump water and grind cereals until the early twentieth century. Then, Poul LaCour, a Dane, constructed the first wind turbine that generated energy in 1891. During World Wars I and II, the Danish engineers improved the technology and employed it to tackle energy shortages. F.L. Wind Turbines, a Danish manufacturer was the one who manufactured the wind turbines [45]. Since then, significant advancements in wind turbine design have been made. Modern technical advancements and improvements of a turbine and its components, in particular, have resulted in considerable increases in produced power output and efficiency. Nowadays, commercially available wind turbines range in size from a few kilowatts to many megawatts.

Modern wind turbines can be divided into two types:

1. Horizontal axis wind turbines (HAWTs)
2. Vertical axis wind turbines (VAWTs)

HAWTs dominate the majority of the wind industry due to their greater efficiency and energy output in comparison to VAWTs.

The diameter of the turbine is among the most important parameter. The recent trend is toward large diameters, as longer blades sweep wind from a larger area and produce greater output energy. Table 3 shows the evolution of wind turbines size over time till 2020.

Table 3 Development of wind turbine size onshore and offshore between 1985 and 2020

Year	Capacity (kW)	Rotor diameter (m)
1985	50	15
1989	300	30
1992	500	37
1994	600	46
1998	1500	70
2001	2000	72
2002	2500	80
2005	3600	120
2010	7580	140
2017	8000	164
2020	12000	220

Practically all modern wind turbines are designed according to the international standard IEC61400. Furthermore, wind turbine certification bodies such as the DNV-GL release their own amendments and additions to the IEC61400 standard [47]. A wind turbine is composed by different components; the main components are listed and described as follows (see Figure 15) [46][48]:

1. Rotor - A rotor consists of large blades resembling an airplane wing. It converts the wind kinetic energy into the rotation of the rotor hub. Wind turbines have normally three blades. Rotor blades can be very large in size.
2. Rotor hub - it connects the blades to the main shaft. It also contains the pitch drive.
3. Pitch drive – It is used to control the pitch of the blades. It changes the angle of attack of the blades with the goal of changing the rotation speed of the rotor. It is used to reduce the lift in high wind speed conditions. This is necessary to guarantee that the generator maintains a speed within an acceptable power system operation range of 1000–3600 RPM (revolutions per minute).

4. Drive train system - it is the part that transfers the energy from the rotor to the generator. There are mainly three types of drive train system: geared, direct-drive and hybrid.
5. Nacelle – The housing of all the elements of the upper part of the wind turbine. The nacelle is located at the top of the turbine tower. It is attached to the rotor, and contains the main technical parts, such as the rotor shaft, gearbox, and generator. The main role of the nacelle is to protect the internal components of the wind turbine against the environment. The nacelle is connected to the tower with bearings and is able to rotate with respect to the wind direction in order to harness maximum wind energy. In addition, there are heaters/coolers fans inside the nacelle to control the temperature. To facilitate the access of operators to large wind turbines, the nacelle may include a helicopter-platform.
6. Gearbox – The turbine rotor typically has a speed of less than 100RPM, but most generators need 1000 to 3600 RPM to generate electricity. Thus, the gearbox converts low rotor speed into higher speeds in order to make the generator operational.
7. Generator – The generator converts the mechanical energy of the rotor into electrical energy. It is placed at the top of the tower, inside the nacelle.
8. Anemometer – the anemometer measures the wind speed, and the wind vane detects the wind direction.
9. Wind orientation control (Yaw control) - controls the rotor to face the wind direction and the yaw angle.
10. Access ladder – Although most modern wind turbines now include elevators to enable easy access to platforms within the towers and all the way to the nacelle, access ladders are still necessary in the event of an emergency lift breakdown or to access to interior tower section between platforms.
11. Tower and foundation –A tower is used to place the rotor at high altitudes in order to capture more wind energy. It is also capable to transfers the vertical and horizontal loads to the ground. The design and configuration depend on where the wind turbine is placed whether onshore or offshore (see Figure 16).
12. Grid connection - In order to reduce electric losses, a transformer converts the medium voltage from the wind turbine generator to high voltage.

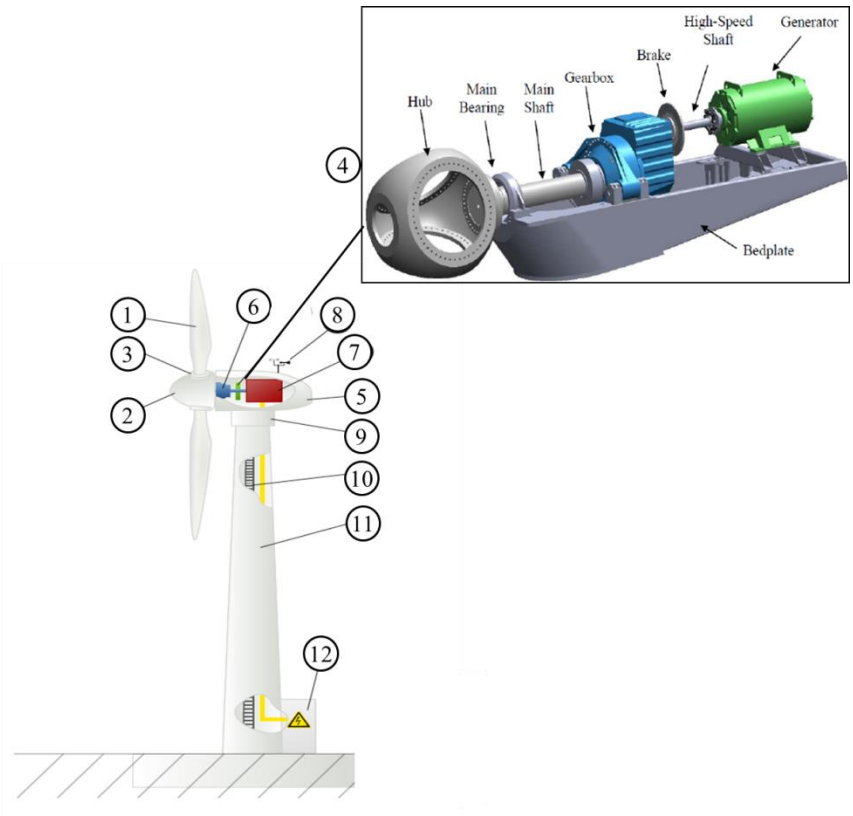

Figure 15 Wind turbine components (Source: [49])

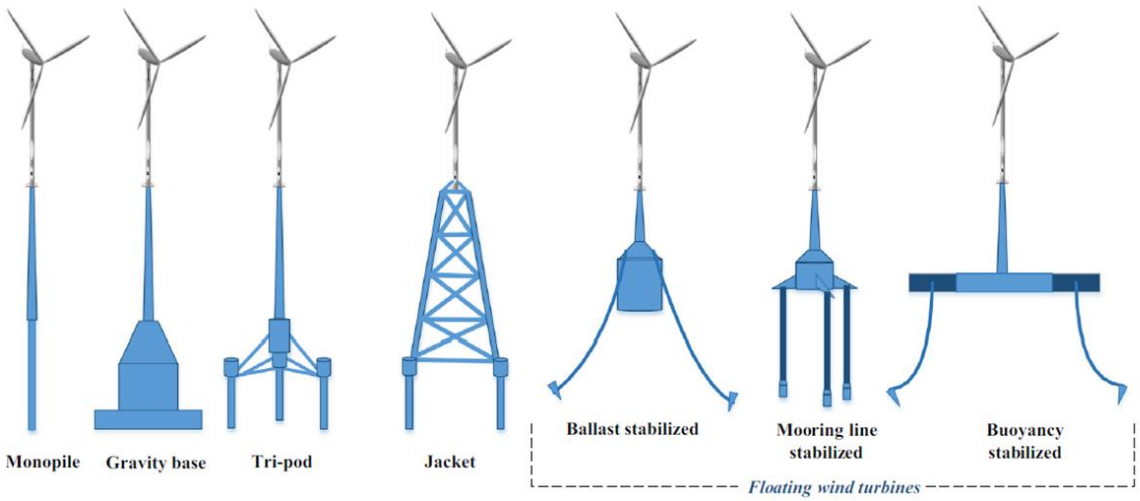

Figure 16 Wind turbine foundations (Source: [46])

2.1.3 Wind turbine power curve

A wind turbine operates from the cut-in wind speed and then increases its power output with increasing wind speed until the wind speed reaches the rated speed, at which point the turbine starts to run at its rated power [12]. Between the cut-in wind speed and the rated wind speed, the power is proportional to the cube of the wind speed. To avoid damage to the rotor, it is halted when the wind speed exceeds the cut-out speed. Typical values ranges are 3–4 m/s cut-in speed (v_c), 11–17 m/s rated speed (v_r) and 25 m/s cut-out speed (v_f) [12][48].

Figure 17 shows the typical power curve of a wind turbine. The main elements are explained as follows (see) [12][48][50]:

1. Cut-in wind speed: the lowest wind speed for which the blades start to rotate and electrical energy is produced. The value of this speed is between 2 and 5 m/s.
2. Below cut-in: until the minimum wind speed is reached, the wind turbine is kept in standby. Once the wind speed reaches the cut-in speed, a start-up routine is carried out.
3. Non-rated region: in this region, the power increases with increasing wind speed it is proportional to the cube of the wind speed.
4. Nominal or rated wind speed: the minimum wind speed for which the maximum output power (rated power) is achieved.

5. Rated region: in this region, the wind turbine produces at rated power. The blade pitch is controlled in order to reduce loads and avoid overspinning of the rotor.
6. Cut-out wind speed: The wind speed for which the wind turbine stops producing electrical energy. As the speed increases above the rate output wind speed, the forces on the turbine structure continue to rise and, at some point, there is a risk of damage to the rotor. As a result, a braking system is employed to bring the rotor to a standstill. This is called the cut-out speed and is usually around 25 m/s.

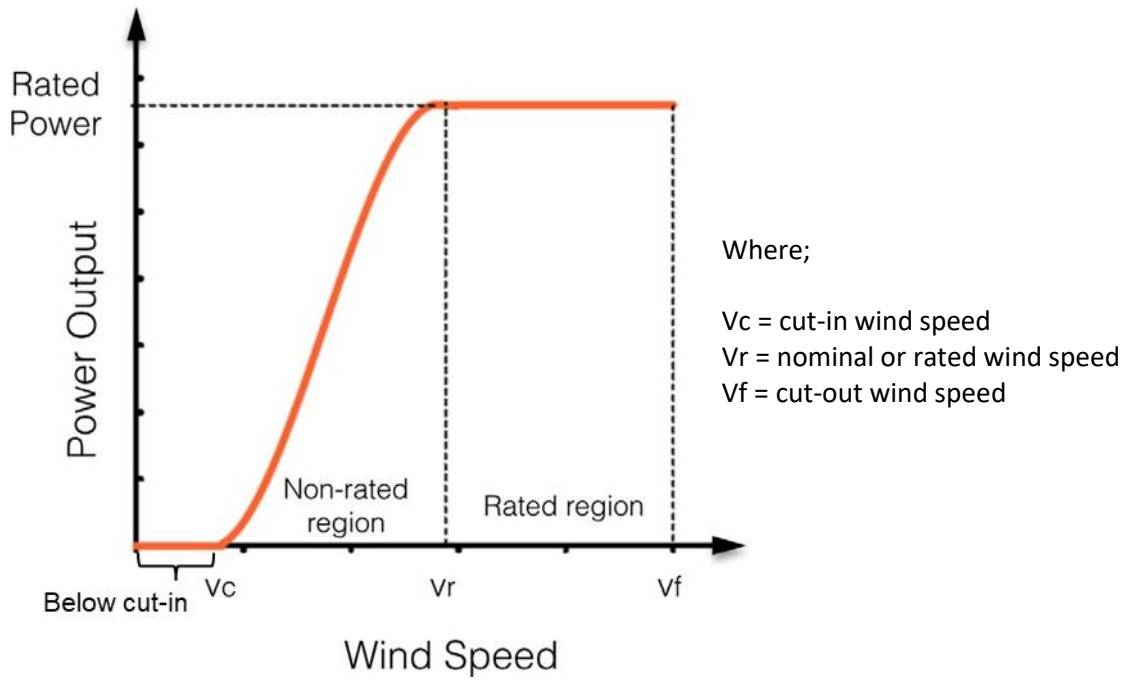

Figure 17 Power curve (Source: Dupont et al [12])

2.1.4 Land based wind turbines

An onshore wind turbine is a category of turbine that is installed on land. Typically, it has 50–100 m tower height with a rotor diameter of 50–100m [46]. The general trend in wind turbine designs is to increase tower height and rotor blade length. The rotational speed of the rotor is typically 12–20 RPM, much lower than those installed during the 1980s, which operated at a 60 RPM [61]. As a result, modern turbines are capable of generating power at much lower wind speeds [46].

In the present day, storm control techniques enable wind turbines to operate even better during very high wind speed conditions. Onshore wind turbines are typically installed together into wind power plants, commonly known as wind projects or wind farms. The 2020 onshore wind energy capacity in Europe is presented in Figure 18.

Figure 18 Onshore wind energy capacity in Europe in 2020 (Source: [55][56])

2.1.5 Near shore/ far offshore wind turbines

Wind turbines installed beyond the coast are known as offshore power systems. The development of offshore wind energy has accelerated in the past decade. The advantages of the offshore environment are that, the wind is typically stronger and more sustained than inland [12][46], and offshore sites can accommodated larger power plants with larger wind turbines [46]. In Europe, the available offshore area for wind turbines deployment is 1,648,000 km², which constitutes 31.5% of the total area [58].

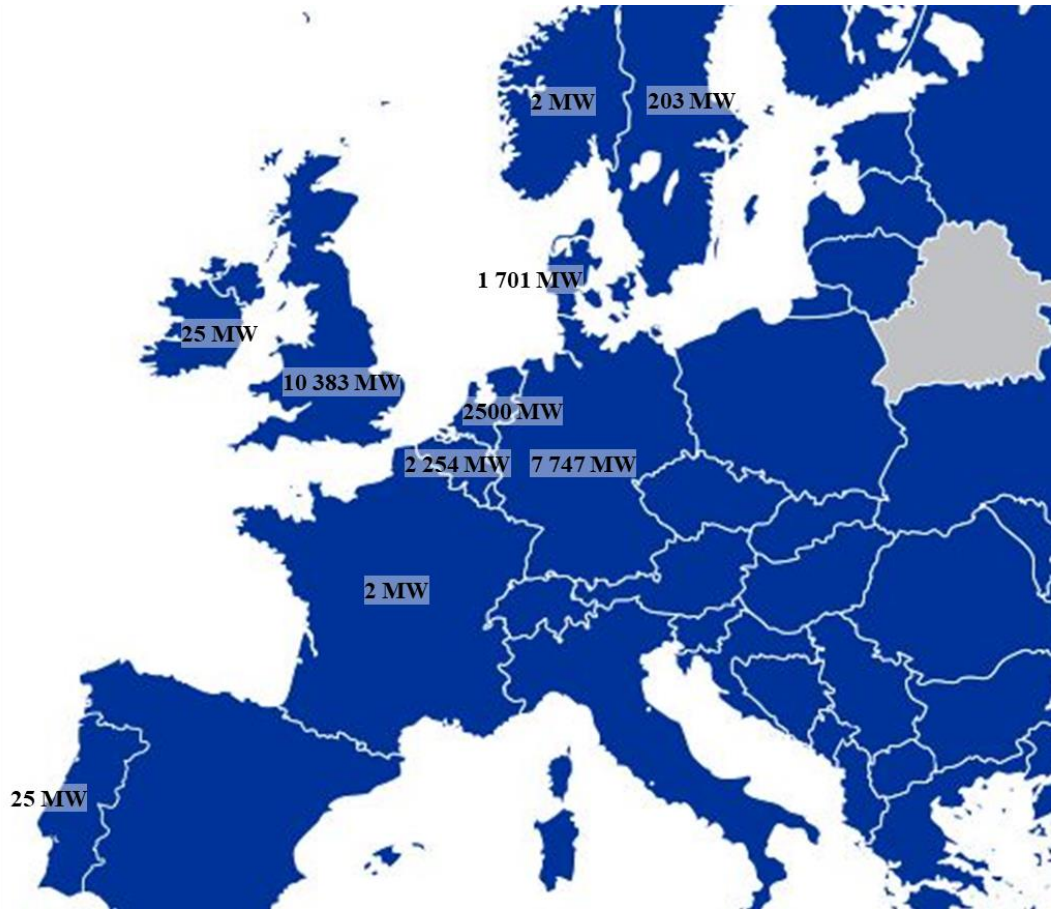

Figure 19 Offshore wind energy capacity for European countries in 2020 (Source: [55])

The first commercial-scale offshore wind farm is Horns Rev 1. It has been installed in Denmark. It has a capacity of 160 MW (Consist of 80 turbines and became operational in 2002. Since then, the capacity of the turbines and the size of offshore wind farms have been increasing. Moreover, they are being installed in deeper waters further from the coast [59].

In 2020, offshore wind has reached a total of 34,367 MW installed capacity globally. Europe holds two-third out of the total offshore wind capacity, with a total of 24,920 MW (see Figure 19). It is followed by Asia with a total capacity of 9,418 MW [55].

The challenges in offshore wind include the higher costs of the installation and operation of the wind turbines, specifically the foundation and the electrical system [67]. The cost of the grid connection is also significantly higher offshore than onshore. Due to these higher costs, larger wind

turbines are required to reduce the overall specific costs per installed kW [46][60]. Table 4 summarizes the advantages and the drawbacks of wind turbine deployment onshore and offshore.

Table 4 Advantages and disadvantages of onshore and offshore wind energy (Source: [59])

Onshore Turbines		**Offshore Turbines**	
Advantage	**Drawbacks**	**Advantage**	**Drawbacks**
Cheap	Highly variable energy source (capacity factor ~25%)	Less variable energy source (capacity factor ~40%)	Expensive
One of the cheapest forms of renewable energy	Can endanger flying wildlife, such as birds and bats	Less turbines required to produce an equal amount of electricity	Increased operation and maintenance costs caused by increased wear from wind and waves and difficult access
Boost local economies	Noise and visual impact	Less visual impact and conflicts of use	Longer wait times required to correct any potential problems due to more limited access
	Inability to produce energy year-round due to reliance on optimal wind conditions	Protects aquatic habitats by restricting access to certain waters	
		Excessive access to wind resources without landforms obstacle	

Offshore wind turbines are similar to that onshore. The only significant difference is the design of the foundations, which requires floating and/or other special foundations to account for underwater tower submergence [46]. There are two main types of offshore foundations that are bottom-fixed and floating wind turbines.

2.1.5.1 Bottom-fixed wind turbines

Figure 20 shows the various types of bottom-fixed foundations that may be used to deploy offshore wind turbines. These foundation types can be categorized based on the water depths in which they are used.

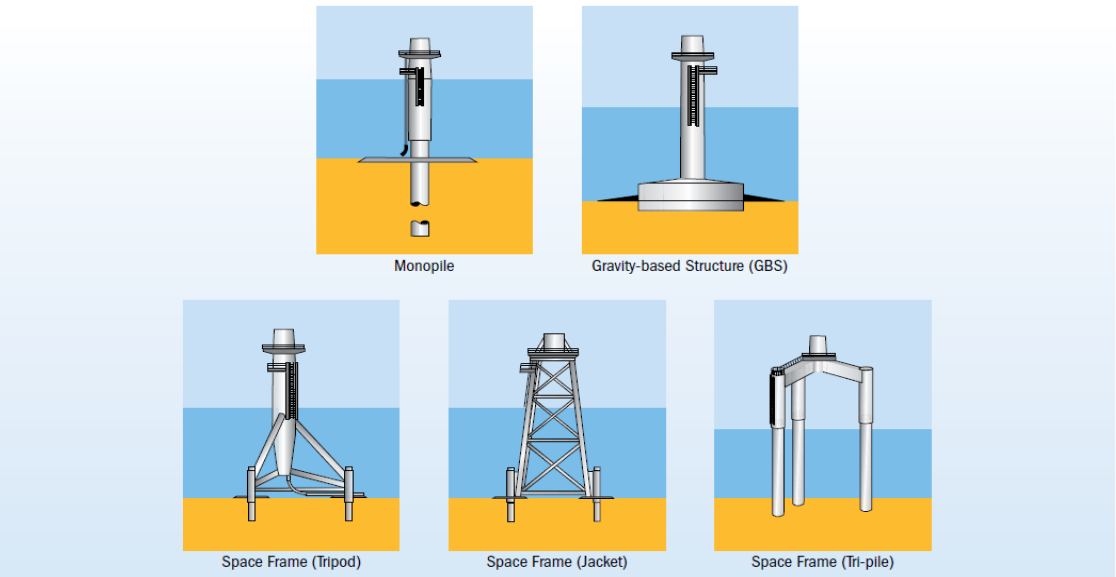

Figure 20 Typical bottom-fixed offshore foundations
(Source: EWEA [54])

2.1.5.2 Shallow water depth (below 35 meter)

The majority of offshore wind turbines is currently installed in shallow water, which are waters depths up to 35 meters [61]. In this range of water depths, the most common type of foundation is the monopile. It is a long and large-diameter steel tubular structure that is hammered or vibrated into the seabed. Monopiles are the most widely utilized foundation type (more than 60% of wind turbines operating worldwide [64]) due to their ease of manufacturing and installation [61]. 'XL-monopiles', with diameters up to 10 meters, are developed to expand their practicality to larger wind turbines and deeper water depths [61].

Gravity based foundation have also been used in shallow water depths. This type of foundation is simply laid on the seafloor and utilizes its own weight to support the wind turbine. Sand, rocks, or iron are commonly used to provide weight for stability. It is worth noting that the gravity-based foundation requires a solid bottom and can only be used in extremely shallow waters. As a result, this type of offshore foundation is rarely utilized nowadays [62].

2.1.5.3 Medium water depth (approximately 35 to 80 meters)

Since the offshore wind industry is now moving toward installing larger wind turbines in deeper waters, shallow-water foundation options may become economically and/or technically unfeasible. As a result, the most widely utilized foundation installations at medium sea depths ranging from 30 meters to 80 meters [61] are as follows:

i. Tripod

Offshore foundations known as tripods are constructed with a central vertical tube attached to three-leg structured cylindrical steel tubes that form a broad base on the seabed [64]. They are frequently connected to small diameter piles placed into the seabed. The broad base offers a solid foundation that can withstand significant overturning. Tripods account for around 5% of all offshore foundations currently in use [61].

ii. Jacket

Jackets, the multi-membered structures are typically made up of three or four legs linked by bracing. This structure is normally deployed in the oil and gas industry; however, it has been optimized for the installation of offshore wind farms [64].

Jackets have relatively high production costs since they are made up of several tubular components that are welded together at nodes. To anchor the structure to the bottom, the legs of the jacket linked to small diameter soil-piles or suction buckets [63]. To anchor the structure to the bottom, the legs of the jacket linked to small diameter soil-piles or suction buckets [63]. Jackets are less sensitive to wave loading than other foundation types [61].

Jacket type foundation has dimensions similarly to tripods, but due to its better adaptability to a variety of conditions and stability, they have become the second most widely used type, just behind monopiles [64].

2.1.5.3 Floating wind turbines (Deep water: 80 meters and beyond)

Significant progress has been made in floating offshore wind in the recent years, including the commissioning of the world's first multi-units installation in 2017 (30 MW Hywind in Scotland). In 2018, several smaller demonstration projects were completed, including Floatgen (2

MW) in France and Hibiki in Japan (3 MW) [65]. Table 5 shows the floating offshore wind turbines and wind farms in operation at the end of 2020. In addition, the 88 MW Hywind Tampen project in Norway, which will have 11 wind turbines, is set to begin commissioning in 2022 [65][69]. The facility was built specifically to supply energy to offshore oil and gas platforms.

Equinor also obtained approval in 2019 to develop a 200 MW floating offshore commercial wind farm off the coast of the Canary Islands, which is projected to be the world's largest floating offshore wind farm [65]

Table 5 Commissioned floating offshore projects at mid-2021 (JAP: Japan; NOR: Norway; UK: United Kingdom; FRA: France; PRT: Portugal) [44][64][65].

Wind Farm	Country	Power (MW)	Turbines	Depth (m)	Distance (km)	Year
Hywind	NOR	2.3	1	220.0	10	2009
Fukushima Floating - Phase 1	JAP	2.0	1	122.5	20	2013
Sakiyama Wind Turbine	JAP	2.0	1	40.0	5	2016
Fukushima Floating - Phase 2	JAP	12.0	2	122.5	20	2018
Hibiki Floating	JAP	3.0	1	55.0	15	2018
Hywind Scotland	UK	30.0	5	103.0	30	2018
Floatgen	FRA	2.0	1	33.0	22	2018
WindFloat Atlantic	PRT	25.2	3	100	20	2020
Kincardine	UK	50	6	80	15	2021

In floating offshore wind, a floating platform and a platform anchoring system make the floating foundation. The platform has a transition piece to install the tower on top. Broadly, spar-buoy, semi-submersible, and tension leg platforms are the three primary types of floating foundations (see Figure 22). Many other variations exist, such as numerous turbines on a single platform and hybrid wind/wave floating systems [65].

i. Floating spar buoy

A spar-buoy is a cylindrical buoy that floats vertically and is large yet slender. To make the construction stable, ballast is used to reduce the center of gravity below the center of buoyancy,

and mooring-lines are used to anchor it to the seabed [61]. Hywind (see Figure 6), the world's first floating 2.3 MW wind turbine, was installed in Norway in 2009 and is supported by a spar-buoy [66].

ii. Semi-submersibles

Semi-submersible structures have a broad base and are partially submerged to provide a solid supporting foundation for the wind turbine [64]. Mooring lines that are moored in the seabed keep the foundation in place. The WindFloat (WF1) is the world's first 2 MW wind turbine to be placed on a semi-submersible platform. It was installed off the Portuguese coast in 2011 and decommissioned in 2016 [61]. All of the lessons learned from the WF1 prototype deployment then applied with additional innovation to the next generation of WindFloat project e.g WindFloat Atlantic (see Figure 21).

Figure 21 Windfloat Atlantic floating offshore wind farm (Source: https://www.offshore-mag.com/renewable-energy/article/14188688/windfloat-atlantic-represents-major-offshore-wind-milestone and [44])

iii. Tension leg platform

A tension leg platform (TLP) is a vertically connected platform with tensioned anchoring lines vertically attached to the floating platform. With the excessive buoyancy of the platform;

these anchoring lines known as tendons or tethers creates tension in the anchoring system [93]. TLP was originally developed by the oil industry for its deep water offshore rigs then expanded in the floating offshore wind industry. The world's first floating wind turbine prototype was installed on a tension-leg platform by Blue H Technologies (small scale TLP with an 80 kW turbine). The 300-ton scale prototype was placed into the Adriatic Sea at a depth of 113 meters, 22 kilometers from the shore, to gather test data on wind and sea conditions [93].

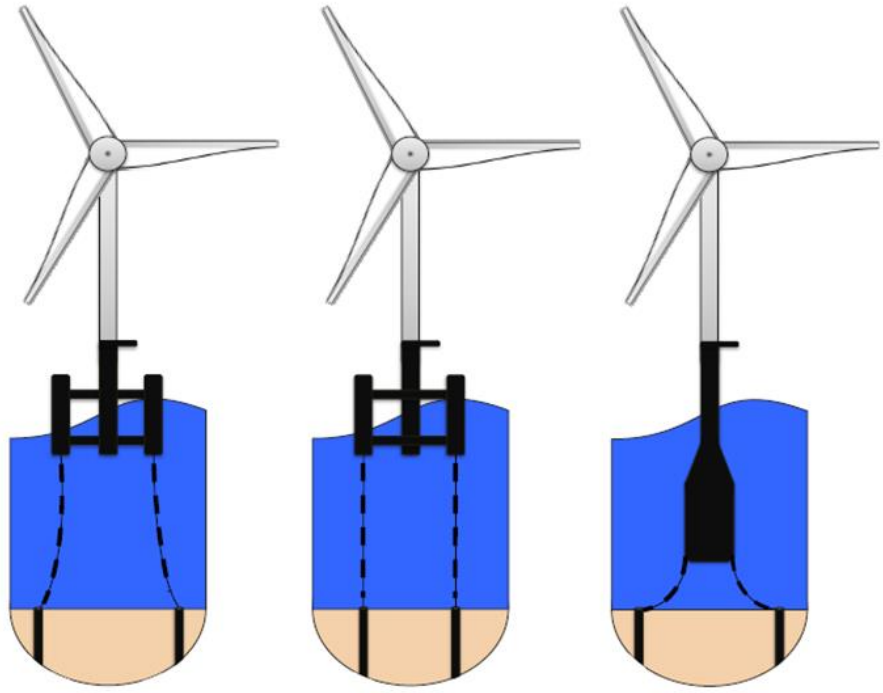

Figure 22 Various types of floating offshore wind turbines (Source: [66])

2.2 Capacity factor of wind turbines

The capacity factor (CF) is the ratio of the average delivered power to theoretical maximum power [54] :

$$C_F = \frac{\int_0^{\mathrm{T}} \mathrm{P}(t)dt}{TP_{rated}} \qquad \text{Eq. 1}$$

Where P is the delivered power, P_{rated} is the maximum power, and T is the duration.

The capacity factor can be computed for a single turbine, a wind farm consisting of several wind turbines or an entire country composed of hundreds of farms. Although geographical location determines in significant part the capacity factor of a wind farm, it is also a matter of turbine design. Indeed, a large rotor combined with a small generator will take advantage of just about any wind and achieve a very high capacity factor, obviously at the cost of a low yearly energy output [55].

The capacity factor of a wind farm and its profitability depends on whether it is adequately sized and sited. This is because the energy produced by a wind farm site depends on many factors, such as variation in wind speed distribution and wind turbine type. Also, taking into consideration the characteristics of speed like the cut-in velocity (v_c), cut-out velocity (v_f), rated velocity (v_r), hub height, and the generator design [39].

2.2.1 Land based wind-turbines

In the United Kingdom, the current average capacity factor of onshore wind turbines is 30% [53]. In mainland Europe, it is 24% [43]. IRENA has presented statistics of the global weighted-average onshore capacity factor over year 2010 to 2019, see Figure 23. It shows that since 2016, the global onshore average capacity factor exceeds 30%. It reached 35.6% in 2019. The capacity factor for onshore wind is significantly higher than that of solar PV (18% in 2019) [55].

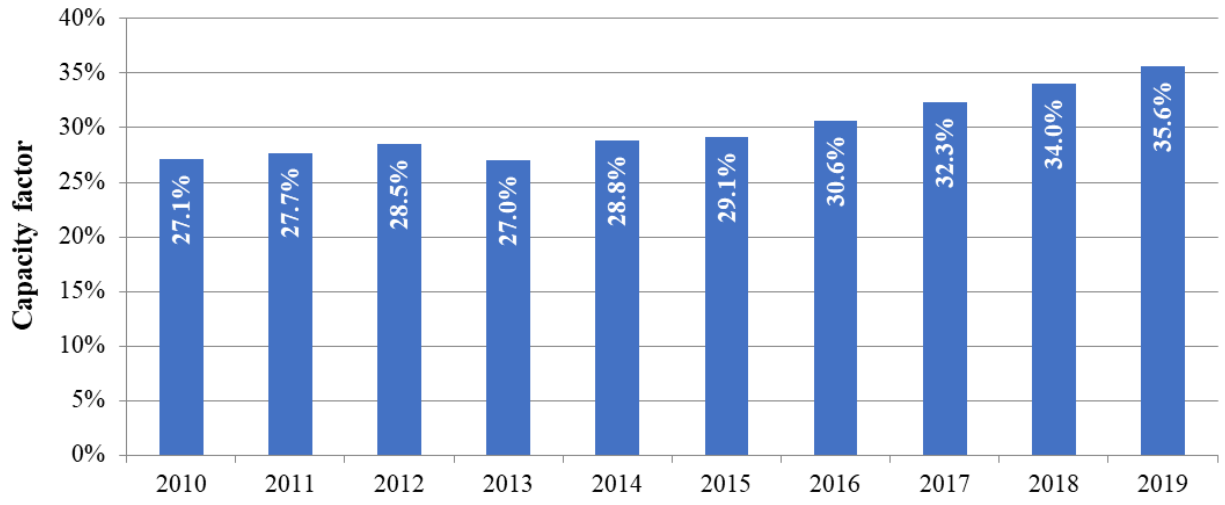

Figure 23 Global weighted-average capacity factor of onshore wind for corresponding year between 2010 and 2019 (Source: IRENA Renewable Cost Database [57]

2.2.2 Near shore wind turbines

Usually, in order to be cost effective, wind farms are installed at class 3 sites [12]. In [7], Capps & Zender showed that the average capacity factor for 5MW offshore wind turbines for locations characterized with class 3 wind speeds and water depth smaller than 200m is in range of 38 to 49%.

In practice, capacity factors of 40 to 50% have been reported for offshore wind farms [25][65]. They are significantly greater than land-based installations; thanks to higher wind speeds in open ocean areas in comparison to areas over land [6]. Note that these capacity factors are for existing offshore wind farms that are located near-shore.

Figure 24 shows the global offshore average capacity factor over the period 2010 to 2019. One can see that there is significant variability over the year. The highest capacity factors, over 45%, were obtained in 2013 and 2017. The lowest was obtained in 2014 (30.2%). Nevertheless, the capacity factor seems to be increasing, reaching values well over 40% over the last years. For 2020, the European Academy of Wind Energy expects that capacity factors will reach 44.6% for offshore wind in Europe [54].

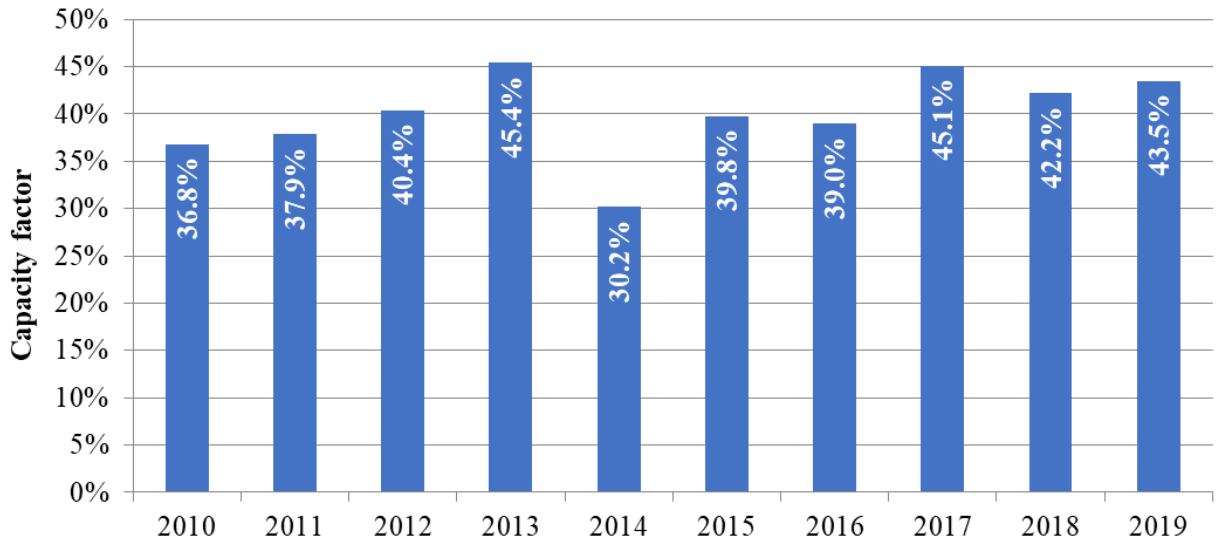

Figure 24 Global weighted-average capacity factor of offshore wind for corresponding year between 2010 and 2019 (Source: IRENA Renewable Cost Database [57])

Dupont et al. [12] estimated a capacity factor of 39% for floating offshore wind farms. Nevertheless, the average capacity factor of the Hywind Scotland offshore wind farm throughout 2 years of operation is 54%, which is significantly greater [68].

2.2.3 Far-offshore

2.2.3.1 Dupont et al. (2017)'s study

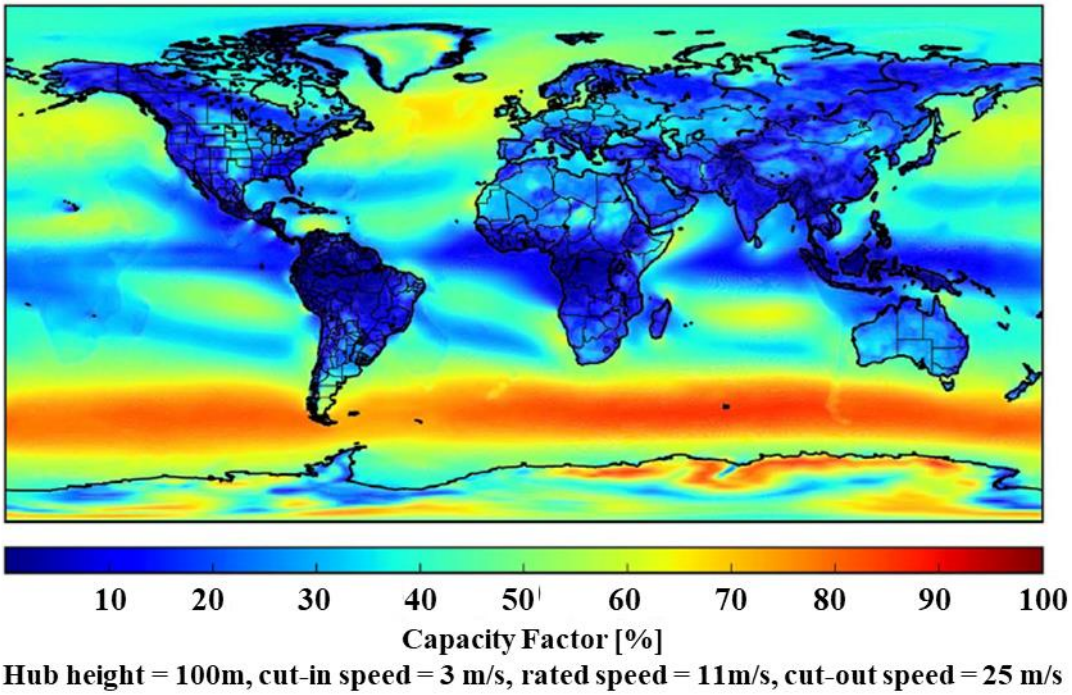

Figure 25 Global map of capacity factor estimates (Source: Dupont et al [12])

Dupont et al. [12] seems to be the first at having performed an extensive assessment of the theoretical global wind potential, including an estimation of the capacity factor of floating wind farms which would be deployed in the far-offshore (see Figure 25).

They considered wind turbines of 120 m diameter offshore (5 MW wind turbines). They used 3 m/s for the cut-in speed, 25 m/s for the cut-out speed, and 11 m/s for the rated wind speed. The wind speed distribution at 100 m hub height from the ERA interim dataset has been used. As the ERA interim dataset does not include the wind speed at hub height, the arithmetic mean of wind

speed at 71 m and 125 m was used. Using that data, they produced a global distribution of capacity factor estimates for wind turbines as shown in Figure 25.

As one can expected, the capacity factor varies significantly depending on the location of the wind turbine. Overall, Figure 25 shows very high capacity factors can be achieved offshore (especially far-offshore). The highest capacity factors (over 80%) could be obtained for wind turbines which would be deployed in the south of the southern hemisphere (between 40°S to 65°S). On the other hand, very low capacity factors (10 to 30%) would be obtained along the equator line (between 10°N to 10°S). In the Northern hemisphere, high capacity factors (in the range 65 – 75%) could be achieved for wind farms in the North of North Atlantic ocean.

2.2.3.2 Verification of the capacity factor of wind farms in the far-offshore

To confirm the results obtained by Dupont et al., an independent investigation of the capacity factor of stationary offshore wind turbines deployed in the far-offshore was carried out.

10m wind speed data for years 2015, 2016 and 2017 from the ERA-Interim dataset reanalysis was used [70]. This dataset provides wind data every 6 h at a 0.75° × 0.75° precision. It was developed by the European Centre for Medium-Range Weather Forecasts (ECMWF).

The assessments of the capacity factor have been performed using a modified version of the QtVlm software. Originally, QtVlm is a free navigation and weather routing software designed for sailing boats. In collaboration with LHEEA, it has been modified in order to extend its capabilities to assess capacity factor of wind turbines and energy ships.

For the assessment of the capacity factor of a wind turbine, the methodology is as follows. A grib-file containing the weather data is loaded in QtVlm. Then, a location is selected for the deployment of the wind turbine.

The wind turbine is modelled in QtVlm through its velocity polar plot and its power polar plot. QtVlm only accepts .pol format for the wind turbine performance input. As the wind turbine is assumed to be stationary, the polar plot for the velocity was set to zero. The polar plot for the power is shown in Figure 26. It was calculated using Eq.1 [95]:

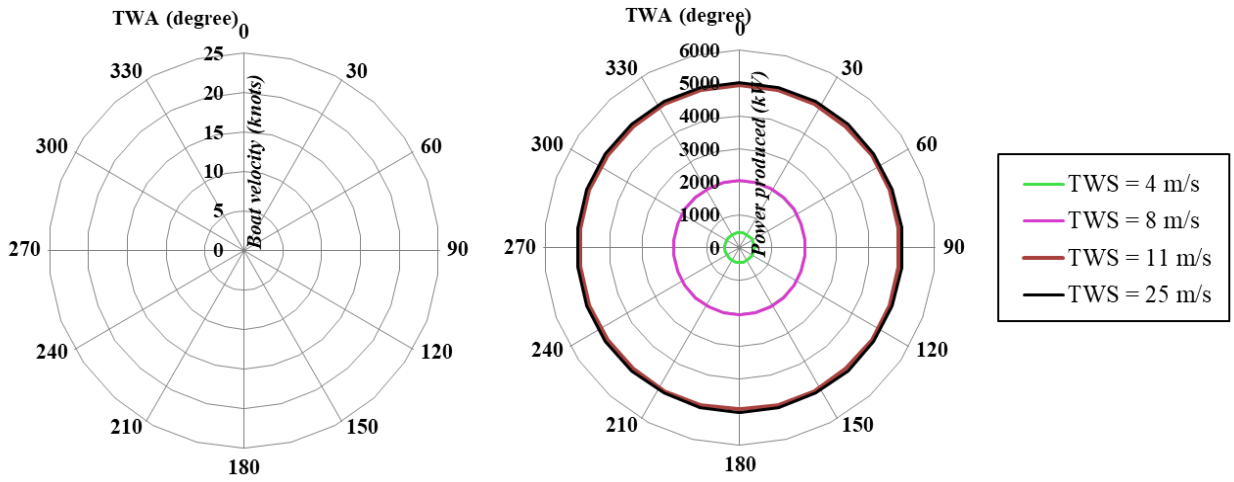

Figure 26 Zero-velocity (left) and wind turbine power production (right) polar contains data of true wind angle (TWA) and true wind speed (TWS) loaded in QtVlm for 5 MW wind turbine capacity factor assessment

$$\tilde{P}(v) = P_{rated} \begin{cases} 0, \ if \ v < \mathrm{v}_c \\ \frac{v^3 - {v_c}^3}{{v_r}^3 - {v_c}^3}, \ if \ v_c \leq v \leq v_r \\ 1, \ if \ v_r \leq v \leq v_f \\ 0, \ if \ v \geq v_f \end{cases} \quad \text{Eq. 1}$$

Where:

- $\tilde{P}$ is the power produced by the wind turbine
- P_{rated} is the rated power of the wind turbine
- v is the wind velocity at the hub height
- v_c, v_r and v_f are respectively the cut-in, nominal and cut-out wind speeds.

The wind velocity at the altitude of the hub (90 m) is obtained from the wind data (which is given for 10 m altitude) using the power law profile:

$$U(z) = U(H)\left(\frac{z}{H}\right)^{\propto} \quad \text{Eq. 2}$$

Where:

- H is the altitude of the wind data (10 m)
- z is the hub height (90 m)
- $\propto$ is the power law exponent. It is taken equal to 0.12 (open sea with waves) (source: [31])

At first, the capacity factor assessment was performed on a regular 20.0° x 20.0° global grid. Grid points located onshore were not considered in this assessment. Then, the assessment was refined for locations were the capacity factor appeared to vary rapidly.

The capacity factor was assessed for year 2015, 2016 and 2017 at 211 different locations covering the world's five oceans. Figure 27 shows the results for the average capacity factor. Figure 28 focuses on the North Atlantic Ocean.

Figure 27 shows that the highest capacity factor (75 to 88%) are obtained between latitude 40°S and 60°S. Symmetrical, very high capacity factors may be achieved in the North of the oceans of the Northern hemisphere (69 to 80% in the North Atlantic ocean between 40°N and 60°N). On the other hand, the lowest capacity factors are concentrated near the equator line (0°) ranging from 30 to 45%. The greatest capacity factor is 88%, meanwhile the lowest capacity factor is 17%.

By comparing Figure 25 and Figure 27, one can see that there is a good agreement between the results of Dupont et al. [12] and the results obtained in this analysis.

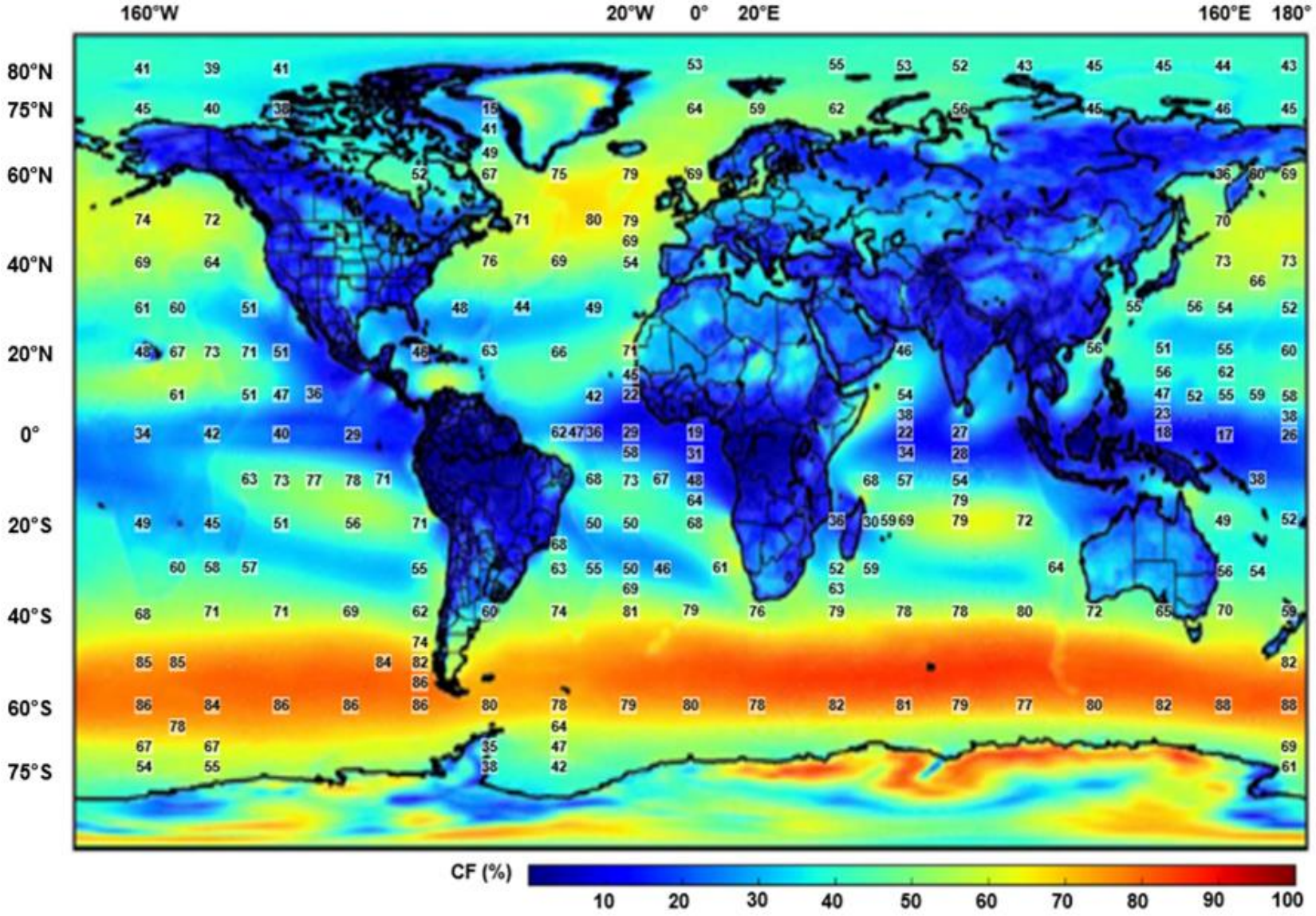

Figure 27 Map of average capacity factor of theoretical floating offshore wind turbines for selected locations (Adapted from Dupont et al [12])

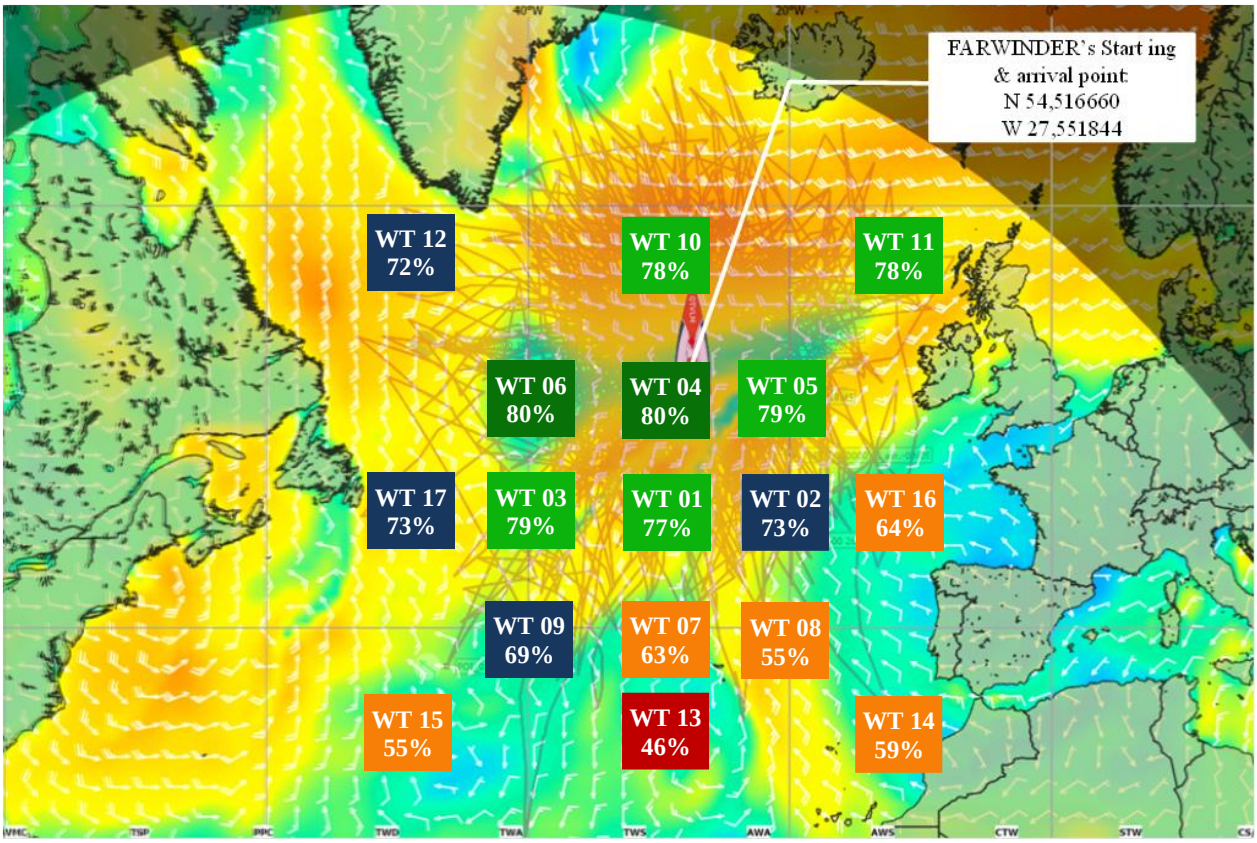

Figure 28 Tested locations for the wind turbines and average capacity factor over the three years of 2015, 2016 and 2017

Figure 28 shows that, in the North Atlantic Ocean, the capacity factor varies significantly depending on the location of the wind turbine. Overall, it can be seen that it is primarily driven by the longitude, and secondly by the latitude. Wind turbines deployed northern than 45° N have capacity factors greater than 75% except in the West of the area (72% for wind turbine #12). Close to 45° N, the capacity factor varies from 64% to 79% depending on the latitude. It can be observed that the capacity factor decreases with getting closer to Europe (64% for wind turbine #16). The smallest capacity factors are obtained for the four wind turbines located on the most southern line (46% to 59%).

2.2.3.3 Annual variability in the North Atlantic ocean

Table 6 shows the annual variability of the capacity factor for the wind turbines hypothetically deployed in the North Atlantic Ocean (Figure 28). One can see that there are year-to-year variations which can be up to 7% in comparison the average over the three years (WT16).

Table 6 Theoretical capacity factor for 5MW floating offshore deployed at 17 locations in North Atlantic ocean for 2015, 2016 and 2017.

Turbine	Latitude (N)	Longitude (W)	2015	2016	2017	3 years average
WT01	46.000000 °	-31.000000 °	0.76 (-1.30%)	0.78 (1.30%)	0.77	0.77
WT02	46.000000 °	-21.500000 °	0.73	0.74 (1.37%)	0.73	0.73
WT03	46.000000 °	-40.500000 °	0.79	0.81 (2.53%)	0.78 (-1.27%)	0.79
WT04	52.000000 °	-31.000000 °	0.77 (-3.75%)	0.84 (5.00%)	0.79 (-1.25%)	0.80
WT05	52.000000 °	-21.500000 °	0.78 (-1.27%)	0.82 (3.80%)	0.76 (-3.80%)	0.79
WT06	52.000000 °	-40.500000 °	0.81 (1.25%)	0.78 (-2.50%)	0.80	0.80
WT07	40.000000 °	-31.000000 °	0.62 (-1.59%)	0.64 (1.59%)	0.63	0.63
WT08	40.000000 °	-21.500000 °	0.55	0.55	0.54 (-1.82%)	0.55
WT09	40.000000 °	-40.500000 °	0.70 (1.45%)	0.70 (1.45%)	0.67 (-2.90%)	0.69
WT10	58.000000 °	-31.000000 °	0.81 (3.85%)	0.77 (-1.28%)	0.76 (-2.56%)	0.78
WT11	58.000000 °	-12.000000 °	0.81 (3.85%)	0.75 (-3.85%)	0.78	0.78
WT12	58.000000 °	-50.000000 °	0.73 (1.39%)	0.74 (2.78%)	0.70 (-2.78%)	0.72
WT13	34.000000 °	-31.000000 °	0.44 (-4.35%)	0.49 (6.52%)	0.45 (-2.17%)	0.46
WT14	34.000000 °	-12.000000 °	0.55 (-6.78%)	0.62 (5.08%)	0.60 (1.69%)	0.59
WT15	34.000000 °	-50.000000 °	0.56 (1.82%)	0.57 (3.64%)	0.53 (-3.64%)	0.55
WT16	46.000000 °	-12.000000 °	0.69 (7.81%)	0.62 (-3.13%)	0.62 (-3.13%)	0.64
WT17	46.000000 °	-50.000000 °	0.75 (2.74%)	0.74 (1.37%)	0.71 (-2.74%)	0.73
			Average wind farm capacity factor			**0.69**

2.2.3.4 Alwan et al. (2019) study

In [71], Alwan et al. have investigated a sailing wind turbine concept for harvesting far offshore wind resources. This concept consists in a floating barge equipped with a wind turbine, a keel and two propellers. It is neither moored nor grid-connected. The sailing wind turbine concept

also includes an on-board energy storage system (e.g. batteries, hydrogen, etc.) as it is not grid-connected.

Figure 29 shows an artist impression of the sailing wind turbine design. Its main characteristics are given in Table 7.

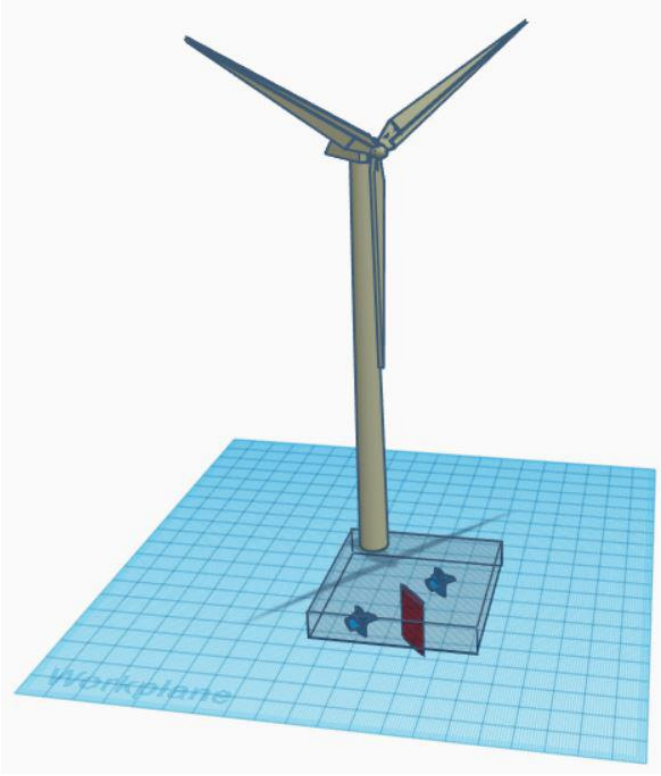

Figure 29 Artist view of a sailing wind turbine. (Source:[71])

Table 7 Design and characteristics of sailing wind turbines

	Unit	Value
Barge dimensions		
Width	m	40
Height	m	10
Draft	m	7.5
Displacement	tonnes	12,000
Propellers		
Diameter	m	6
Number of Blades	-	3
Keel		
Surface Area	m2	15
Wind turbine dimensions		
Rotor Diameter	m	78

Rated Power	MW	2
Nacelle Height	m	90
Wind turbine fig		
Cut-in wind speed	m/s	3.5
Nominal wind speed	m/s	11.4
Cut-out wind speed	m/s	25

The concept is that the foundation's position can be controlled via the combined action of the propellers and the keel. In particular, the propellers can give the platform a forward velocity, thus enabling the generation of a lift force by the keel, which counteracts the drift force from the wind turbine.

A model was developed which enables the velocity and power performance of a sailing wind turbine to be estimated as a function of the environmental conditions.

Using the model, it is shown that there exist two operating regimes that can lead to positive net power production. They are the drifting regime and the sailing regime. In the drifting regime, the propellers are stopped. Nevertheless, thanks to the significant water resistance on the platform, the drift velocity is much smaller than the wind velocity. Thus, the apparent wind velocity is large, which leads to high levels of power production. However, a drawback of the drifting regime is that only downwind sailing conditions can be achieved in this regime.

In contrast, maintaining position and net power production can be achieved in the sailing regime. However, for a given wind speed, the power production is less than in the drifting regime because of the power consumed by the propellers.

The simplest mode of operation for a sailing wind farm is to use the sailing regime. Net power production of a sailing wind turbine at a true wind speed of 8 m/s is in order of 800 kW. According to Alwan et al., capacity factors up to 36% could be achieved by sailing wind turbines operated in the North Atlantic Ocean. It is approximately half that of stationary wind turbines which would be deployed in the same area (Figure 28). However, note that 2 MW wind turbines (hub height 90 m) wind were considered in Alwan et al.’s study, whereas 5 MW wind turbines (hub height of 100 m) were used in Dupont et al. [12] and in our investigation. Thus, one can expect that the capacity factor of 5 MW sailing wind turbines could be greater. Moreover, as point out by

Alwan et al., other exploitation strategies for the operation of sailing wind turbines may be developed, potentially resulting in significantly higher capacity factors.

2.3 Conclusion

Overall, in this chapter, we presented the state-of-the-art of wind energy technology. Capacity factor of wind were discussed and compared for land based wind turbines and offshore wind turbines. Noticeably, the global average capacity has reached 35.6% for the land based wind turbines and 43.5% for offshore wind turbines in 2019.

We also investigated the capacity factor of stationary offshore wind turbines in the far-offshore and compared it with the investigation by Dupont et al. [12].

A good agreement is obtained. Results show that very high capacity factors (over 70%) can be achieved for wind turbines which would be deployed in the far offshore. Furthermore, the annual variability of 5MW floating wind farm at North Atlantic ocean was also investigated. Results indicate that the year-to-year variation is in the order of a few percent.

Finally, we presented the alternative sailing wind turbine concept for far-offshore wind energy conversion which was proposed by Alwan et al. [71]. Its advantage is that it requires neither moorings nor grid-connection. However, its capacity factor is significantly smaller than that which could be obtained by moored stationary wind turbines.

CHAPTER 3

CAPACITY FACTOR OF WEATHER-ROUTED ENERGY SHIPS IN THE FAR-OFFSHORE

In this chapter, the capacity factor of energy ships which would be deployed in the far-offshore is investigated and compared to that of stationary floating wind turbines deployed at the same locations. The capacity factor is optimized using a modified version of the weather-routing software QtVlm [27]. This chapter also presents the results of the sensitivity studies of boat performances (i.e polar speed and polar power plots) on the capacity factor and the energy production of the energy ship.

3.1. Ship weather-routing

3.1.1. Review of existing methods and tools

In contrast to stationary floating offshore wind turbine, energy ships are mobile. Therefore, their trajectories (routes) can be optimized taking into account weather-forecast in order to maximize energy production [19][28]. This concept is called weather-routing [72]. It is commonly used by offshore racers and in commercial shipping.

In this study, capacity factor is obtained using hindcast data. Thus, they correspond to perfect forecast. Errors and uncertainties in weather forecast can lead to smaller capacity factors in practice. However, this effect is expected to be limited as the routes are flexible and that they can be re-optimized as new weather forecast become available.

Based on marine weather forecast data and ship performances, ship weather routing calculates an optimal route at sea. The optimization criteria may correspond to maximum safety and crew comfort, minimum fuel consumption, minimum time underway, or any combination within defined weather and sea conditions [28][73][75]. Traditionally, the basis of the weather routing is the recommended route which is based on a review of weather and sea forecasts between the starting point and the endpoint (destination). It considers the vessel type, hull type, speed capability, safety considerations, cargo, and loading conditions, among several other criteria [84]. The vessel progress is monitored, and if bad weather or rough seas are predicted along the vessel present route, a diversion recommendation or weather advisory is sent to the

user [72]. By utilizing this method of initial route selection and constant progress monitoring for possible changes in projected weather and sea conditions along a route, it is possible to maximize both speed and safety of the voyages.

Matthew Fontaine Maury first introduced the concept of weather-routing [72]. It started with the massive compilation of atmospheric and oceanographic data from ships' logbooks by Maury in the mid-19th century. Thus, the mariner had access to global climatology data consisting of ocean weather and currents for the first time. Towards the late 19th century, Maury used this information to construct seasonally recommended routes for sailing ships and early steam-powered vessels [72].

Nowadays, weather routing and route optimization has been recognized in the shipping industry as an effective technique to assure ships safety, earn more economic advantage, and reduce environmental impact [77]. During the route planning process, ship captains frequently employ a weather routing tool to avoid potentially dangerous and harsh weather conditions, to limit the risk of ship/cargo damage and human injuries, to predict the expected arrival time (ETA), and many more [28][72][73]. Based on current weather forecasts and ship performance models, a route optimization system uses optimization algorithms in computers to plan a ship sailing course and schedule in the most efficient way possible from a long-term perspective (until destination) [74].

Figure 30 shows the usual route optimization technique: a grid of waypoints along a ship sailing area is first generated, and then a path searching method is used to find the best route based on specific end-user objectives [73].

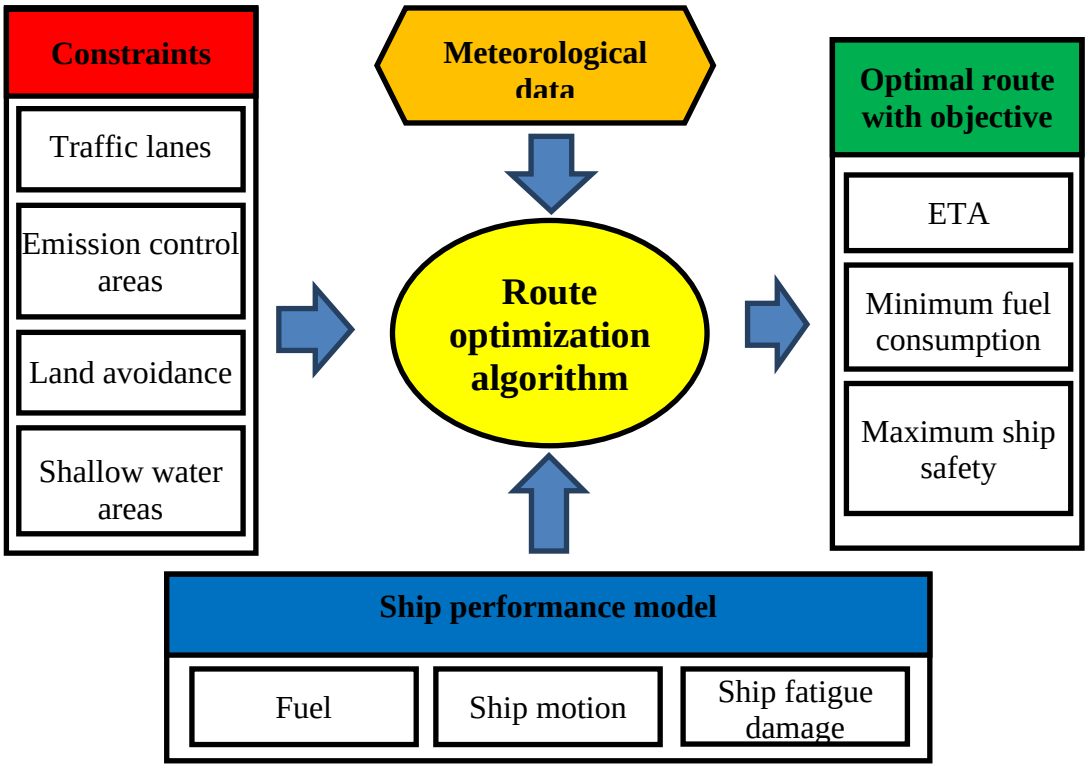

Figure 30 Overview of route optimization system (Source: [73])

Numerous route optimization methods and algorithms are available to deal with route planning problems [28][73].

Walther in [28] presents a comprehensive comparative overview of existing optimization methods for ship weather routing. They include calculus of variations [76], 3D Dynamic programming (Shao, Zhou & Thong, 2012) [28], dynamic programming method (Wit,1990) [28], Iterative dynamic programming (Luus, 2000) [28], isopone method (Klompstra et al.,1992) [28], original isochrones method (James, 1957) [28], modified isochrone method [19][88], 3D modified isochrones method (Lin et al. 2013) [28], Dijkstra's algorithm (Dijkstra, 1959; Padhy et al, 2008) [28], real coded genetic algorithm (Maki et al. 2011) [28], Pareto-optimized multi objective genetic algorithm [78], multi objective evolutionary algorithm, SIMPLEX algorithm, DIRECT (Diving Rectangles) method and many more [28]. They are summarized in Table 8 along with their advantages and drawbacks (not an exhaustive list).

Table 8 Existing route optimization methods and algorithms

Optimization Methods /Algorithms	**Principle / Implementation**	**Advantages**	**Drawbacks**
Calculus variations	- Pontryagin's maximum principle - Optimization based on dynamic programming - minimize or maximize functionals often expressed as integrals, in order to find extremals - the optimization is achieved through variation of the parameters that control the trajectory - Numerical Euler-Lagrange equations solver equivalent	Powerful and elegant mathematical approach	- Difficult to apply in practice - need a lot of calculation time and memory space for objective functions
Dynamic programming	- Using Forward Dynamic Programming method based on Bellman's principle of optimality - Deterministically solve the optimization problem with one objective function and several constraints	Can provide the solution giving the global minimum to an objective function and can easily incorporate the constraints into the routing algorithm.	- Extensively depends on the fineness of the grid system used for the computation - needs many grid points for the search routine to obtain an accurate solution, thus it uses a lot of calculation time and memory space
Isochrones method	- practical method of route planning process - treats the ship routing as a discrete optimization problem - work on a set of connected points dependent on weather factors, that a ship can reach within a given time limit starting from one point and going in all possible directions.	Convenient to obtain the isochrones by hand	Not applicable for computer programs due to "isochrones loops" - an irregularity in shape of an isochrone

Modified Isochrone method	- Deterministic routing - Applied to minimum fuel/cost routing. - can be extended to stochastic routing by incorporating the stochastic nature of the environmental forecasts into the routing algorithm.	- straightforward and very suitable for computerization - remove “isochrones loops” problem thus applicable to computer application - determine the correct isochrones; thus it can calculate the accurate minimum time route and easily take into consideration the constraints	Not suited for a narrow strait.
Dijkstra’s algorithm	- Finds the shortest path between two given nodes in a graph with positive edge weights - Uses a deterministic method for solving a discrete optimization problem consisting of one objective and only implicitly defined constraints.	Low numerical complexity (almost linear)	- the resulting path is not smooth - only deal with single-objective optimization problems (route)
Real coded genetic algorithm	- evolutionary calculation technique considers real-valued vectors	Robust and efficient method for strongly inter-variable dependencies	Computationally expensive and time consuming
Multi-Objective Genetic Algorithm (MOGA)	- stochastically solves a discretized nonlinear optimization problem containing several objective functions and several constraints.	Higher capability to find the global optimum	Higher computational effort
SIMPLEX algorithm	Use deterministic method with working principle as follows: - requires n + 1 initial designs or starting points - objective function is evaluated for all n + 1 points. If one of the designs is good enough the algorithm stops. - Otherwise the worst point is deleted and replaced by a new one and create a new polytope	- Fast - Can solve nonlinear unconstrained optimization problem	- Convergence to local minima - Rely on a convex solution space may or may not yield the optimal result.

Along with the development of optimization methods and algorithms, various weather routing software are now available on the market. They include PredictWind, Adrena, TimeZero, FastSeas and QtVlm (not an exhaustive list) [79] to [83]. In this thesis, the weather routing software QtVlm [27] developed by Meltemus [83] was used.

3.1.2. The QtVlm weather-routing software

QtVlm is a free navigation and weather routing software developed for sailing boats [27]. Its primary function is to calculate routings and routes based on weather data and boat performance polar. In QtVlm, the weather data are provided in Gridded Binary (GRIB) format [86] while boat performance polars are provided as text files (.pol).

A polar diagram describes how fast a sailing boat may go at different wind speeds (TWS) and in different angles to the wind (TWA). The true wind speed (TWS) is the actual speed of the wind as it passes the surface of the sea. While the true wind angle (TWA) is the angle between the boat's heading and the true wind direction (TWD).

Each type of boat has its specific polar diagram, which can computed using a velocity and power prediction program (VPPP) [22] or obtained from sea-trials.

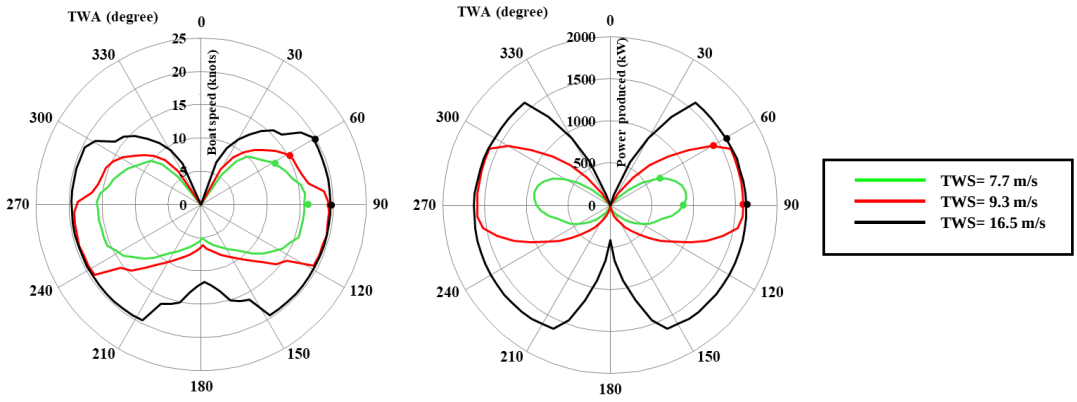

Figure 31 Example of 1.6 MW catamaran boat speed (left) and power production (right) polars

Figure 31 shows an example of the boat speed polar and the power production polar of a 1.6 MW energy ship. The boat speed polar shows the boat speed as function of the true wind angle while the power production polar shows the generated power as function of the true wind angle. Both polar are plotted for three true wind speeds (7.7 m/s, 9.3 m/s, 16.5 m/s).

3.1.2.1. Route optimization algorithm

QtVlm uses the isochrones method to find the optimal route. The isochrone method was initially proposed by James in 1957 [28]. Then Hagiwara [19] proposed a modified isochrone method.

As defined by James, an isochrone is a set of connected points that a ship may reach in a certain amount of time by starting at one point and travelling in all possible directions within the time limit. These points are influenced by weather conditions such as wave direction and height. Based on the definition of the isochrone, the first isochrone visualizes the ship's speed characteristic. The characteristics are dependent on factors like the vessel's dimensions and contractual speed.

A perpendicular line to the tangent is determined from each point belonging to the first isochrone for the second isochrone (see Figure 32). The point of the second isochrone is defined by a segment of the line depicting the distance that the ship can reach within the next time limit. The second isochrone is made up of a group of such connected points. Following that, the next isochrones are generated with the same method.

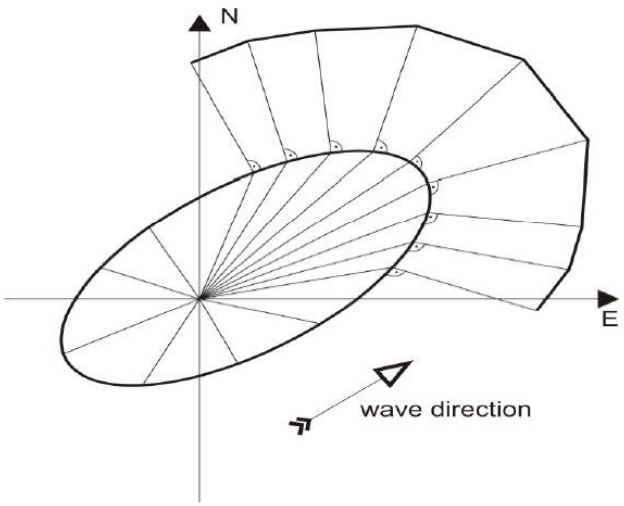

Figure 32 Construction of first and second isochrones [88]

The original isochrone method was intended for manual use by navigators as an aid for route planning process. In 1989, Hagiwara had made an improvement to the original method and developed the modified isochrone method. The modified isochrone method formulates the ship routing problem as a discrete optimization problem for easier computer calculation [19].

The algorithm (see Figure 33) extends the basic isochrone algorithm by treating points obtained at the first iteration as initial points for the second iteration and so on.

To maintain a reasonable number of points, the search space is divided into a limited number of subsectors (see Figure 34). The number of subsections may vary depending on the chosen number of reference routes and the subsector width, which determines the accuracy of the result. The furthest point along the great circle route (GCR) connecting the departure point and the point under consideration are chosen to be part of the next isochrone within each subsector. The selected points are then treated as initial points for the next iteration, and the same procedure is repeated until the first point on an isochrone coincides with the destination. The optimal path may be found by tracing it back.

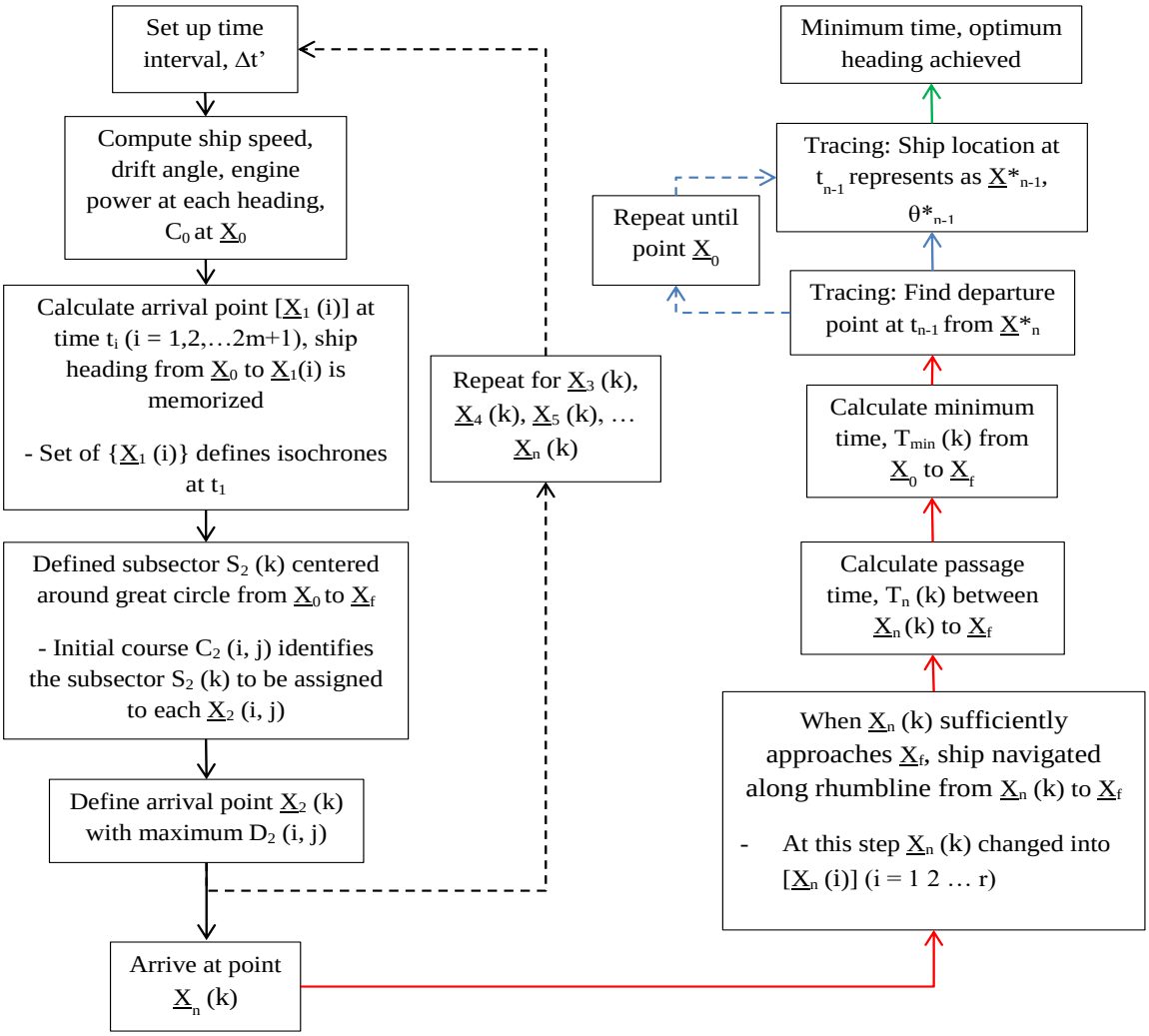

Figure 33 Modified isochrones algorithm (Adopted from Hagiwara (1989) [19]

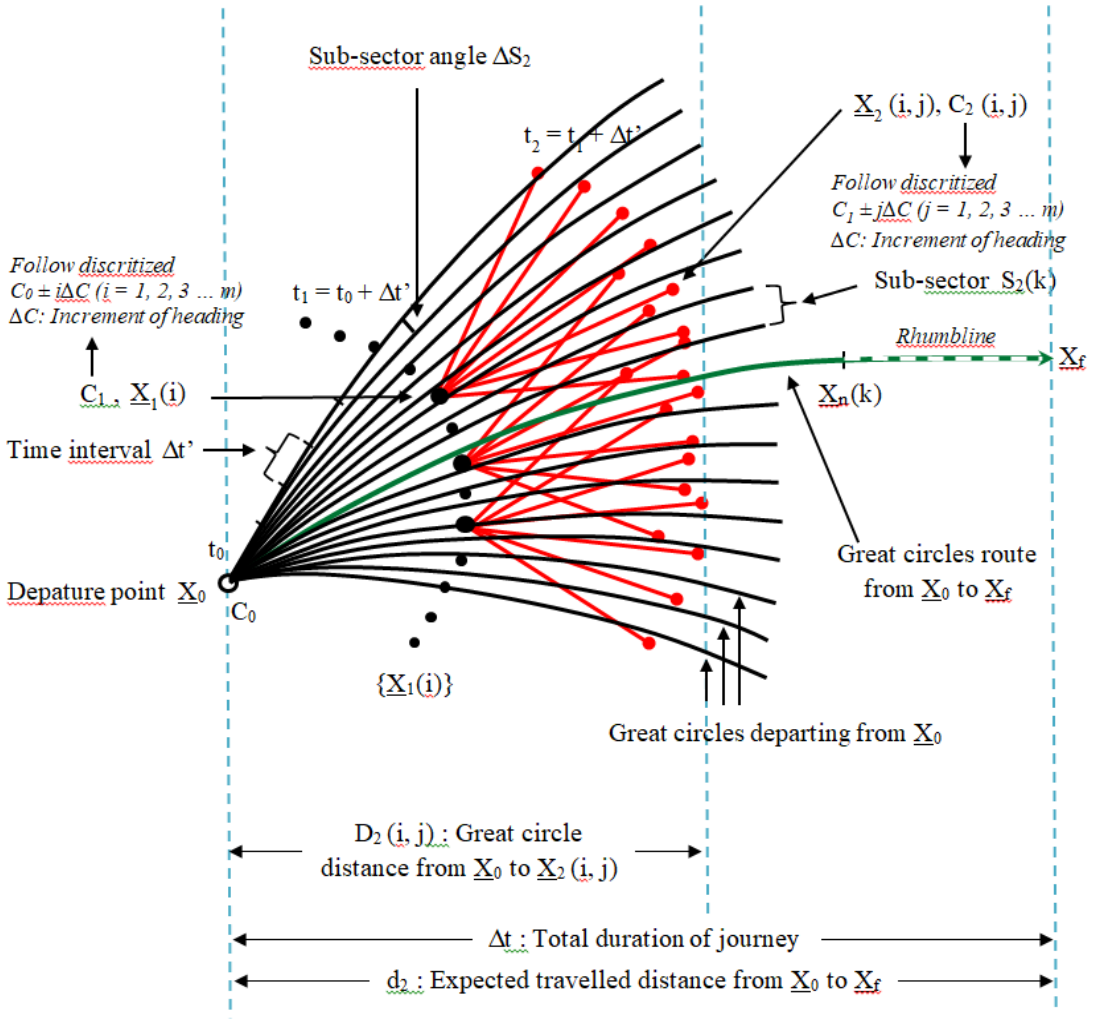

Figure 34 Modified isochrone algorithm diagram adapted from [19]

3.1.2.2. Nodes location optimization

The QtVlm software also includes the possibility to further improve the travel duration by optimizing the location of the nodes of the route determined by the modified isochrone method using the SIMPLEX method.

The SIMPLEX algorithm was developed by Nelder and Mead (1965). It is a popular deterministic method for solving nonlinear unconstrained optimization problem (see Figure 35) [78]. The algorithm basic principle is as follows [78]:

1. It requires n + 1 initial designs or starting points, i.e. for a 2-dimensional problem it starts with a triangle, a tetrahedron for a 3-dimensional problem, and a polytope (SIMPLEX) with n + 1 vertices for a n-dimensional problem.

2. The objective function is evaluated for all n + 1 points. If one of the designs is good enough the algorithm stops.

3. Otherwise the worst point is deleted and replaced by a new one. In this way a new polytope is built.

4. Continue the loop with step (2).

The core of the algorithm is the strategy in step (3) to build the new simplex:

a) Reflect the worst point about the centroid of all others.

b) If this point is now better than all the other ones, expand the step in the same direction.

c) If it is simply better than before, continue with step (2).

d) However, if the point gets worse in either case, shrink the simplex e.g. to half size around the best point and continue at step (2).

The algorithm terminates if the attainable improvement at successive optimization loops falls below a preset convergence limit.

The SIMPLEX algorithm is widely used in high dimensional optimization problems [78]. Extensions have been developed for the SIMPLEX method. They include the capability to preserve an equable shape of the simplex or even some random capabilities to overcome the issue of convergence towards local optima.

QtVlm uses a combination of the isochrone and SIMPLEX methods for its routing optimization algorithm [83].

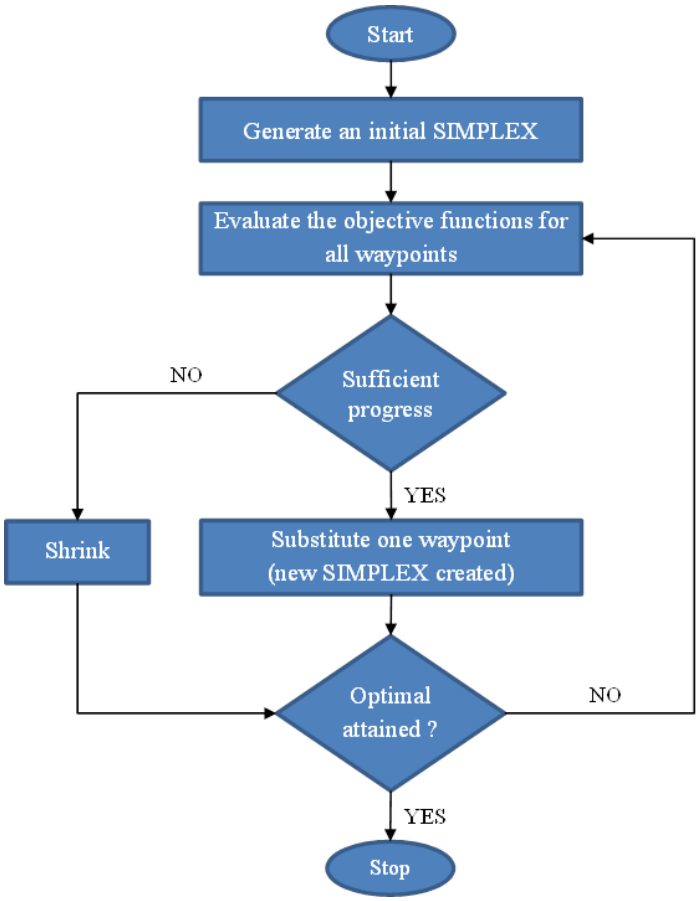

Figure 35 Simplex optimization algorithm [78]

3.2. Weather-routing optimization of energy ships using QtVlm

3.2.1 Weather data

In this thesis, 10-meter wind speed data for the year 2015, 2016 and 2017 are used. It was obtained from the ERA-Interim dataset which was developed by the European Centre for Medium-Range Weather Forecasts (ECMWF) reanalysis [86]. The time step is 6 hours and the spatial resolution is 0.75° (approximately 80 km). It is coarse in comparison to other meteorological data. For example, the ERA5 dataset has a spatial resolution of 0.28° (approximately 31 km) and the ECMWF's operational high-resolution forecast (HRES) has a resolution of 0.25° [87].

In [92], five global reanalysis have been analyzed and compared in order to identify the most accurate dataset for the wind speed at the height of wind turbines' hub. The reanalysis are ERA5, ERA-Interim, the Japanese 55-year Reanalysis (JRA55), the Modern Era Retrospective Analysis for Research and Applications-2 (MERRA2), and the National Centers for

Environmental Prediction (NCEP)/National Center for Atmospheric Research (NCAR) Reanalysis 1 (R1). Table 9 shows the datasets' main characteristics. The accuracy of the surface and near-surface winds were evaluated by comparison to measurements at 77 instrumented tall towers.

Table 9 Summary of the basic characteristics of the five reanalysis datasets (Source: Ramon et al. (2019) [92])

Name	ERA-Interim	ERA5	JRA55	MERRA2	R1
Institution	ECMWF	ECMWF	JMA	NASA GMAO	NOAA/NCEP and NCAR
Period coverage	1979 to present (Dicontinued August 2019)	1980 to present (Expanded back to 1950 in August 2019)	1978 to present	1980 to present	1948 to present
Time resolution	6-hr	1-hr	6-hr	1-hr	6-hr
Horizontal grid spacing	0.75° × 0.75°	0.3° × 0.3°	1.25° × 1.25°	0.5° latitude × 0.625° longitude	1.875° latitude × 2° longitude

The study highlighted differences in DJF (December-January-February) mean wind speed, year-to-year variability, and long-term trends between the five global reanalysis datasets. Particularly, the most significant discrepancies were encountered within continental areas. Mean wind-speed differences can be partly explained by different representations of land-surface roughness and elevation at the various grid resolutions employed in the reanalysis models.

The verification process with the in-situ tall tower measurement wind offered insights into which reanalysis perform better than others on daily and seasonal time-scales. Amongst all five surface wind datasets plus the multi-reanalysis mean (MR), ERA5 shows the best results in terms of correlation and standard deviation. Indeed, the improvement in both correlation and variability with respect to the MR is statistically significant in 35% of tall tower sites, which is significantly higher than other reanalysis such as MERRA2 (9.1%) and ERA-Interim (1.3%) [92]. Neither JRA55 nor R1 is better than the MR in any of the tower locations. Overall, Ramon et al. concluded that the ERA5 near-surface wind dataset provides the most accurate estimations of mean wind speed and variability at turbine hub heights. Unfortunately, the ERA5 dataset was not available at the beginning of this thesis, which is why ERA-Interim was used.

In addition, in this thesis, the MERRA2 dataset and the ERA-INTERIM dataset wind datasets have been compared. The MERRA2 data was obtained through the website www.renewable.ninja. Figure 36 shows a comparison of the distribution of wind speed for the whole year 2017 at the exact location of 52°N 31°W. The mean wind speed for the MERRA2 dataset (11.18 m/s) is significantly greater than the ERA-INTERIM dataset (9.54 m/s). The maximum wind speed for MERRA2 also is 33.5 m/s, which is higher than that for ERA-INTERIM, 23.9 m/s. One may also note that the spatial resolution for the MERRA2 dataset is 0.5° latitude × 0.625° longitude (see Table 9). Thus, the data provided by MERRA2 is finer than ERA-INTERIM.

The significant differences between these two datasets indicate that there is a significant uncertainty on the results of the thesis. Thus, these results should be considered as preliminary estimates.

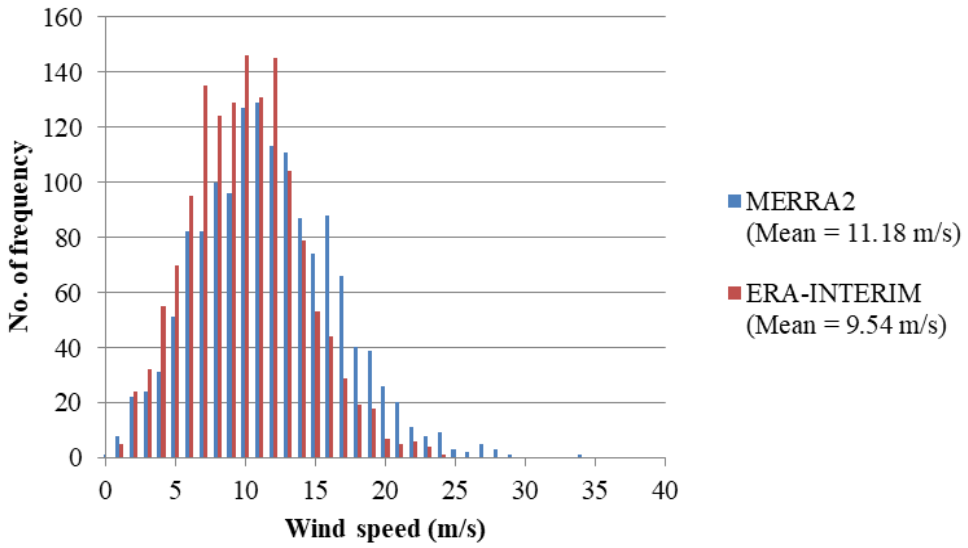

Figure 36 Wind distributions for MERRA2 and ERA-INTERIM dataset for year 2017

3.2.2 Energy ships and stationary wind turbines performances

As already mentioned, a preliminary design of an energy ship has been developed at LHEEA. It is an 80m long catamaran fitted with four (30m tall, 5m diameter) Flettner rotors [22]. The mode of operation of the energy ship at far offshore is described in Chapter 1.

The performance of the energy ship is characterized by polar plots for its speed and power production. Those plots relate the speed of the boat (U) or the produced power to the true wind speed (TWS) and true wind angle (TWA). They were obtained using an in-house velocity and power performance program (VPPP) [22]. The polar plots are shown in Figure 37. Five values for the true wind speed were considered ranging from 7.5 to 19.5 m/s. Note that the wind speed of the energy ship is at 10 m altitude.

The rated power of 1.6 MW for energy ship was chosen in order to allow a fair comparison to the 5MW wind turbine discussed in Chapter 2. Indeed, the 1.6 MW rated power is achieved for a true wind speed of 10.5 m/s at 10 m which corresponds to rated wind speed of 11.4 m/s at a nacell height of 90 m (which is a typical hub height for a floating offshore wind turbine).

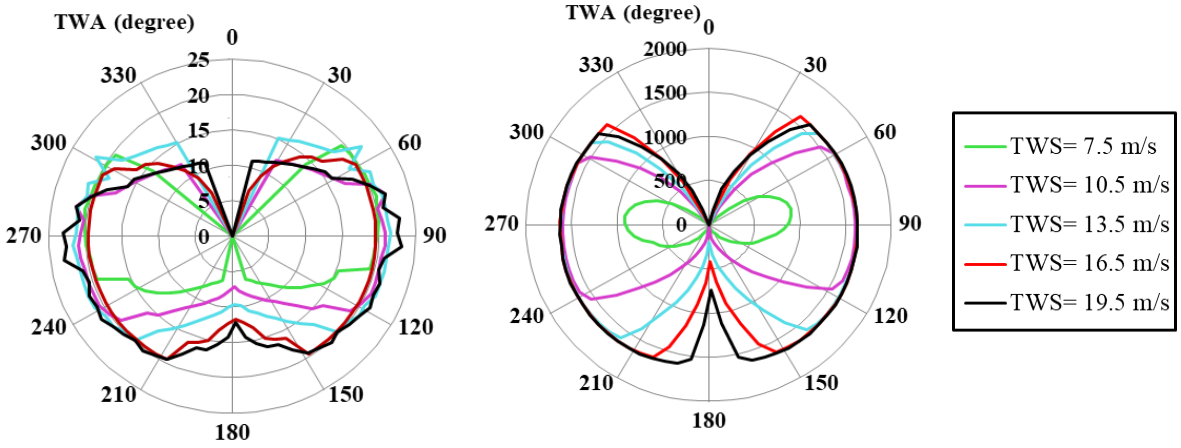

Figure 37 Polar plots for the boat velocity (left, in knots) and power production (right, in kW) for the energy ship of 1.6 MW rated power (Design #01); 5 different true wind speeds (TWS) are shown in both plots ranging from 7.5 m/s (innermost curve) to 19.5 m/s.

3.2.3 Optimization criterion

In the standard version of QtVlm, the optimization criterion is the travel duration from the starting point A to the arrival point B. In this study, the aim is to optimize the energy production. Therefore, a dedicated batch-mode version of QtVlm had to be developed in order to optimize the capacity factor over the route instead of the travel duration. The optimization algorithm defined for this version of QtVlm is shown in Figure 38.

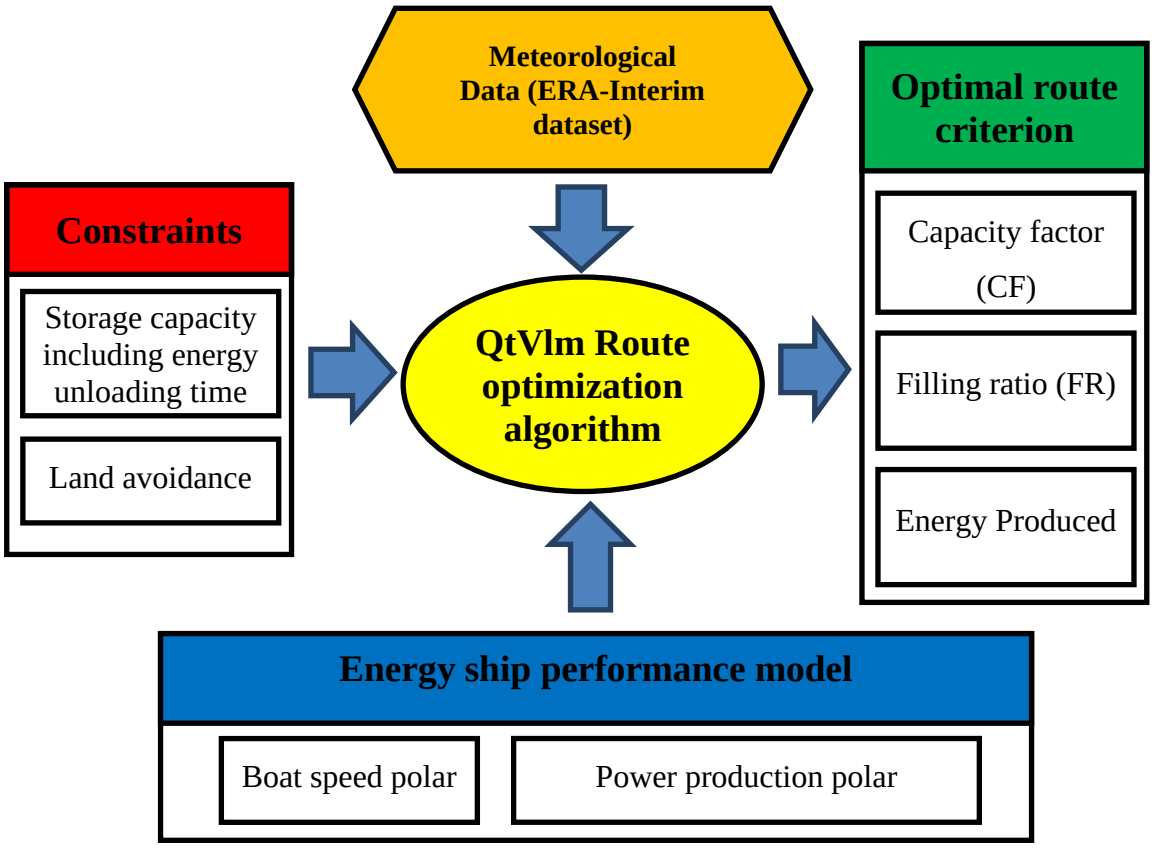

Figure 38 Overview of energy ship route optimization system using QtVlm

The new optimization criterion is defined by:

$$C_F = \frac{\int_0^T \tilde{P}(t)dt}{(T+T_0)P_{rated}} \quad \text{(Eq. 2)}$$

Where:

- C_F is the capacity factor
- T is the route duration
- T_0 is the duration of the loading/unloading operations of the stored energy
- $\tilde{P}$ is the power produced by the energy ship (MWh)
- P_{rated} is the rated power of the ship (MWh)

In the criterion, the duration T_0 at the denominator is to account for the time necessary to unload the stored energy. This parameter is particularly useful to avoid the optimization converge to very short routes.

An important constraint to take into account in the optimization process is the limited energy storage capacity aboard the ship. Thus, we introduced the filling ratio F that we define as the ratio of the energy stored in the energy reservoir $E = \int_0^T \tilde{P}(t)dt$ to the reservoir capacity, E_{max}. The reservoir capacity is N hours at rated power ($E_{max} = NP_{rated}$).

Thus, the filling ratio is:

$$F = \frac{\int_0^T \tilde{P}(t)dt}{NP_{rated}} \quad \text{(Eq. 3)}$$

To take into account the limited storage capacity, the produced power is set to 0 if the filling ratio reaches 1. If not, the produced power is obtained by interpolating in the power production polar plot (Figure 45) as function of the true wind speed and true wind angle at the ship location

($\tilde{P} = P(TWS, TWA)$) except during maneuvers. It is assumed that maneuvers (which correspond to events during which the axis of the ship crosses the axis of the wind) last for 15 minutes. During maneuvers, the produced power and ship velocity is reduced to 25% of the power and velocity in the polar plots.

Finally, the produced power $\tilde{P}$ is given by:

$$\tilde{P}(t) = \begin{cases} 0 \; if \; F \geq 1 \\ 0.25P(TWS, TWA) \text{ during maneuver} \\ P(TWS, TWA) \text{ otherwise} \end{cases} \quad \text{(Eq. 4)}$$

3.2.4 Optimization strategy

The optimization process requires the specifications of a starting point and an arrival point for the energy ship. It has been assumed that those points are one and the same point. This is because we assume that the energy ship meets at this location a platform or a tanker for unloading the stored energy. The mode of operations of the energy ship at far offshore was presented in chapter 1 (see Figure 11 and Figure 12).

The weather routing optimization in this chapter uses a batch-mode version of QtVlm which generates the optimized route automatically. Apart from the boat performance curves (polars of velocity and power production as function of true wind speed and true wind angle, storage capacity, unloading time), it depends on four numerical parameters:

- The search step angle (in degrees). It is used to initialize the first step of the simplex and to increase the search range. It is a distance where one minute latitude is equal to one NM. It has nothing to do with the boat position or boat heading. It represents how far away from a point of the route the simplex will initially look when optimizing the capacity factor over the route.
- The number of waypoints of the route. The locations of the waypoints are the optimization variables. They are optimized by QtVlm using the SIMPLEX algorithm in order to maximize the capacity factor (see Figure 35).
- The initial route direction: North, West, South or East.
- The initial Filling Ratio (FR).

QtVlm starts the optimization process by creating a draft route which starts and comes back to the one and same point. The heading is set such as the true wind angle is 90° and the ship goes in the initial route direction (North, West, South or East) set in the QtVlm configuration.

A first point is created in that direction at a distance equal to one-hour sailing. Next, the return trip is generated and the capacity factor and filling ratio at the time of arrival are calculated. If the filling ratio is less than the target initial filling ratio, QtVlm repeats the process, starting from the last point created, until the target initial filling ratio is reached. Then, all the waypoints are removed except the last one. Finally, waypoints are inserted regularly along the path to match the target number of waypoints parameter.

Last but not least, the draft route generated by this process is optimized using a SIMPLEX optimization algorithm as discussed in subsection 3.1.2.2. Figure 39 shows the example of the initially generated draft route (left) and the route after optimization (right). The draft route duration is 36.58 hours and the initial capacity factor is 59%. After the optimization, the route duration has reduced to 24.83 hours and the capacity factor has increased to 83%. The optimized data is saved in the route logbook and route comparator table. The data can be exported in .csv format.

The details of QtVlm setting and configurations are presented in Appendix 2.

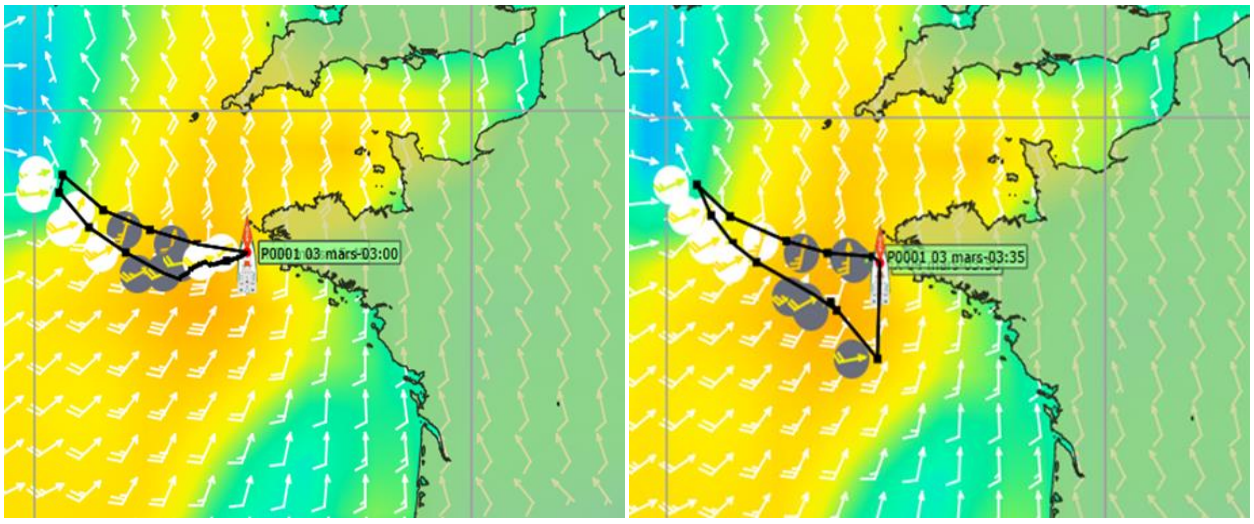

Figure 39 Example of the draft route initially generated (left) by QtVlm and the route after optimization (right).

3.3. Sensitivity analysis of the effect of the numerical parameters and initial filling ratio on the weather routing optimization results

The route optimization software QtVlm involves two main numerical parameters, the optimization search step angle and the number of initial optimization waypoints.

In this section, the effect of these parameters and initial filling ratio on the capacity factor is investigated. This sensitivity study was performed for the 1.6 MW rated power energy ship equipped with 168-hours storage capacity and 6-hours unloading time deployed in North Atlantic ocean in 2015. A small 10% initial filling ratio was selected to avoid long initial draft routes.

Table 10 Sensitivity to weather routing numerical optimization parameters for the energy ship deployed in the North Atlantic Ocean for 2015.

8° INITIAL SEARCH STEP ANGLE		**WAYPOINTS**					
		2	4	6	7	12	15
10% INITIAL FILLING RATIO	CAPACITY FACTOR (%)	73	78	78	80	80	80
	AVERAGED FILLING RATIO (%)	52	71	72	73	76	83
	SINGLE ROUTE DURATION (h)	114	147	150	147	153	169
	ENERGY PRODUCED (MWh)	10247.06	10874.22	10881.24	11168.75	11219.05	11218.52

Table 10 shows the optimization results for 6 values of the number of optimization waypoints and an 8° initial search step angle. One can see that the capacity factor increases with increasing number of waypoints. A capacity factor as high as 80% is achieved for 7 waypoints and more. As the simulation time increases with increasing number of waypoints, a combination of 8° initial search step angle and 7 waypoints was chosen as the optimal numerical parameters for the weather routing optimization of the energy ship in the far offshore.

3.4. Results and discussion

3.4.1 Optimized capacity factor of the energy ship

Let us first consider the case of an energy ship with starting point and destination at location N 54, 516660; W 27,551844. This point was selected because it is in the North Atlantic storm track (see Figure 40) which offers high density of wind resources [4][6][7].

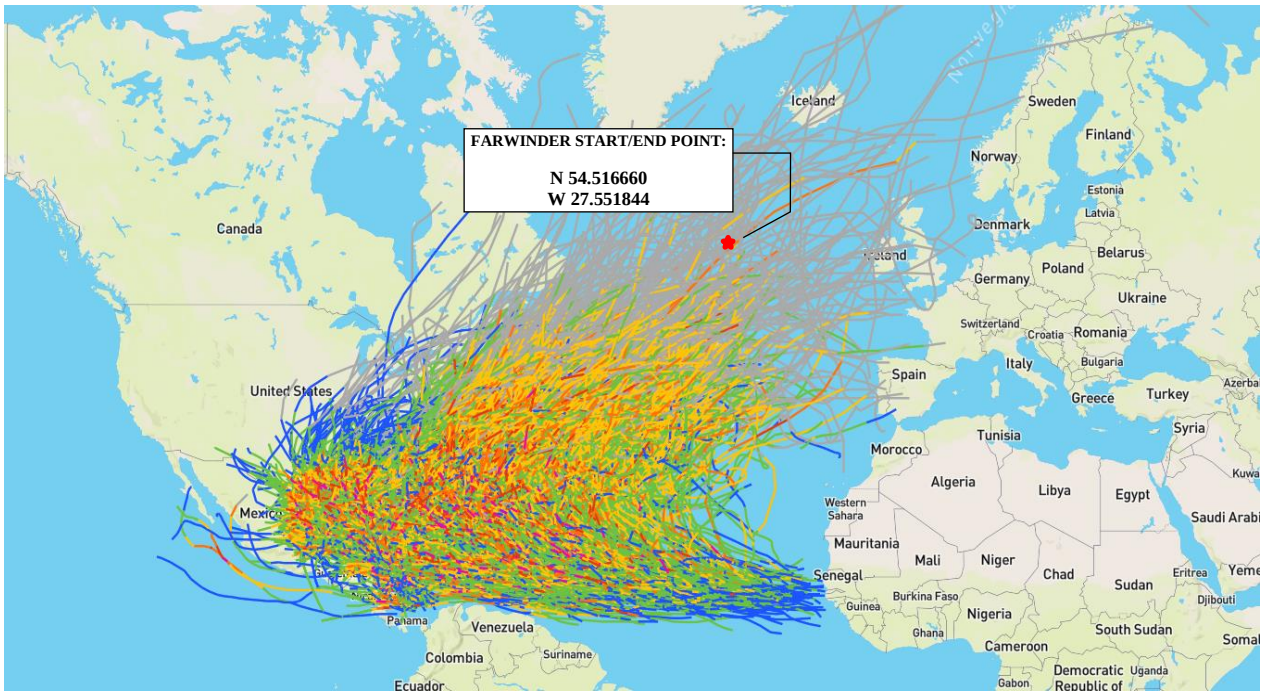

Figure 40 North Atlantic Ocean Historical Storm and Hurricane Tracks (Source: NOAA, https://coast.noaa.gov)

The optimization process was applied to calculate the optimized capacity factor over the three years of 2015, 2016 and 2017. The initial filling ratio was set to 10%. An 8° search step angle and 7 waypoints were selected for the optimization parameters. The storage capacity was set to 174-hour storage capacity (7 days). The unloading time was set to 6 hours.

The weather routing optimization results are shown in Table 11.

Table 11 Capacity factor of the 1.6MW energy ship equipped with 174-hour storage capacity and 6-hour unloading time and optimization parameter of 8° search steps angle and 7 initial waypoints

Year	-	2015	2016	2017
Annual average capacity factor	%	79	82	82
Best capacity factor over one route	%	99	99	97
Worst capacity factor over one route	%	40	44	39
Average route duration	Hour (s)	162	156	142
Longest route duration	Hour (s)	398.5	393.2	437.3
Shortest route duration	Hour (s)	22.5	22.9	38.6
Longest route distance	NM	3921.2	5010.4	5187.0
Shortest route distance	NM	460.8	470.3	752.8
Annual average filling ratio at the end of the routes	%	77	76	70

One can see that the annual average capacity factor is very high. It consistently exceeds 80% for the three years. The average over the three years is 81% and it reaches 82% for the best the year of 2016 and 2017.

The best capacity factor achieved over one route is 99% for both year 2015 and 2016; and 97% for year 2017, which means that route optimization enabled the energy ship to sail in highly favorable conditions over the whole duration of the route. Nevertheless, the worst capacity factor over the three years is quite high (41%). This shows that despite the wind resource is very high in average, there happens to be some time when the wind is low.

Figure 41 shows the seasonal variability of the average capacity factor. One can see that the lowest monthly average capacity factors are achieved during the month of May to August. Nevertheless, despite the low wind, the worst average capacity factor is still relatively high.

The average filling ratio over the three years is moderately high, 74% and the average route duration is 153 hours (approximately 6 days). However, these results need to be confirmed by running sensitivity studies for the effect of storage capacity on the capacity factor and route duration.

For comparison, the average capacity factor over years 2015, 2016 and 2017 of a stationary floating offshore wind turbine which would be deployed at the same location was performed. It is found to be also very high (over 80%).

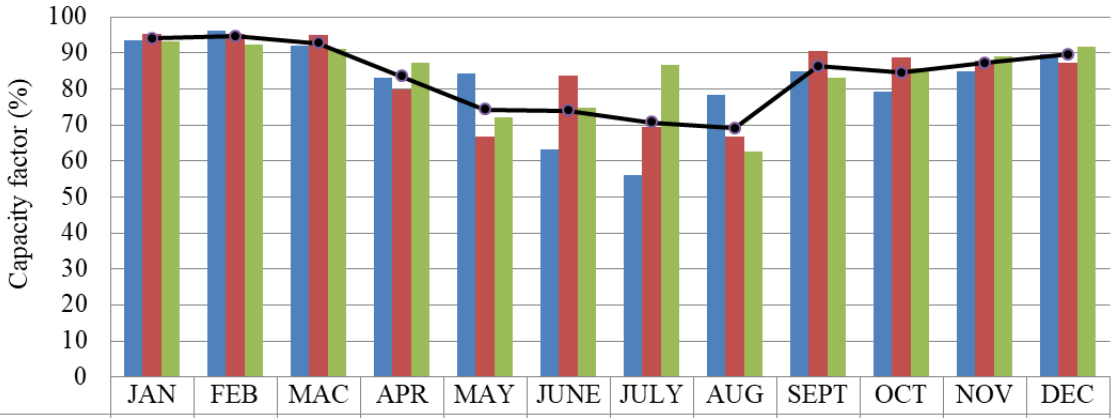

	JAN	FEB	MAC	APR	MAY	JUNE	JULY	AUG	SEPT	OCT	NOV	DEC
2015	94	96	92	83	84	63	56	78	85	79	85	90
2016	95	95	95	80	67	84	69	67	91	89	88	87
2017	93	92	91	87	72	75	87	63	83	86	89	92
AVERAGE	94	95	93	83	74	74	71	69	86	85	87	90

Figure 41 Monthly average capacity factor and three years average for 1.6 MW energy ship equipped with 174-hour storage capacity and 6-hour unloading deployed at North Atlantic ocean

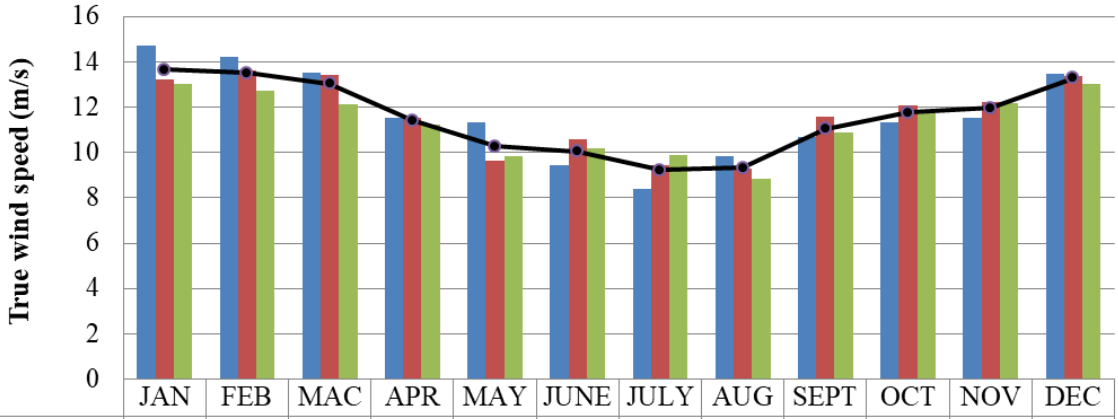

	JAN	FEB	MAC	APR	MAY	JUNE	JULY	AUG	SEPT	OCT	NOV	DEC
2015	15	14	14	12	11	9	8	10	11	11	12	13
2016	13	14	13	12	10	11	9	9	12	12	12	13
2017	13	13	12	11	10	10	10	9	11	12	12	13
AVERAGE	14	14	13	11	10	10	9	9	11	12	12	13

Figure 42 Monthly average true wind speed (TWS) at North Atlantic ocean for 2015 (blue), 2016 (red) and 2017 (green)

Figure 42 shows the monthly average true wind speed at the location within North Atlantic ocean passed by the energy ship. Overall, the annual averages of true wind speed were 12 m/s for

year 2015 and 2016, and 11 m/s for 2017. One can see that the wind is the lowest from May till August, which explains the lower capacity factors during those months.

Figure 43 also shows the distribution of capacity factor as function of the delivery time for each route in 2015, 2016 and 2017. It can be observed that during the months with low wind, the route duration increases.

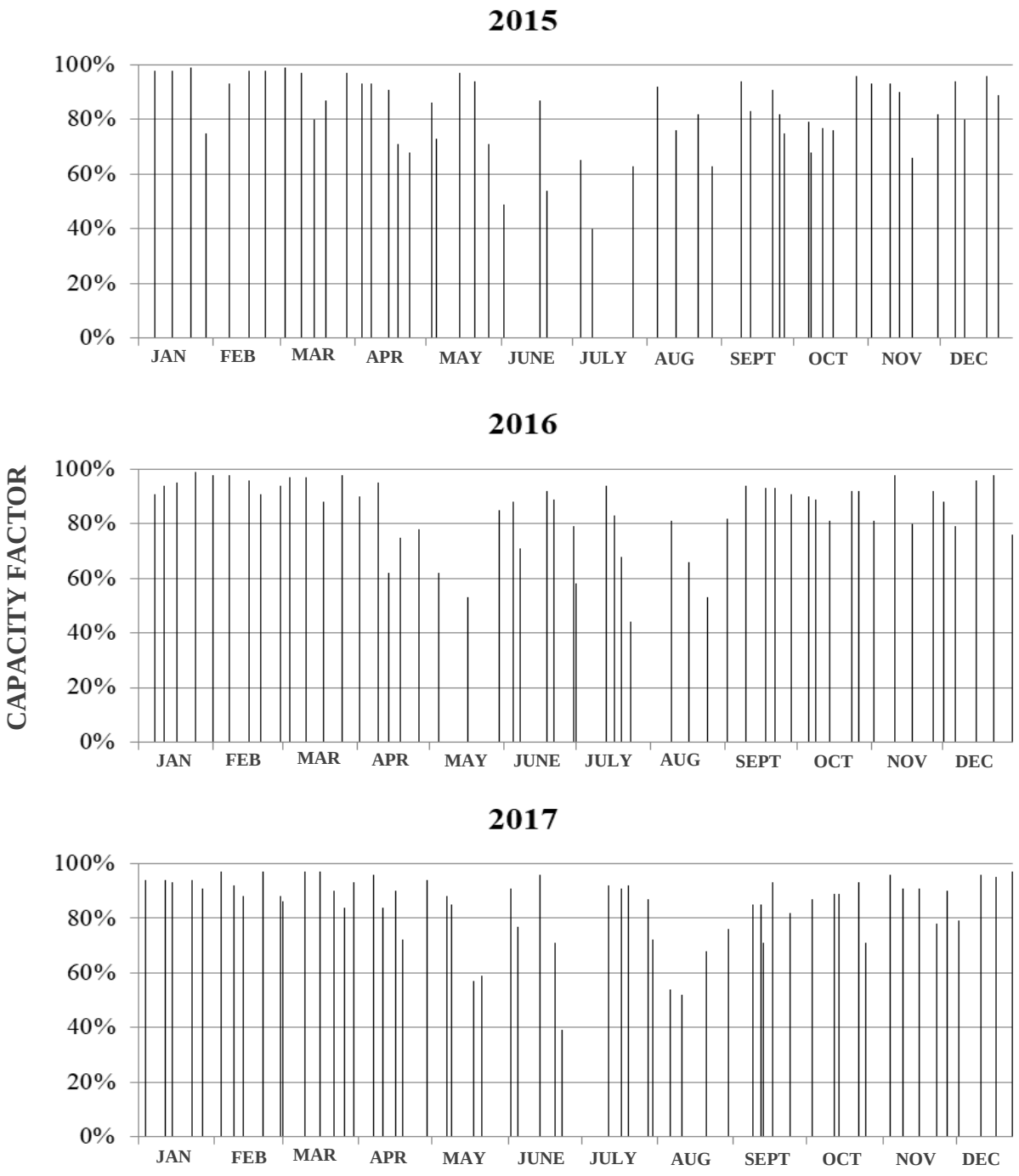

Figure 43 Capacity factor at the end of each route plotted as function of the delivery time

3.4.2 Sensitivity to storage duration and unloading time

In this section, the sensitivity of the capacity factor to storage capacity and unloading time is investigated.

According to Eq. 4, the maximum capacity factor is:

$$CF_{max} = \frac{N}{N+T_0} \quad \text{(Eq. 5)}$$

Where we recall that N is the storage capacity (in hours at rated power) and T_0 is the unloading time (in hours). For 7 days storage capacity (174 hours) and 6 hours unloading time, the maximum capacity factor is 96.7%.

Three configurations of storage capacity and unloading time have been considered:

- 3.5- days (87-hours) storage capacity and 3-hour unloading time,
- 7-days (174-hours) storage capacity and 6-hour unloading time,
- 14-days (339-hours) storage capacity and 12-hour unloading time

The unloading time was set proportional to the storage capacity in order to keep the same maximum capacity factor for all the configurations.

Table 12 shows the capacity factor, filling ratio and the annual energy production production for the years 2015, 2016 and 2017; and for the three years average for each configuration.

Capacity factors are in the range 75 to 81%. The best average capacity factor is obtained by the energy ship equipped with 174hours storage capacity (81.2%). The worst capacity factor is obtained for the energy ship with the greatest storage capacity (339 h). This result is unexpected as one could expect that the greatest capacity factor would have been obtained for the energy ship with the greatest storage capacity. It can be explained by the fact that the optimization method in qtVlm may not always converge to the global optimum.

Table 12 Capacity factor, filling ratio and energy production for 1.6 MW energy ship equipped with 3 configurations of storage capacity and unloading time in North Atlantic ocean for 3 years (2015, 2016 & 2017)

		NORTH ATLANTIC OCEAN					
		1.6 MW					
		Capacity factor (CF) (%)		Filling ratio (FR) (%)		Energy Produced (MWh)	
		8°; 7 WPs	Average over 3 years	8°; 7 WPs	Average over 3 years	8°; 7 WPs	Average over 3 years
87h storage capacity / 3h unload time	2015	78.72	80.73	83.22	82.59	11005.05	11297.56
	2016	81.81		84.10		11468.89	
	2017	81.67		80.43		11418.72	
174h storage capacity / 6h unload time	2015	79.48	81.19	76.78	74.37	11115.88	11362.90
	2016	81.97		76.41		11492.27	
	2017	82.11		69.93		11480.54	
339h storage capacity / 12h unload time	2015	74.51	76.48	60.09	53.91	10427.42	10713.43
	2016	79.62		54.20		11172.39	
	2017	75.32		47.43		10540.49	

3.4.3 Sensitivity to energy ship rated power

In this section, the effect of rated power on the capacity factor is investigated. It is expected that the capacity factor will increase with decreasing rated power, and vice-versa. Note that total energy production is expected to decrease with decreasing rated power.

Three rated powers were considered: 1 MW, 1.3 MW and 1.6 MW. The same velocity polar was used for the three configurations. The power production polar of configurations with rated power below 1 MW and 1.3 MW were derived from the polar of the 1.6 MW energy ship (Figure 37) by limiting the output power to the rated power (see Figure 44). In fact, in this study, the derivation of power production for 1 MW and 1.3 MW is the simplified way and considered as a conservative estimate to assess the effect on capacity factor for the energy ship. Thus, an individual derivation of boat performance for 1 MW and 1.3 MW using VPPP must be done in future.

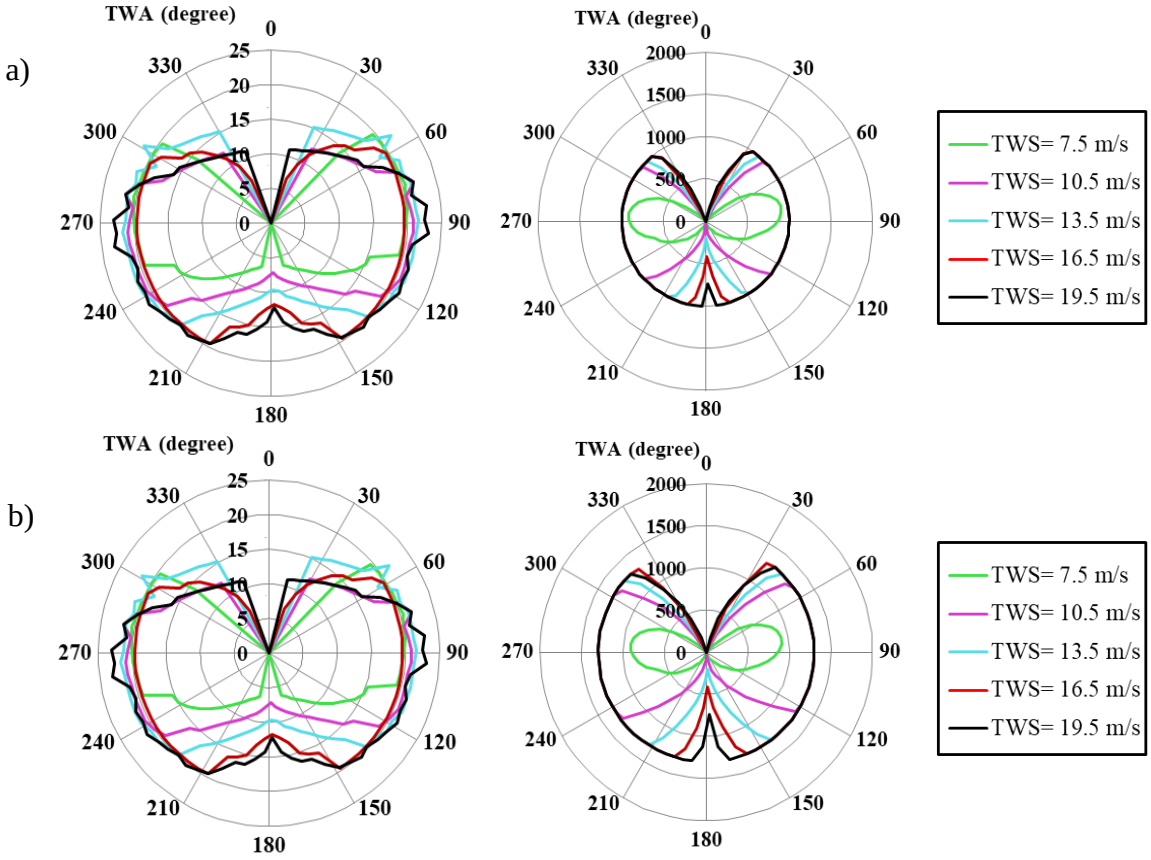

Figure 44 Polar plots of the speed (left, in knots) and power production (right, in kW) of a) 1MW and b) 1.3MW energy ship as function of the true wind direction (0-360°) and true wind speeds (TWS) ranging from 19.5 m/s (outer curve), 16.5 m/s, 13.5 m/s, 10.5 m/s and 7.5 m/s (innermost curve).

The initial optimization waypoints were set to 7 and the search steps angle was set to 8°. The storage capacity and unloading time of the energy ship was fixed to respectively 174 hours and 6 hours as it was shown in the previous section that it gives the best results. The resulting 3 years capacity factor, filling ratio and energy production are presented in Table 13.

As expected, the capacity factor increases with decreasing rated power. The greatest average capacity factor (84.3%) is obtained by the 1 MW energy ship. The 1.3 MW energy ship achieves a capacity factor of 81.3% which is only 0.1% greater than the 1.6 MW energy ship.

The greater capacity factor of the smaller rated power configurations comes at the cost of a significant reduction in annual energy production. Indeed, the energy production of the 1 MW energy ship is 35% smaller than that of the 1.6 MW energy ship, whereas its capacity factor is only

3.7% greater. Therefore, regarding the cost of energy, it is unlikely that the benefit of the greater capacity factor of the 1 MW energy ship outweighs the loss in revenues due to smaller energy production. This is even more the case for the 1.3 MW energy ship as it has almost the same capacity factor as the 1.6 MW energy ship but 20% less energy production. Those results indicate that an energy ship with 1.9 MW or even greater rated power may actually lead to better economic performance.

Table 13 Capacity factor, filling ratio and energy production for 1 MW, 1.3 MW and 1.6 MW energy ship in North Atlantic ocean for 3 years (2015, 2016 & 2017)

				NORTH ATLANTIC OCEAN					
				1MW		1.3MW		1.6MW	
				8°; 7 WPs	Average over 3 years	8°; 7 WPs	Average over 3 years	8°; 7 WPs	Average over 3 years
174-hour storage capacity / 6-hour unloading time	Capacity factor (CF)	%	2015	82.70	84.34	78.35	81.29	79.48	81.19
			2016	85.59		82.93		81.97	
			2017	84.72		82.60		82.11	
	Filling ratio (FR)	%	2015	81.40	79.48	80.24	76.84	76.78	74.37
			2016	79.67		78.69		76.41	
			2017	77.37		71.60		69.93	
	Energy Production	MWh	2015	7227.39	7372.84	8901.7241	9239.09	11115.88	11362.90
			2016	7486.53		9430.3331		11492.27	
			2017	7404.61		9385.2152		11480.54	
	Annual routes options	-	2015	51	53	49	53	52	55
			2016	54		53		54	
			2017	55		58		59	
	Average single route duration exclude unloading time	h	2015	165	158	172	159	162	153
			2016	156		159		156	
			2017	153		145		142	
	Total annual route duration including unloading time	h	2015	8739.48	8742.21	8739.83	8742.53	8741.17	8747.58
			2016	8746.81		8747.10		8762.57	
			2017	8740.33		8740.66		8739.01	

3.4.4 Sensitivity to polars

In this section, a sensitivity analysis to changes in the energy ship velocity polar is presented. In this respect, two different designs of a 1 MW energy ship are considered. Their characteristics are summarized in Table 14. The architecture and boat performance has been published in other study. Details can be found in [21][22].

Table 14 Ship characteristics of two different designs of the energy ship.

		Design # 01 (1MW)	Design # 02 (1MW)
	Unit	Value	
Hull			
Length	m	80	80
Breadth	m	31.7	12
Displacement	t	660	123
Wind propulsion			
Type	–	Flettner rotors	
Number	–	4	4
Rotor height	m	30	27
Rotor diameter	m	5	4
Rotor mass	t	59	9
Rotor rated power	kW	110	38
Water turbine			
Area	m2	12.57	3.14
Rotor diameter	m	4	2
Rotor-to-electricity efficiency (η3)	–	80%	70%

Figure 45 shows the polars of the two considered energy ships. For Design #01, the 1 MW power production polar was derived from the 1.6 MW power production polar (see Figure 37) in order to allow a fair comparison between both designs.

One can see that the shape of the velocity and power production polar between both designs is significantly different. Both velocity polars look like butterfly curves, but the opening angle of the polar of Design #02 is smaller than that of Design #01. Design #02 also has the greatest boat velocity when sailing upwind, whereas the velocity polar of Design #01 looks more like general cardioids curves.

For both Design #01 and Design #02, the rated power produced is achieved at a 10.5 m/s true wind speed. However, one can see that the rated power is achieved for a wider range of true wind angles for Design #02 than for Design #01.

The optimized capacity factor was investigated for both designs. The storage capacity was fixed to 174-hour (7 days). A 6-hour unloading time was also used and the numerical optimization parameters were set to 8° search step angle with 7 initial number of waypoints. As in the other weather routing optimizations, the initial filling ratio was set to 10%.

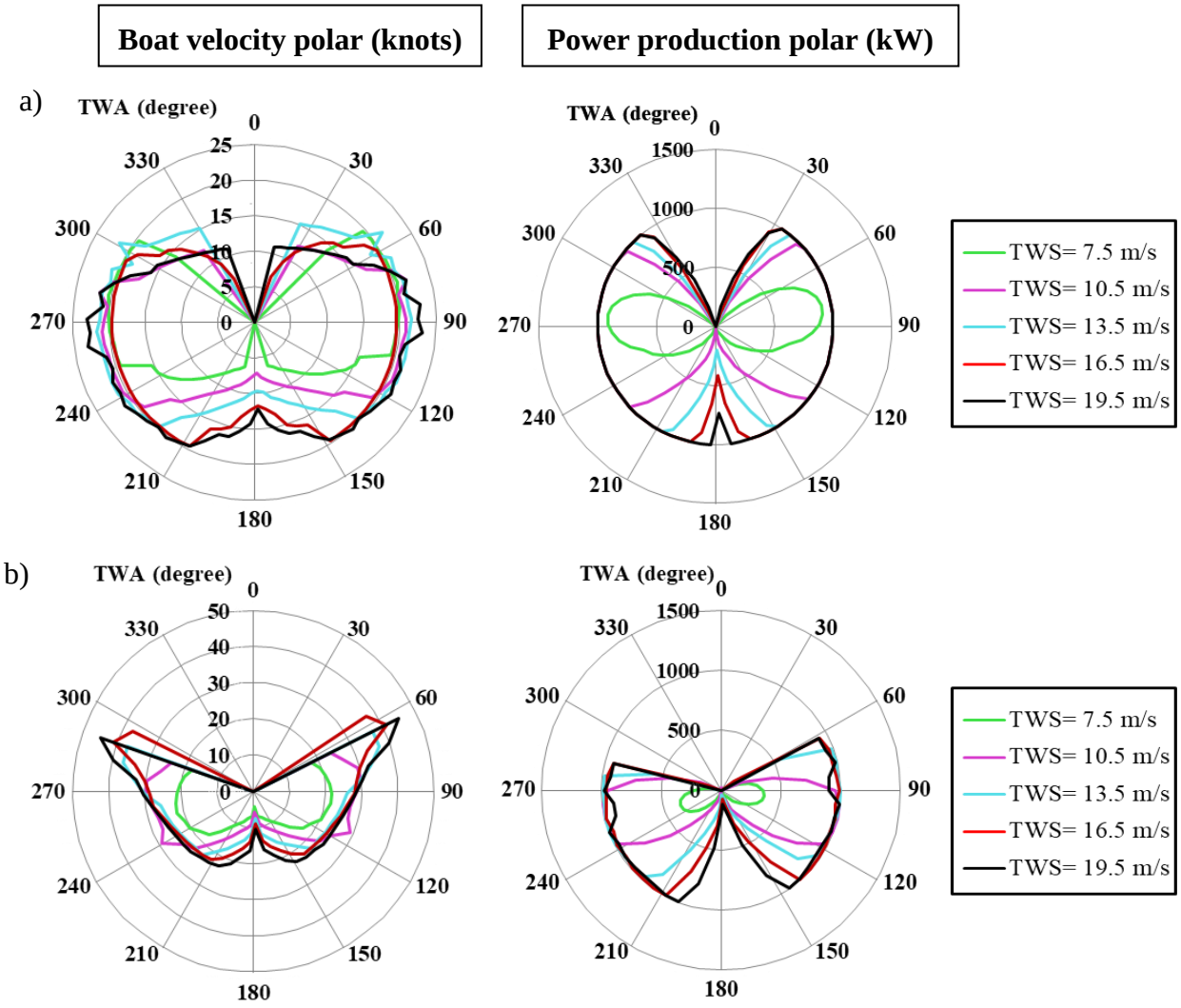

Figure 45 Polar plots for the velocity (left, in knots) and power production (right, in kW) of proposed 1MW energy ship derived from a) Design #01 [21]for true wind speed of 7.5, 10.5, 13.5, 16.5, and 19.5 m/s (most outer curves)

Table 15 Comparison of optimized capacity factor, filling ratio and total energy produced for 1MW deployed at far offshore for 2 different boat performance polars.

			Design #01		Design #02	
			8°; 7 WPs	Average over 3 years	8°; 7 WPs	Average over 3 years
1MW equipped with 174-hour storage capacity / 6-hour unloading time	Capacity factor (CF) (%)	2015	82.70	84.34	70.95	71.53
		2016	85.59		71.50	
		2017	84.72		72.13	
	Filling ratio (FR) (%)	2015	81.40	79.48	64.88	64.69
		2016	79.67		66.69	
		2017	77.37		62.50	
	Energy Production (MWh)	2015	7227.39	7372.84	6202.30	6257.27
		2016	7486.53		6266.64	
		2017	7404.61		6302.87	

Table 15 shows the results. In average, the annual energy production and capacity factor of Design #01 are 18% greater than that of Design #02. This confirms that the shape of the velocity and power polars have a significant impact on energy performance of energy ships.

3.5. Conclusion

In this chapter, we investigated the capacity factor of energy ships that would be deployed far-offshore in the North Atlantic Ocean. It is optimized using weather-routing. We found that energy ships can achieve capacity factors exceeding 80%, which is similar to that of a 5MW stationary offshore wind turbine which would be deployed in the same area.

Sensitivity studies were also performed. It is found that storage capacity and velocity and power polars of the ship have a significant effect on the energy performance.

CHAPTER 4

INVESTIGATION OF THE CAPACITY FACTOR OF WEATHER-ROUTED ENERGY SHIPS DEPLOYED IN THE NEAR-SHORE

In this chapter, we explore the capacity factor of weather-routed energy ships deployed nearshore and with batteries energy storage. Two case studies are considered: the island of Ile de Sein and the archipelago of Saint-Pierre-et-Miquelon.

Results show that weather routed optimization for 1.6 MW energy ship at nearshore can achieve an average capacity factor of 43% at Saint-Pierre-et-Miquelon and 39% at Ile de Sein for the three years of 2015, 2016 and 2017. Such capacity factors are similar to that of currently operating offshore wind farms.

This chapter also investigates the sensitivity of the optimization results on the numerical optimization parameters (number of initial optimization waypoints and search step angle).

4.1. Description of the case studies

4.1.1. Ile de Sein island and Saint-Pierre-et-Miquelon archipelago

Figure 46 shows the locations of Ile de Sein and Saint-Pierre-et-Miquelon. Their population is respectively 249 and 6,057 inhabitants [89][90]. Accordingly, their energy needs are limited. The installed power generation capacity at Ile de Sein is 900 kW. That of Saint-Pierre-et-Miquelon is 25 MW.

At present, power supply for these islands is based on fossil fuels (diesel generation), which is an issue because of GHG emissions (over 700 gCO2/kWh). Moreover, as the fuel is imported and as the size of the power plants are relatively small, the electricity generation cost is very high (of the. order of 509 €/MWh at Saint-Pierre-et-Miquelon according to the Commission de Régulation de l'Energie (CRE, French Energy Regulation Authority))[90].

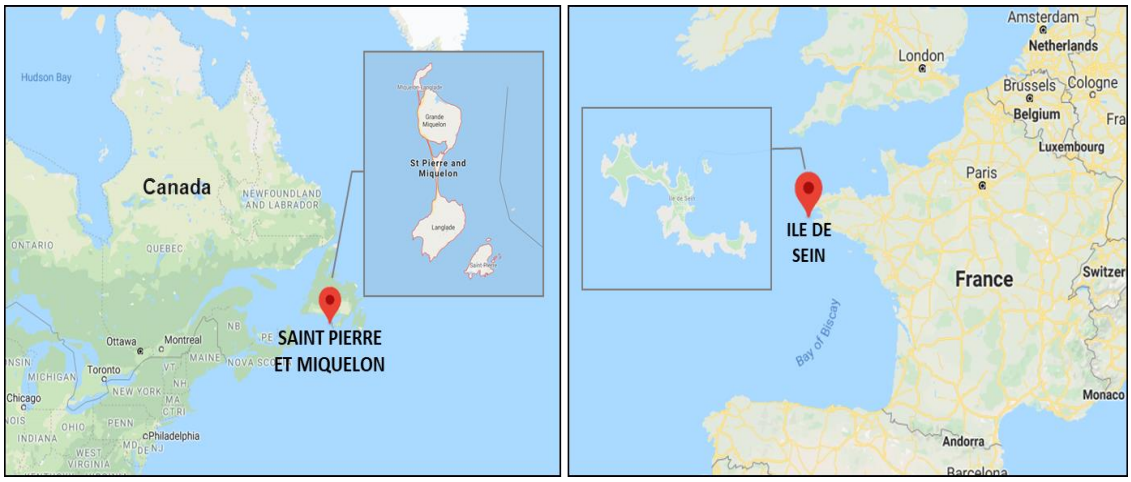

Figure 46 Locations of the Saint-Pierre-et-Miquelon and Ile de Sein Island
(Source : Google Maps)

Energy ships could represent a relevant alternative for the power supply of these islands. In this scenario, the produced energy would be stored in batteries. The mode of operation of the energy ship at near shore has been described in Chapter 1. In summary, the island grids would be powered by virtual power plants consisting in several batteries containers. The plants would be located in porst. Once a battery container stationed at the port would be empty, it would be loaded aboard an energy ship which would then set sail and start a charging cycle (see Figure 12).

The trajectory of the charging cycle is optimized using weather-routing in order to charge the batteries as fast as possible. Once the batteries would be charged, the energy ship would come back to the port, unload the filled batteries containers, load empty batteries containers, and start again a new charging cycle.

4.1.2. Energy ship characteristics

As explained in chapter 3, the energy ship is modelled in QtVlm through its polar curves of velocity and power production. Three versions of the ship have been considered: one with 1 MW rated power, a second one with 1.3 MW rated power and a third one with 1.6 MW rated power. Their velocity and power production polar curves are shown in Figure 37 and Figure 44 (in Chapter 3).

In comparison to hydrogen or methanol storage [21][22], batteries have better round-trip efficiency, but their energy density is an order of magnitude smaller (approximately 2 kWh/kg for

hydrogen storage vs 0.1 kWh/kg for battery storage). Therefore, in this chapter, only 12 to 48 hours of energy storage capacity have been considered.

4.1.3. Wind data

The same three years (2015, 2016, and 2017) global data of 10 m altitude wind speeds as in Chapter 3 is considered. The data being global, it covers the surrounding of the two considered islands: Saint-Pierre-et-Miquelon (SPM) and Ile de Sein (IDS).

4.1.4. Optimization method and strategy

The weather routing optimization is performed using the QtVlm software as presented and discussed in Chapter 3.

4.1.5. Statistical analysis data and method for energy production, sailed distance, boat speed and true wind angle (TWA) distribution

As the optimized trajectories of the energy ship appear to be complex and diverse. At first look, no typical pattern can be identified. Therefore, a statistical analysis has been implemented in order to determine whether there exist relationships patterns and trends in the data.

Thus, the statistical analysis was performed using the weather routing optimization results for the 1.6 MW rated power energy ship. The boat speed and power production polar diagram is shown in Figure 37. Four configurations of energy storage and unloading time (6-hour storage capacity and 1-hour unloading time, 12-hour storage capacity and 2-hour unloading time, 24-hour storage capacity and 4-hours unloading time, 48-hour storage capacity and 8-hour unloading time), and two deployment locations (Saint-Pierre-et-Miquelon and Ile de Sein) were considered.

Based on the optimization results of qtVlm, two datasets were generated and analyzed. For each energy storage configuration and deployment location, Dataset 1 corresponds to a table of energy production, sailed duration and sailed distance at the end of each route travelled by the energy ship. It covers the three years of 2015, 2016 and 2017. It typically includes the number of data points depends on the size of the storage capacity as follows (see Table 16):

Table 16 Three-year average number of data points for two deployment locations available in Dataset 1

	6-hour storage capacity and 1-hour unloading time	12-hour storage capacity and 2-hour unloading time	24-hour storage capacity and 4-hours unloading time	48-hour storage capacity and 8-hour unloading time
Saint-Pierre-et-Miquelon	828	410	207	102
Ile de Sein	728	374	187	99

Dataset 2 is more precise and extensive as it corresponds to data with a time sample of 5 minutes. It was obtained by gathering the raw data produced by QtVlm for each route of the year 2017, both for Saint-Pierre-et-Miquelon and Ile de Sein. In addition to power production at each time step includes the true wind speed, true wind angle, and boat speed. It contains 89,634 number of data points for Saint-Pierre-et-Miquelon and 90,185 number of data points for Ile de Sein.

The frequency distribution produced in this analysis is the relative frequency distribution. The data in Dataset 1 were calculated for individual class intervals by dividing them by the average observed frequencies or data points. Each storage capacity has a different number of data points for each of 2015, 2016 and 2017. Thus, the average observed data points were used as a baseline. Then the relative frequencies were visualized into a Histogram (for energy production distribution) and line graph (for the sailed distance over maximum distance). The frequencies were written in percentage (%).

Meanwhile, the frequency distribution for true wind angle (TWA) using Dataset 2 was produced using the joint frequency distribution. This method was used to analyze several occurrences simultaneously at each possible joint occurrence of two variables (energy ship power production and true wind angle). The contour diagram was produced to visualize the joint frequency distribution. All data calculations and diagrams were produced using Microsoft Excel software.

4.2. Sensitivity analysis of the effect of the numerical parameters on the weather routing optimization results

It is recalled that the route optimization software QtVlm involves two main numerical parameters:

a) The optimization search step angle: used as a first distance to initialize the first step of the simplex and to increase the search range
b) The number of initial optimization waypoints: the points to be created by QtVlm in the optimization process to calculate and optimize the capacity factor based on the set filling ratio target.
c) In this section, the effect of these parameters on the capacity factor is investigated. The aim is to determine which parameters give the best results.

This sensitivity study was performed for the 1.6 MW rated power energy ship. Deployments in Saint-Pierre-et-Miquelon and Ile de Sein were both considered. The search step angles which were considered are: 0.5°, 1°, 2°, 4°, 6° or 8°. The number of initial optimization waypoints that were considered are: 2, 4, 6, 12 and 18 waypoints.

In this numerical parameter optimization, the default setting for the energy ship's storage capacity is 24 hours. The unloading time was set to 4 hours.

At the beginning of the sensitivity analysis, the analysis was started with 0.5° search step angle and 12 waypoints as the reference configuration. Then, the value of the search step angle was doubled up to 64°. The effect of the number of waypoints was also studies separately.

4.2.1. Saint-Pierre-et-Miquelon case study

Figure 47 shows the average capacity factor for the three years (2015, 2016 & 2017) as function of the search step angle and the initial number of waypoints at Saint-Pierre-et-Miquelon.

Results show that the capacity factor depends significantly on the numerical parameters. Overall, the capacity factor appears to decrease with increasing number of initial optimization waypoints. This is unexpected as the optimization waypoints correspond to the variables of the optimization problem. It was thus expected that a greater number of optimization waypoints would allow more flexibility in the route, thus greater capacity factors. It indicates that the current

optimization method (initialization procedure + simplex) in QtVlm is not able to find the global maximum.

The other parameter of the optimization is the search step angle. For this parameter, Figure 47 shows that an 8° search step angle is optimal.

4.2.2. Ile de Sein case study

Figure 48 leads to the same conclusion for Ile de Sein as for Saint-Pierre-et-Miquelon. The capacity factor also decreases with increasing number of initial optimization waypoints. As for the Saint-Pierre-et-Miquelon case study, the greatest average capacity factor is obtained for 2 initial optimization waypoints. However, in this case study the optimal search step angle is 6° whereas it is 8° for Saint-Pierre-et-Miquelon.

In chapter 3, it was found that the optimal parameters for far offshore deployment are 8° search step angle and 7 waypoints. Therefore, it appears that the optimal numerical parameter depends on the deployment locations.

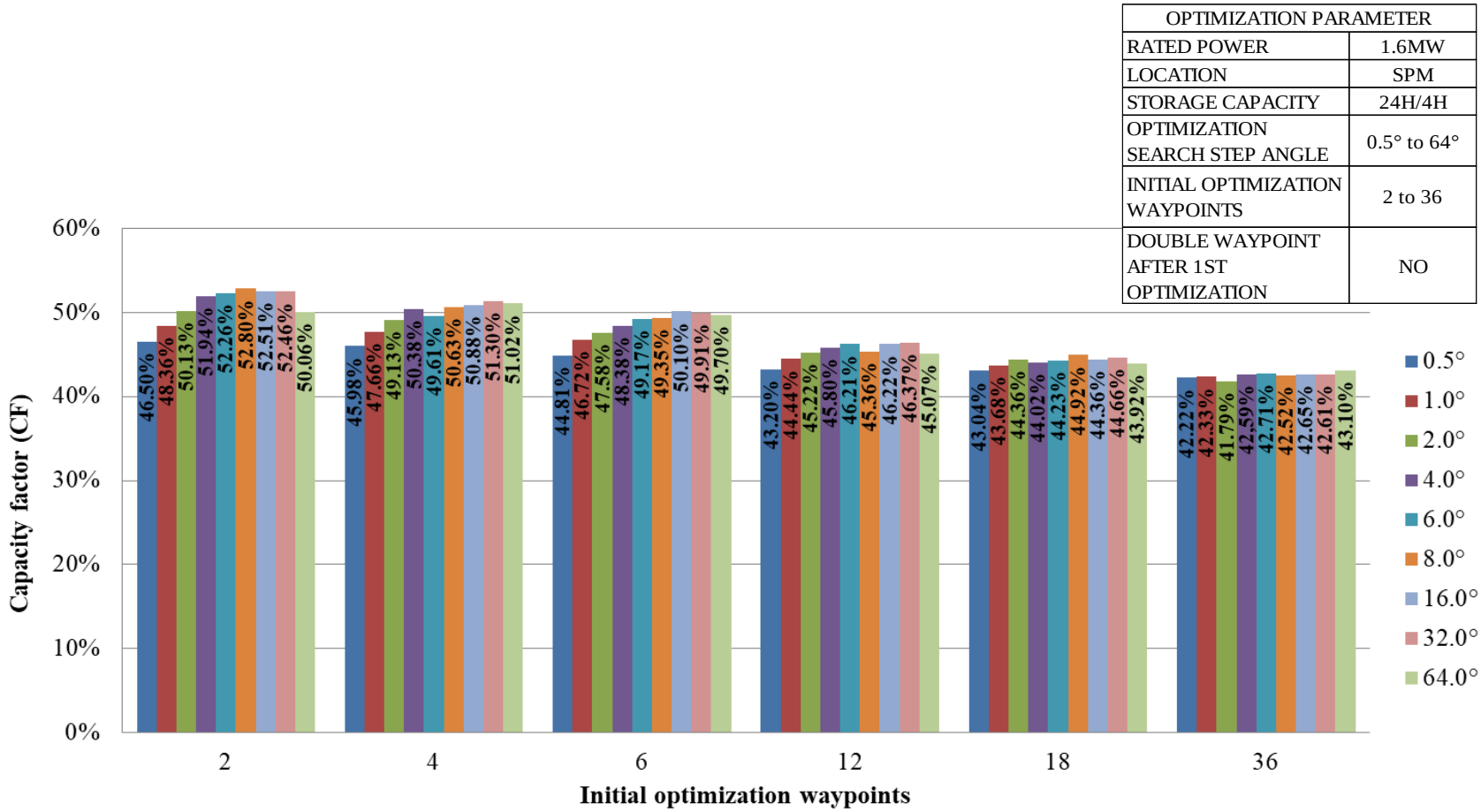

Figure 47 Sensitivity study on weather routing optimization criteria. The results of the 6 clustered initial optimization waypoints and 9 clustered optimization search steps angle for 1.6 MW energy ship in Saint-Pierre-et-Miquelon (average of 2015, 2016 & 2017) are presented. These results influence by 6 different initial waypoints of optimization that are set to 2, 4, 6, 12, 18 and 36; and 9 different optimization search steps.

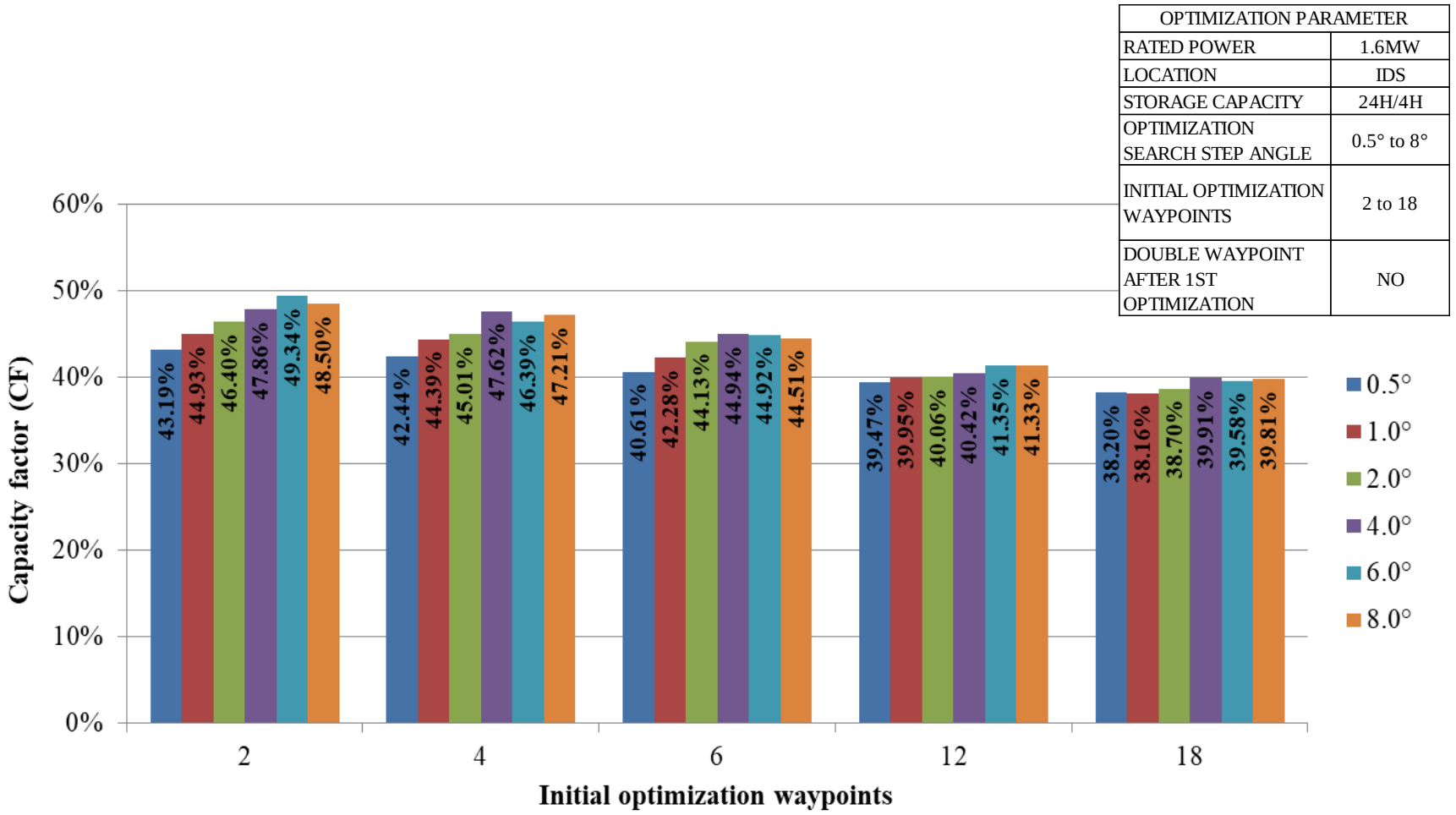

Figure 48 Sensitivity on weather routing numerical optimization criteria. The results of the 5 clustered initial optimization waypoints and 6 clustered optimization search steps angle for 1.6 MW energy ship in Ile de Sein (average of 2015, 2016 & 2017) are presented. These results influence by 5 different initial waypoints of optimization that are set to 2, 4, 6, 12, and 18; and 6 different initial optimization search steps.

4.2.3. Sensitivity to the doubling of waypoints after the first optimization

In QtVlm, there is a possibility to double the number of waypoints after the first optimization. This means that, at the end of the first optimization, the number of initial optimization waypoints is doubled and that the optimization algorithm is re-run including the new waypoints.

A sensitivity analysis to this capability has been performed. The test case is the 1.6 MW energy ship with 24-hour storage capacity and 4-hour unloading time. The search step angle was set to 8° and the initial number of waypoints to 4. Indeed, even though a total of 2 initial waypoints was found to be the best setting in the previous section, it has been found to be too small in practice for the purpose of this analysis.

Table 17 shows the results of the optimized capacity factor of a 1.6 MW energy ship deployed at Saint-Pierre-et-Miquelon and Ile de Sein for the year 2015, 2016 and 2017 and the average optimized capacity factor for those three years. For Saint-Pierre-et-Miquelon (respectively Ile de Sein), doubling the number of waypoints increases the capacity factor from 53% to 55% (respectively 48% to 50%). It represents an increment of 3.6% (respectively 4%). Furthermore, the average for a single route duration remains the same. Therefore, the difference is small. Since using this option increases significantly the simulation time, it was not activated for the remaining of this study.

Table 17 Comparison of optimized capacity factor (CF), filling ration (FR), and route duration with and without using the option to double the number of waypoints after the first optimization

		1.6MW (Saint-Pierre-et-Miquelon) 24h storage capacity / 4h unload; 8° / 4WP (Starting time 03:00:00)			1.6MW (Ile de Sein) 24h storage capacity / 4h unload; 8° / WP (Starting time 03:00:00)		
		FR	CF	Average single route duration (h)	FR	CF	Average single route duration (h)
Without doubling the number of waypoints after the first optimization	2015	92%	52%	38	95%	51%	41
	2016	93%	52%	39	94%	45%	46
	2017	93%	54%	37	95%	50%	42
	Average	93%	53%	38	94%	48%	43
With the doubling of the number of waypoints after the first optimization	2015	95%	55%	38	96%	55%	38
	2016	95%	54%	38	96%	46%	46
	2017	95%	55%	38	98%	50%	42
	Average	95%	55%	38	97%	50%	42

4.3. Capacity factor of energy ships deployed at Saint-Pierre-et-Miquelon

In this section, the capacity factor of energy ships deployed at Saint-Pierre-et-Miquelon is investigated. The optimization parameters are set to two initial optimization waypoints and 8° search step angle as they give the best results according to Figure 47.

Table 18 shows the capacity factor over the three years of 2015, 2016 and 2017. The annual average capacity factor consistently exceeds 52% for the three years. The best annual capacity factor is obtained in 2017, 54%. Overall, the annual variability of the capacity factor appears to be limited (1 to 2%).

The average filling ratio is very high, 92.8%. The best capacity factor achieved over one route is 87% for each year. It corresponds to the maximum capacity factor which can be achieved taken into account the unloading time. The worst capacity factor is 11%.

Table 18 Results for the optimization of the capacity factor of the 1.6 MW energy ship in Saint-Pierre-et-Miquelon; equipped with 24 hours storage capacity and 4 hours unloading time and optimization parameter of 8° search steps angle and 2 initial waypoints

Year	-	2015	2016	2017
Annual average capacity factor	%	52	52	54
Best capacity factor over one route	%	87	87	87
Worst capacity factor over one route	%	16	11	13
Average route duration	Hour (s)	38.3	38.9	37.4
Longest route duration	Hour (s)	140.5	212.9	173.4
Shortest route duration	Hour (s)	10.1	9.6	8.5
Longest route distance	NM	1892.4	1331.8	1551.4
Shortest route distance	NM	147.6	198.6	180.1
Average filling ratio at the end of the routes	%	92.5	93.4	92.6

In comparison to other renewable power generation technologies such as solar photovoltaics or land-based wind energy, a capacity factor of 53% is high. It is of the same order of magnitude as that of currently operating offshore wind farms as discussed in Chapter 2. However, it is almost 20% less than the capacity factor that was obtained for energy ships deployed in the North Atlantic ocean and with hydrogen storage. It can be explained by weaker winds and smaller energy storage capacity which cause shorter route duration and limits the weather-routing options.

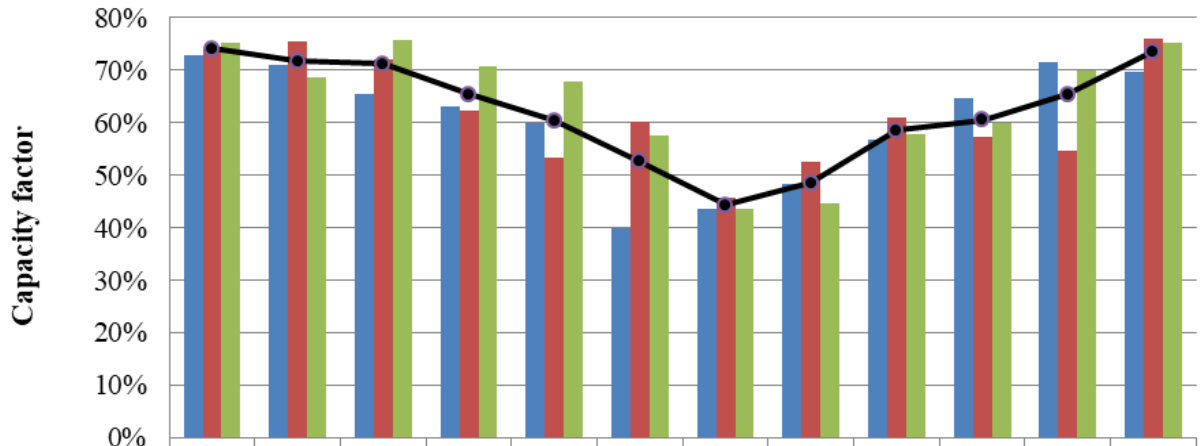

	JAN	FEB	MAC	APR	MAY	JUNE	JULY	AUG	SEPT	OCT	NOV	DEC
2015	73%	71%	66%	63%	60%	40%	44%	48%	57%	65%	72%	70%
2016	74%	76%	72%	62%	53%	60%	46%	53%	61%	57%	55%	76%
2017	75%	69%	76%	71%	68%	58%	44%	45%	58%	60%	70%	75%
AVERAGE	74%	72%	71%	65%	60%	53%	44%	49%	59%	61%	65%	74%

Figure 49 Monthly average capacity factor for 1.6 MW energy ship deployed at Saint-Pierre-et-Miquelon in 2015, 2016 and 2017

Figure 49 shows the monthly average capacity factor. The lowest capacity factor (44%) is obtained in July of 44% due to low wind resource during that month as shown in Figure 50.

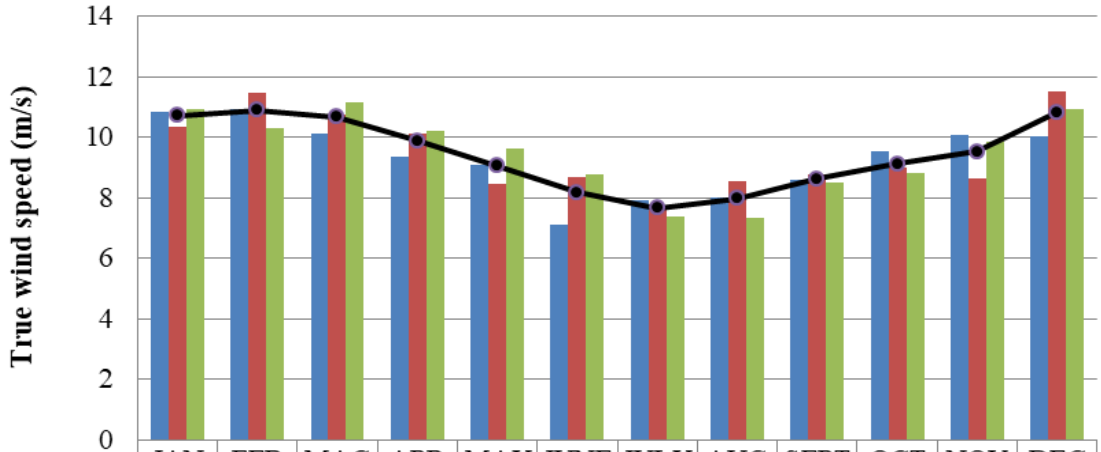

	JAN	FEB	MAC	APR	MAY	JUNE	JULY	AUG	SEPT	OCT	NOV	DEC
2015	11	11	10	9	9	7	8	8	9	10	10	10
2016	10	11	11	10	8	9	8	9	9	9	9	12
2017	11	10	11	10	10	9	7	7	9	9	10	11
AVERAGE	11	11	11	10	9	8	8	8	9	9	10	11

Figure 50 Seasonal variability of wind speed at Saint-Pierre-et-Miquelon in 2015, 2016 and 2017

Figure 51 shows the superimposition of the traces of all the optimized routes followed by the 1.6 MW energy ship in 2015, 2016 and 2017. It shows that the ship's trajectories cover a large part of South Saint-Pierre-et-Miquelon. The trajectories appear to be random; no typical pattern can be identified. It is also shown that some routes go through land. It is due to a bug in qtVlm. Their number being limited, this issue is not expected to affect significantly the results.

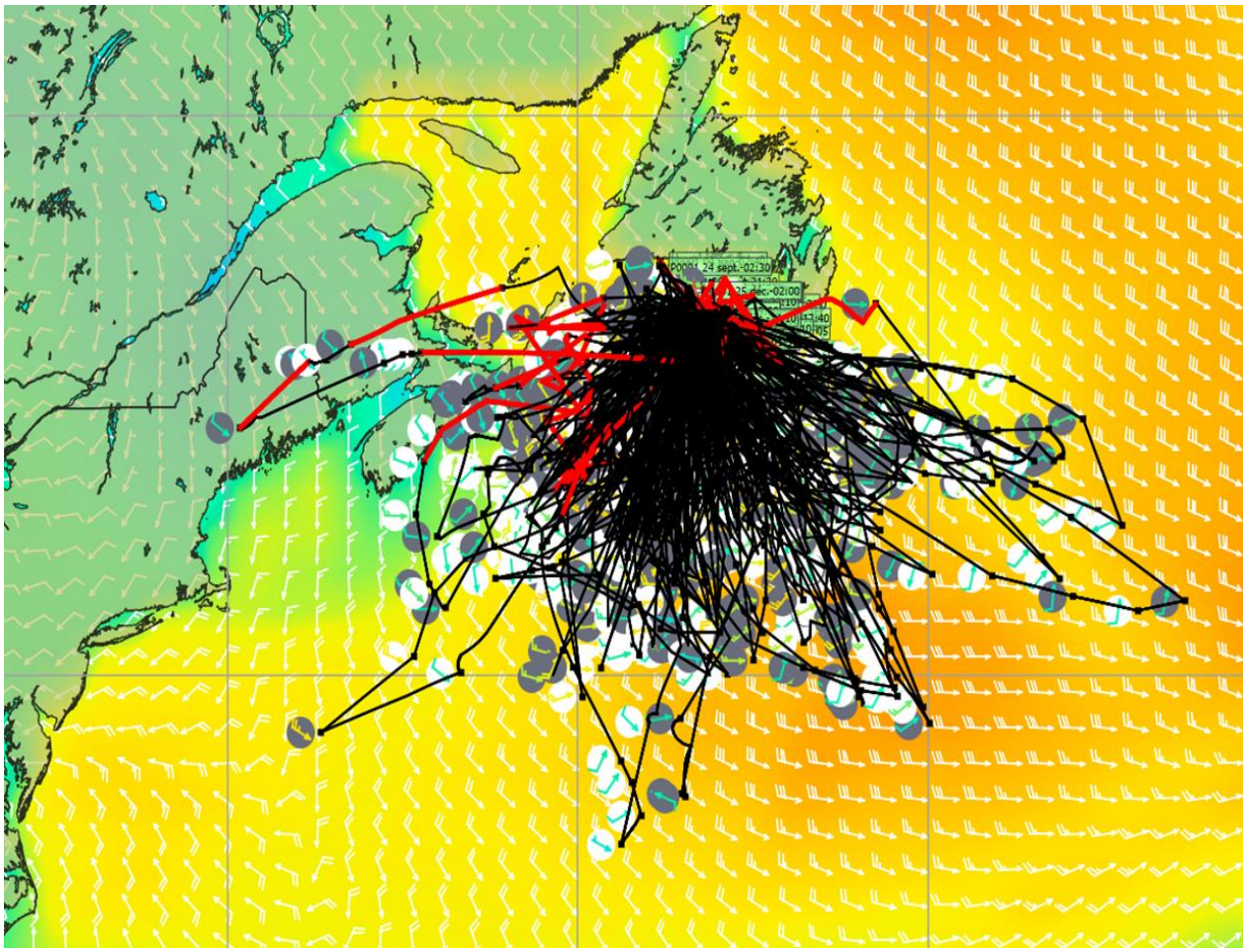

Figure 51 1.6 MW energy ship route traces for 24-hour storage capacity & 4-hour unloading time in 2015, 2016 and 2017 at Saint-Pierre-et-Miquelon

4.3.1. Effect of rated power

A sensitivity study on the rated power was performed. It follows the same methodology as in Chapter 3. Three versions of the energy ship with rated power 1 MW, 1.3 MW and 1.6 MW are considered. All ships are equipped with 24-hour storage capacity. The unloading time is 4 hours. The numerical parameters were fixed to 2 initial optimization waypoints and 8° search step angle.

It is expected that the capacity factor will increase with decreasing rated power, and vice-versa. Note that the total energy production is expected to decrease with decreasing rated power.

Table 19 shows the average capacity factor for the 1 MW, 1.3 MW and 1.6 MW energy ship over the years (2015, 2016 & 2017. One can see that, as expected, the capacity factor decreases with increasing rated power. The greatest average capacity factor (58.8%) is obtained for the 1 MW energy ship. Regarding the average filling ratio, it exceeds 94% for all configurations. Thus, the weather routing enables an intensive use of the energy reservoir.

Regarding the annual energy production, even though the capacity factor decreases with increasing rated power, it appears to increase with increasing rated power. For instance, the energy production of the 1.6 MW energy ship is 22% greater than the 1 MW energy ship despite a 11% smaller in capacity factor. It is likely that even greater annual energy production may be achieved by further increasing the rated power.

Table 19 Capacity factor, filling ratio and total annual energy production for 1MW, 1.3MW and 1.6MW energy ship in Saint-Pierre-et-Miquelon for 3 years (2015, 2016 & 2017)

			1 MW		1.3 MW		1.6 MW	
			8°; 2 WPs	Average over 3 years	8°; 2 WPs	Average over 3 years	8°; 2 WPs	Average over 3 years
24h storage capacity / 4h unload time	Capacity factor (CF) (%)	2015	59.94	58.83	55.81	55.13	52.39	52.80
		2016	59.08		54.77		52.31	
		2017	57.46		54.80		53.70	
	Filling ratio (FR) (%)	2015	94.38	94.66	94.30	93.93	92.48	92.82
		2016	94.54		93.85		93.39	
		2017	95.06		93.63		92.59	
	Total annual energy production (MWh)	2015	5233.43	5142.74	6328.34	6263.42	7311.22	7378.73
		2016	5174.75		6237.78		7317.95	
		2017	5020.05		6224.14		7507.00	

4.3.2. Effect of storage capacity and unloading time

Table 20 shows the sensitivity of the capacity factor to storage capacity and unloading time. The rated power is 1.6 MW. The numerical parameters are 8° for the search step and 2 waypoints.

Table 20 Capacity factor (%) of the 1.6 MW energy ship in Saint-Pierre-et-Miquelon with optimization parameter 8° search step angle & 2 number of waypoints and 4 storage capacity configurations.

		Capacity factor (CF) (%)		Filling ratio (FR) (%)		Total annual energy production (MWh)	
		8°; 2 WPs	Average over 3 years	8°; 2 WPs	Average over 3 years	8°; 2 WPs	Average over 3 years
6h storage capacity / 1h unload time	2015	55.97	53.76	93.96	94.45	7808.28	7513.39
	2016	54.21		94.00		7593.11	
	2017	51.10		95.38		7138.79	
12h storage capacity / 2h unload time	2015	54.52	53.16	94.02	94.49	7620.28	7432.68
	2016	53.29		94.73		7454.48	
	2017	51.68		94.72		7223.27	
24h storage capacity / 4h unload time	2015	52.39	52.80	92.48	92.82	7311.22	7378.73
	2016	52.31		93.39		7317.95	
	2017	53.70		92.59		7507.00	
48h storage capacity / 8h unload time	2015	49.72	50.97	91.55	91.12	6955.43	7021.69
	2016	52.48		93.06		7360.10	
	2017	50.70		88.74		6749.54	

The obtained capacity factors are in the range 50 to 54%. The best capacity factor is obtained for 6-hour storage capacity and 1-hour unloading time. Both capacity factor and total annual energy production decrease with increasing storage capacity and unloading time. The annual energy production for 24-hour storage capacity and 6-hour unloading time is 7% less than that with 6-hour storage capacity and 1-hour unloading time.

These results are surprising as one may have expected that greater storage capacity would lead to a greater number of weather-routing options, and thus a greater capacity factor and total energy production. One may note that the unloading time is also greater, but it does not change the

theoretical maximum capacity factor (85.7%) for all the configurations. An explanation is that the optimization algorithm converges to a local maximum.

Regarding the filling ratio, the minimum is 91% obtained with 48-hour storage capacity and 8-hour unloading time. Thus, the filling ratio is high but is it comparable to the filling ratio of the energy ship deployed at far offshore.

Overall, one can see that the capacity factor and total energy production at Saint-Pierre-et-Miquelon is sensitive to the storage capacity and unloading time configuration.

4.3.3. Distribution of energy production

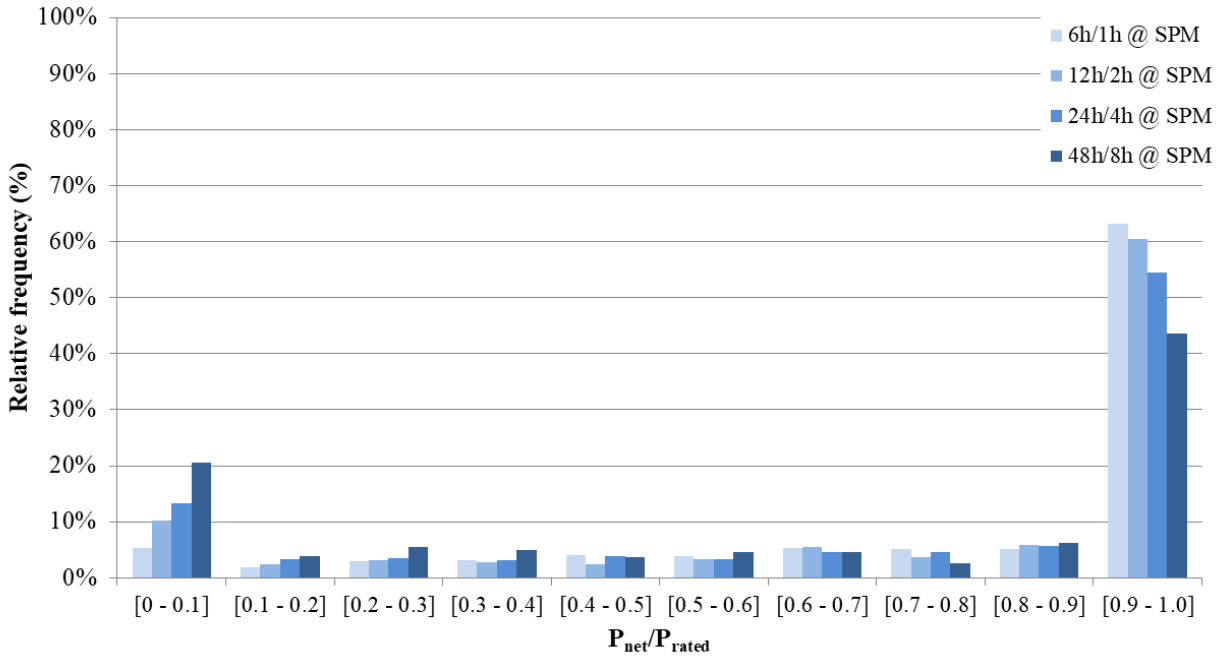

Figure 52 Frequency distribution of energy production for 1.6 MW energy ship in Saint-Pierre-et-Miquelon for 3 years (2015, 2016 & 2017)

Figure 52 shows the distribution of the ratio of the energy delivered by the 1.6 MW energy ship to the maximum energy which could have been produced over the same period of time (rated power times duration of the route). One can see that, most of the time and for all storage capacities, the energy delivery is equal to the maximum energy. However, it also shows that the frequency of routes for which is the energy delivery is very small is relatively high. The other cases are relatively

evenly distributed. These results could be explained by weaker wind or no wind available at certain time. This is particularly the case during the months of June to August (Summer) (see Figure 50).

One can see in Figure 52, as the storage capacity duration increases, the frequency of deliveries for which the amount of energy is equal to the maximum decreases (vice versa for the lowest energy delivery class).

4.3.4. Frequency distributions of sailed distance over maximum distance

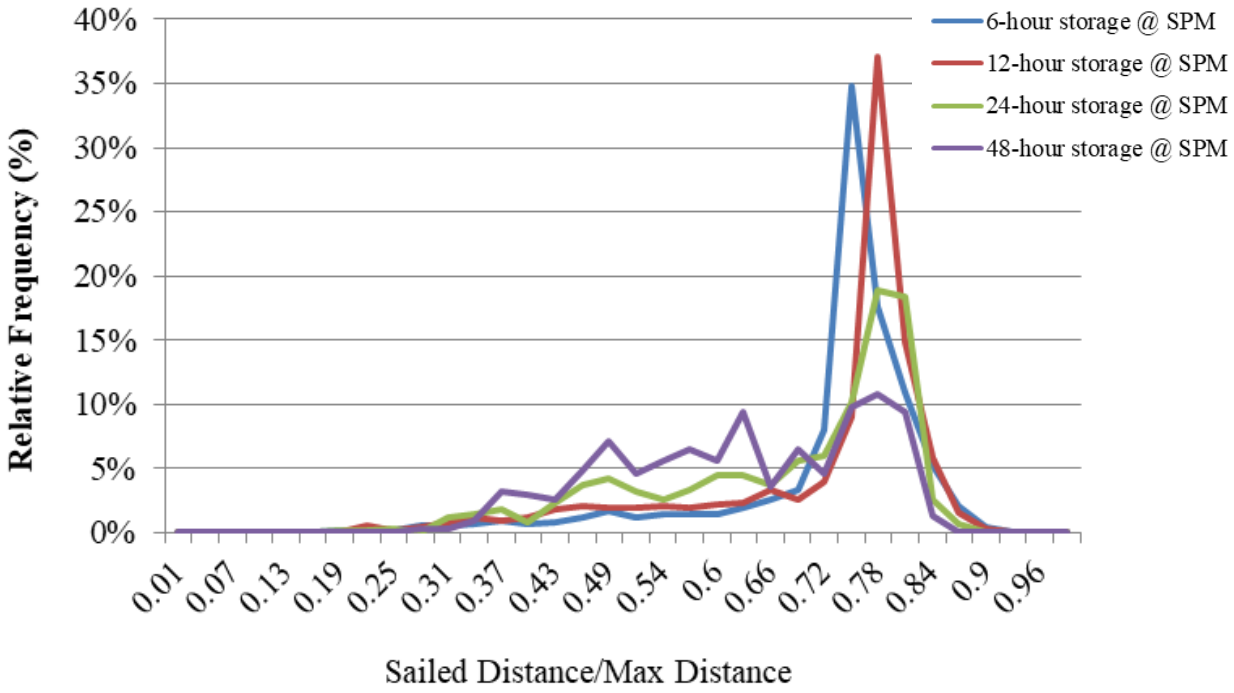

Figure 53 Frequency distributions of sailed distance over maximum distance of 1.6 MW energy ship in Saint-Pierre-et-Miquelon for 3 years (2015, 2016 & 2017)

Figure 53 shows the frequency distribution of the sailed distance (total distance travelled by the energy ship when arriving back to port). For the ships with the smallest storage capacities, one can see that, most of the time, the energy ship covers 80% of the maximum distance (which is defined as the distance that it could cover in the same amount of time if sailing at its maximum speed, e.g. 20 knots). For the energy ship equipped with 48-hour storage capacity, the distribution is broader. Through-out the year, most of time, this energy ship travels between 40% and 80% of its maximum distance.

This pattern could be explained by the distribution of the true wind speed at Saint-Pierre-et-Miquelon shown in Figure 55. Note that, the true wind speed is the average true wind speed at current boat locations for each route options available in a year 2015, 2016 and 2017. As shown, for all configurations, the energy ship experienced true wind speed of 20 knots (10.3 m/s) at most of the time and routes. These could be explained by the maximum performance derived from the energy ship polar. As shown in boat performance polar diagram in Figure 37, the 1.6 MW energy ship achieved its maximum boat speed and maximal power production at 10 m/s true wind speed.

4.3.5. Frequency distributions of True Wind Angle (TWA) in 2017

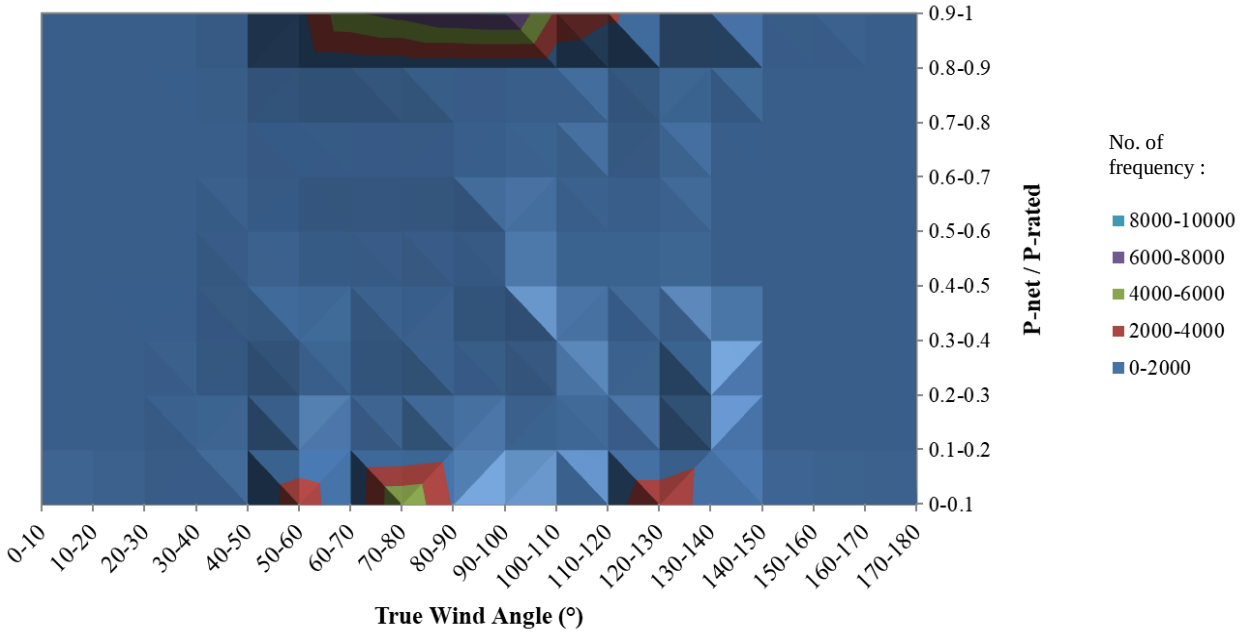

Figure 54 Frequency of true wind angle (°) in response to produced energy over rated power of the 1.6 MW energy ship at Saint-Pierre-et-Miquelon

Figure 54 shows the frequency distribution of true wind angle power production of the 1.6 MW energy ship. It has been produced using dataset 2. As expected, one can see that the optimized routes correspond to routes for which the energy ship sails close to 90° true wind angle (beam reach). It can also be observed that the distribution is slightly distorted towards the upwind conditions, which means that, for optimized routes, the energy ship sails more often in upwind conditions than in downwind conditions.

4.3.6. Comparison with a stationary offshore wind turbine

The capacity factor obtained by the 1.6 MW energy ship is compared to that of a stationary offshore wind farm. The capacity factor of the offshore wind turbine is obtained using the web application https://www.renewables.ninja. This application estimates the energy production of wind or solar farms at any location [91]. It uses the MERRA-2 weather data [70].

Nine different locations were considered for the wind farm (indicated by the boxes in Figure 56). The wind farm area was bounded within 46.3° to 42.3 ° North and 56.5° to 58.5° West approximately covering the area of navigation of the energy ship. The rated power of the offshore wind turbine was set to 1.6 MW. The hub height was set to 90 m. The wind distribution and the power curve of the floating wind turbine are shown in Figure 55.

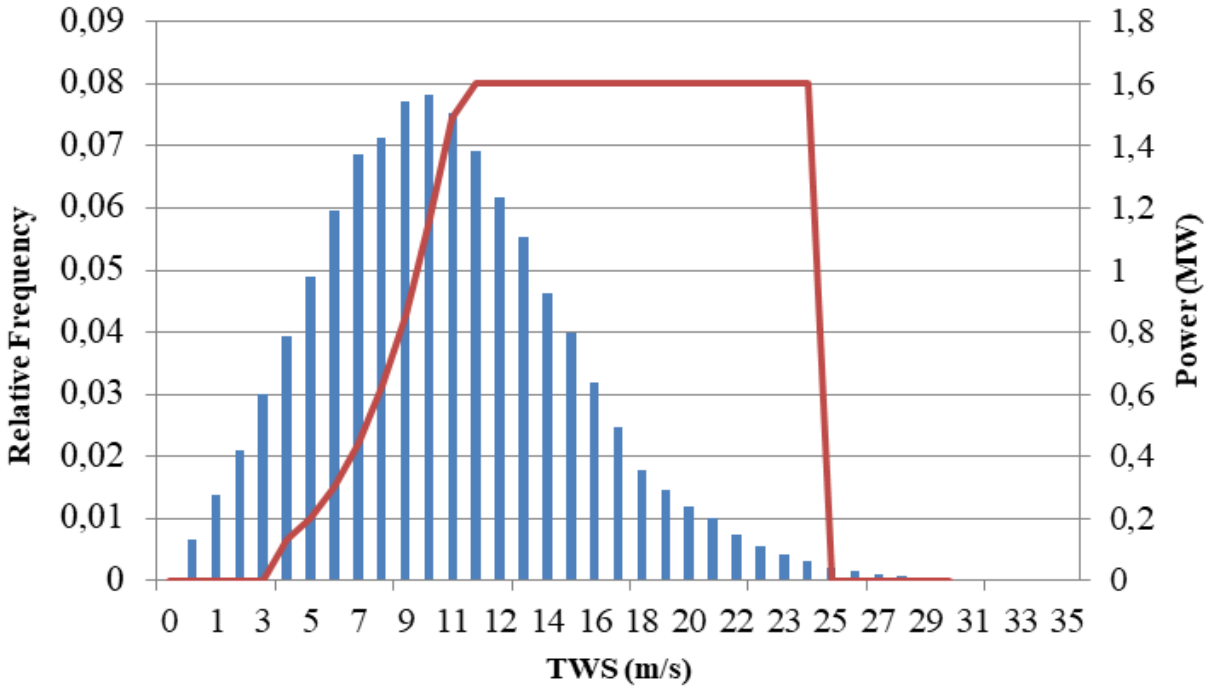

Figure 55 Wind distribution and power curve for the 1.6 MW stationary wind turbines over the three years of 2015, 2016 and 2017 in Saint-Pierre-et-Miquelon
(Mean TWS = 10.28 m/s; Standard deviation = 4.92)

Table 21 shows the capacity factor for the 1.6 MW floating offshore wind turbines for 3 years (2015, 2016 & 2017) and its average over the 3 years.

One can see that the capacity factor varies from 61% to 65% depending on the location of the wind farm. The smallest capacity factor (62%) is obtained for location #1 which is one of the

nearest to the energy ship start/end point. The greatest capacity factor 64.6% is obtained for locations #3 and #6 which are located in the northern part of the area, away from shore towards the middle of the North Atlantic Ocean.

The spatial average capacity factor of floating offshore wind farms is 63% which is 10% greater than the capacity factor obtained by the energy ship (53%).

Table 21 Capacity factor for 1.6 MW floating offshore wind turbines in Saint-Pierre-et-Miquelon for 3 years (2015, 2016 & 2017)

	Latitude (N)	Longitude (W)	2015	2016	2017	AVERAGE
FWT01	46.3 °	58.5°	62.7%	62.4%	60.3%	61.8%
FWT02	46.3 °	55.5°	63.4%	62.7%	62.0%	62.7%
FWT03	46.3 °	52.5°	65.8%	64.1%	64.0%	64.6%
FWT04	44.3 °	58.5°	62.2%	62.6%	63.5%	62.8%
FWT05	44.3 °	55.5°	63.2%	63.4%	64.0%	63.5%
FWT06	44.3 °	52.5°	64.5%	65.1%	64.3%	64.6%
FWT07	42.3 °	58.5°	60.5%	63.2%	63.6%	62.4%
FWT08	42.3 °	55.5°	61.1%	63.2%	62.4%	62.2%
FWT09	42.3 °	52.5°	61.2%	63.1%	61.5%	61.9%
						63.0%

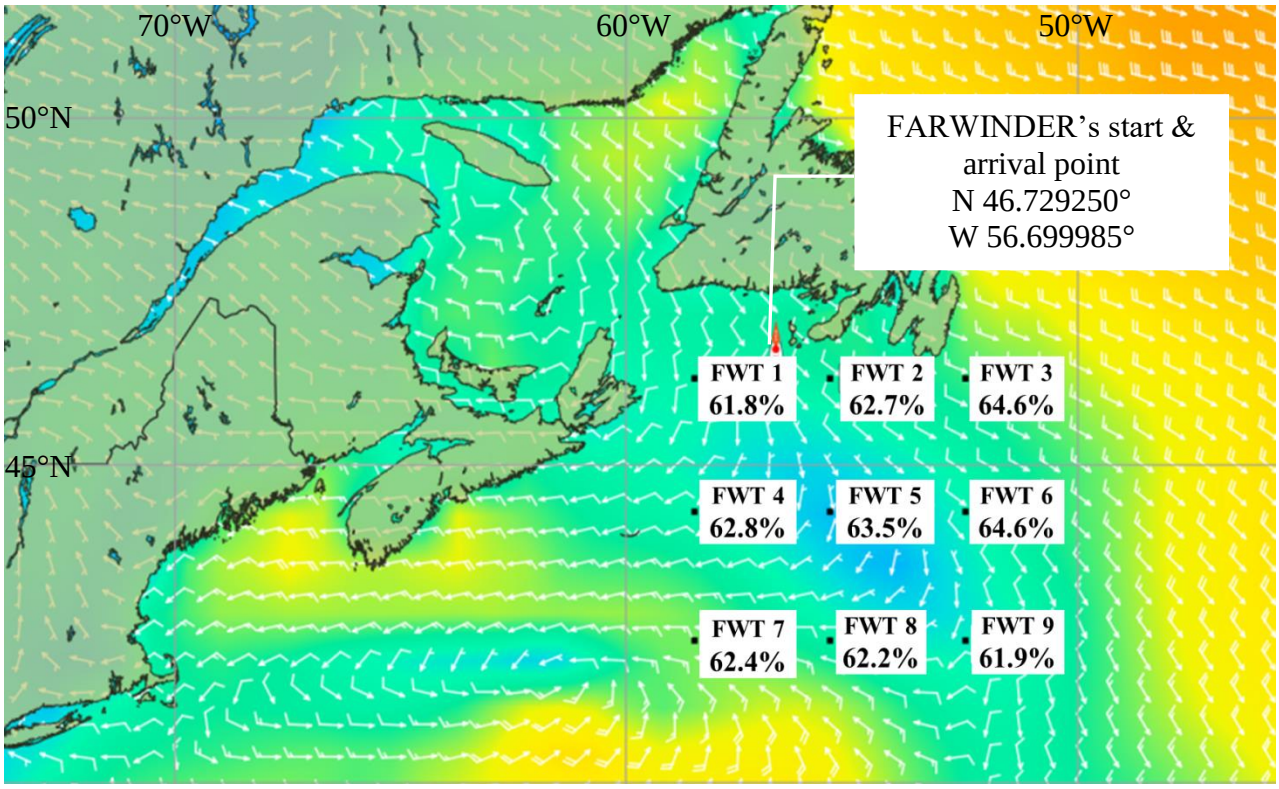

Figure 56 Tested locations for the 1.6 MW floating wind turbines and average capacity factor over the three years of 2015, 2016 and 2017 in Saint-Pierre-et-Miquelon

4.4. Capacity factor of energy ships deployed at Ile de Sein case

In this section, we consider a second case study which is the deployment of an energy ship for the power supply of Ile de Sein (Figure 46). The capacity factor of the 1.6 MW energy ship was estimated for the three years of 2015, 2016 and 2017. The same optimization parameters as for Saint-Pierre-et-Miquelon were used (two initial optimization waypoints and 8° search step angle). The storage capacity is 24 hours and the unloading time is 4 hours. The start/end point is N 48.044997°, W 5.146862°.

Table 22 shows the capacity factor over the three years. It shows that an average capacity factor of 49% can been achieved. It is 8% smaller than the average capacity factor obtained at Saint-Pierre-et-Miquelon (53%).

The year-to-year variability appears to be significant as the annual average capacity factor exceeds 50% both in 2015 and 2017, but falls to 45% in 2019. The best capacity factor over one

route is 87%, corresponding to the achievable maximum taking account the unloading time. The worst capacity factor over one route (6%) is almost half that in Saint-Pierre-et-Miquelon (11%).

As for Saint-Pierre-et-Miquelon, the average filling ratio is very high (94.4%). This shows that the route optimization algorithm tends to converge towards solutions for which the batteries are fully charged when the ship comes back to port.

Table 22 Results for the optimization of the capacity factor of the 1.6 MW energy ship in Ile de Sein; equipped with 24 hours storage capacity and 4 hours unloading time and optimization parameter of 8° search steps angle and 2 initial waypoints

Year	-	2015	2016	2017
Annual average capacity factor	%	51	45	50
Best capacity factor over one route	%	87	87	87
Worst capacity factor over one route	%	7	6	11
Average route duration	Hour (s)	40.6	46.1	41.8
Longest route duration	Hour (s)	337.5	401.4	215.3
Shortest route duration	Hour (s)	10.3	5.8	10.8
Longest route distance	NM	3051.6	1959.1	2303.8
Shortest route distance	NM	208.4	51	227.8
Average filling ratio at the end of the routes	%	94.5	93.6	94.9

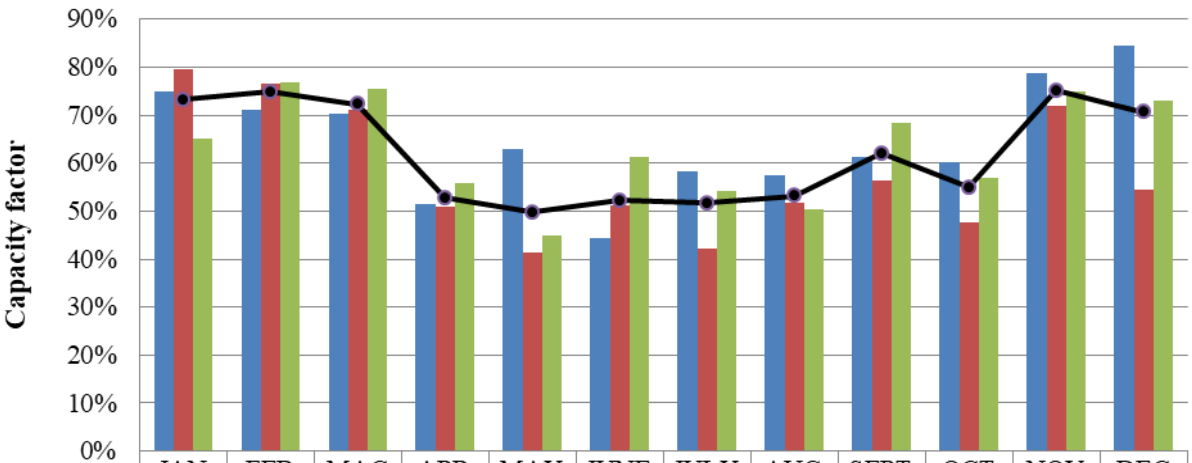

	JAN	FEB	MAC	APR	MAY	JUNE	JULY	AUG	SEPT	OCT	NOV	DEC
2015	75%	71%	70%	52%	63%	44%	58%	58%	61%	60%	79%	85%
2016	80%	77%	71%	51%	41%	51%	42%	52%	56%	48%	72%	55%
2017	65%	77%	75%	56%	45%	61%	54%	50%	68%	57%	75%	73%
AVERAGE	73%	75%	72%	53%	50%	52%	52%	53%	62%	55%	75%	71%

Figure 57 Monthly average capacity factor for 1.6 MW energy ship deployed at Ile de Sein in 2015, 2016 and 2017

Figure 57 indicates the monthly average capacity factor obtained by the 1.6 MW energy ship deployed at Ile de Sein. In contrast to the Saint-Pierre-et-Miquelon case, the lowest capacity factor is obtained in May, which corresponds to the month with the lowest wind resource as can be seen in Figure 58.

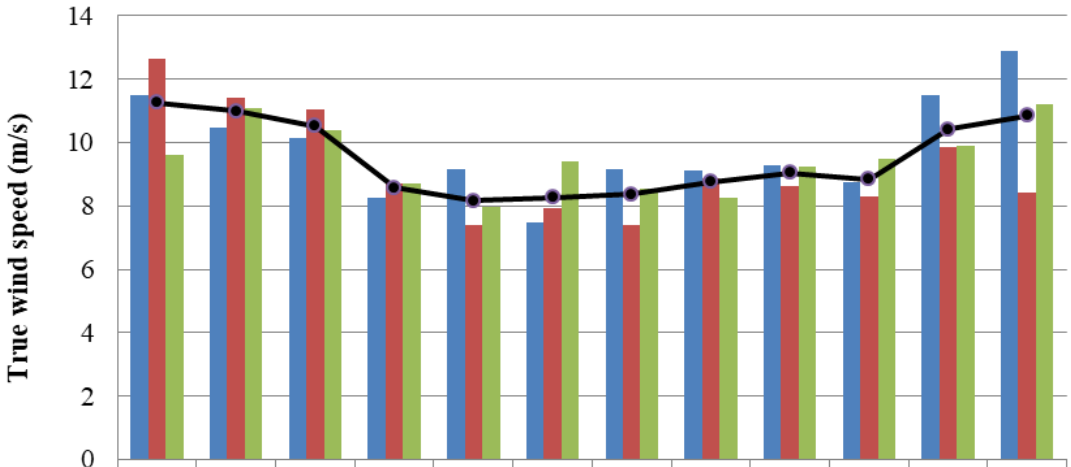

	JAN	FEB	MAC	APR	MAY	JUNE	JULY	AUG	SEPT	OCT	NOV	DEC
2015	12	10	10	8	9	7	9	9	9	9	11	13
2016	13	11	11	9	7	8	7	9	9	8	10	8
2017	10	11	10	9	8	9	9	8	9	10	10	11
AVERAGE	11	11	11	9	8	8	8	9	9	9	10	11

Figure 58 Seasonal variability of wind speed at Ile de Sein in 2015, 2016 and 2017

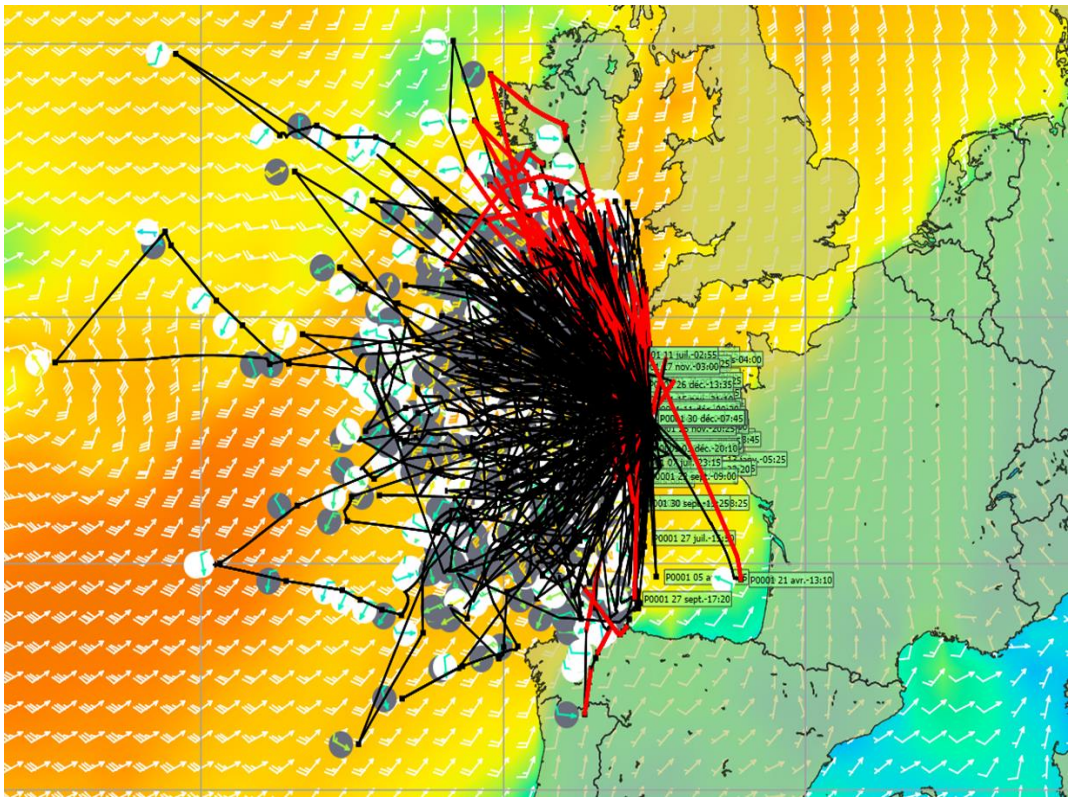

Figure 59 Superimposition of the traces for 1.6 MW energy ship route traces equipped with 24-hour storage capacity & 4-hour unloading time in 2015, 2016 and 2017 at Ile de Sein

Figure 59 shows the superimposition of the traces of all the optimized routes followed by the 1.6 MW energy ship in 2015, 2016 and 2017. It shows that the ship's trajectories cover a large part of West Ile de Sein. As in previous cases, the trajectories appear to be random which no typical pattern is can be identified. Thus, a statistical analysis on frequency distributions of power, sailed distance, speed and true wind angle (TWA) for all case studies will be presented in next subsections. The figure also shows that in a few cases, the ship is routed over land areas. This bug in the software shall be fixed in future work.

4.4.1. Effect of rated power

The same sensitivity study to rated power of the energy ship as for Saint-Pierre-et-Miquelon (see subsection 4.3.1.1) was performed. The results are shown in Table 23.

Similar to the Saint-Pierre-et-Miquelon case study, one can see that the energy production increases with increasing rated power. However, the capacity factor decreases. The maximum capacity factor of 55.3 % is obtained for the 1 MW energy ship, compared to only 48.5% (12% less) for the 1.6 MW energy ship. The effect of the rated power on the filling ratio appears to be limited as the average filling ratio exceeds 92% in all studied configurations.

Table 23 Capacity factor, filling ratio and energy production for 1 MW, 1.3 MW and 1.6 MW energy ship in Ile de Sein for 3 years (2015, 2016 & 2017)

			1 MW		1.3 MW		1.6 MW	
			8°; 2 WPs	Average over 3 years	8°; 2 WPs	Average over 3 years	8°; 2 WPs	Average over 3 years
24h storage capacity / 4h unload time	Capacity factor (CF)	2015	59.49%	55.34%	54.99%	51.07%	50.87%	48.50%
		2016	51.61%		47.98%		44.85%	
		2017	54.93%		50.23%		49.77%	
	Filling ratio (FR)	2015	95.33%	94.63%	95.28%	94.73%	94.54%	94.36%
		2016	93.20%		93.70%		93.61%	
		2017	95.36%		95.20%		94.94%	
	Total annual energy production	2015	5198.18	4835.71	6246.38	5806.17	7110.62	6786.01
		2016	4522.51		5465.55		6287.91	
		2017	4786.45		5706.59		6959.51	

4.4.2. Effect of storage capacity and unloading time

In this section, the effects of storage capacity and unloading time are investigated. As for Saint-Pierre-et-Miquelon, 4 configurations were considered (6-h storage capacity/1-h unloading time, 12-h storage capacity/2-h unloading time, 24-h storage capacity/4-h unloading time, 48-h storage capacity/8-h unloading time).

Results are shown in Table 24. As expected, and in contrast to Saint-Pierre-et-Miquelon, the average capacity factor increases with increasing storage capacity. Conversely, the filling ratio decreases, albeit the reduction is limited.

Table 24 Capacity factor (%) of the 1.6 MW energy ship in Ile de Sein with optimization parameter 8° search step angle & 2 number of waypoints

		Capacity factor (CF)		**Filling ratio (FR)**		**Energy Produced (MWh)**	
		8°; 2 WPs	Average over 3 years	8°; 2 WPs	Average over 3 years	8°; 2 WPs	Average over 3 years
6h storage capacity / 1h unload time	2015	52.16%	47.78%	96.07%	95.59%	7291.28	6670.25
	2016	45.79%		94.84%		6374.22	
	2017	45.40%		95.87%		6345.26	
12h storage capacity / 2h unload time	2015	52.56%	48.94%	95.15%	95.33%	7346.57	6847.07
	2016	46.16%		94.92%		6471.27	
	2017	48.10%		95.91%		6723.37	
24h storage capacity / 4h unload time	2015	50.87%	48.50%	94.54%	94.36%	7110.62	6786.01
	2016	44.85%		93.61%		6287.91	
	2017	49.77%		94.94%		6959.51	
48h storage capacity / 8h unload time	2015	53.53%	50.20%	93.14%	92.56%	7441.51	7013.52
	2016	48.08%		92.43%		6744.09	
	2017	49.00%		92.10%		6854.96	

4.4.3. Frequency distributions of energy produced by the energy ship

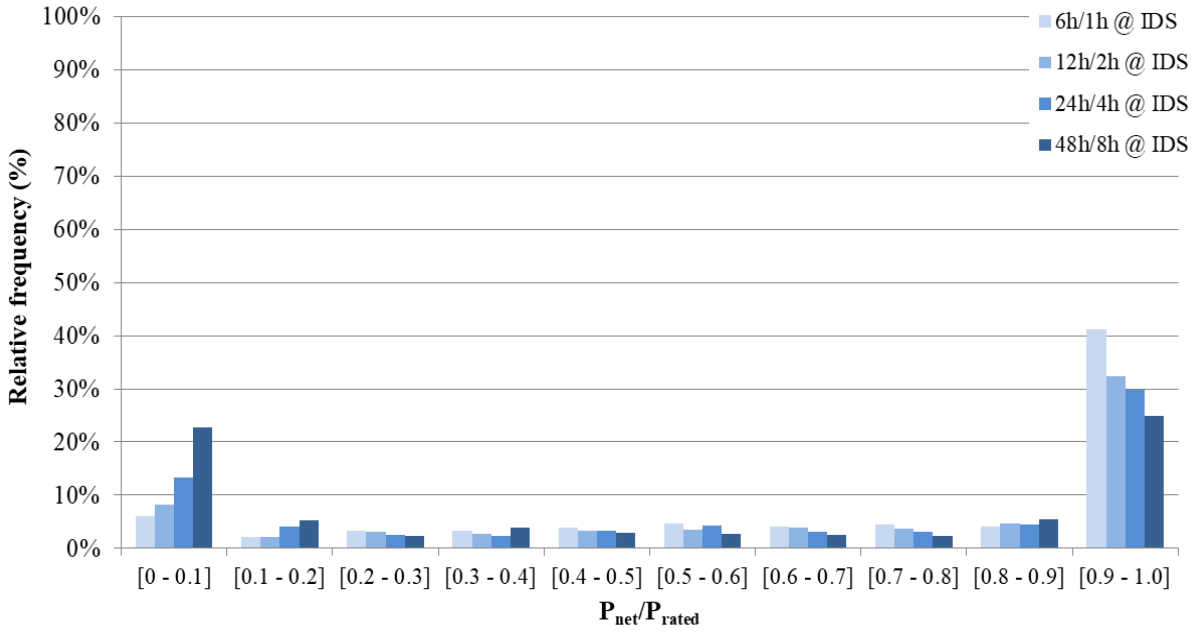

Figure 60 Frequency distribution of energy production for 1.6 MW energy ship in Ile de Sein for 3 years (2015, 2016 & 2017)

Figure 60 shows the distribution of the ratio of the delivered energy to the maximum energy which could have been delivered over the same period of time. The distribution appears to be similar to that for Saint-Pierre-et-Miquelon: the two most frequent cases are that for which the delivered energy is equal to the maximum and that for which it close to 0. This result can be explained by weaker wind or no wind available at certain time especially in month of April to July (see Figure 63).

It also appears in Figure 60 that the frequency of energy deliveries for which the amount of energy is equal to the storage capacity decreases with increasing storage capacity (vice versa for the lowest energy delivery class). This effect was also observed for Saint-Pierre-et-Miquelon.

4.4.4. Frequency distributions of sailed distance over maximum distance

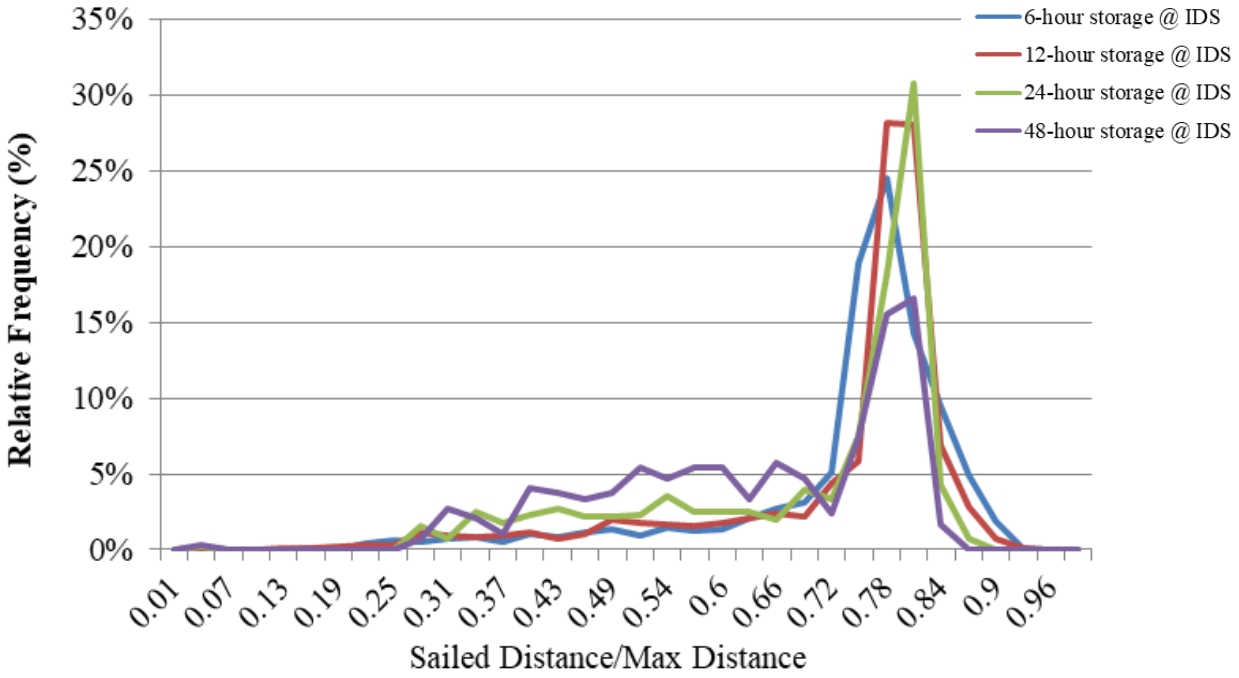

Figure 61 Frequency distributions of sailed distance over maximum speed of 1.6 MW energy ship in Ile de Sein for 3 years (2015, 2016 & 2017)

Figure 61 shows the frequency distribution of the traveled distance at Ile de Sein. One can see that the energy ship travels 80% of the maximum distance for most of the deliveries. As in Saint-Pierre-et-Miquelon, the true wind speed at Ile de Sein was centered at 19 knots (9.8 m/s).

4.4.5. Frequency distributions of True Wind Angle (TWA) in 2017

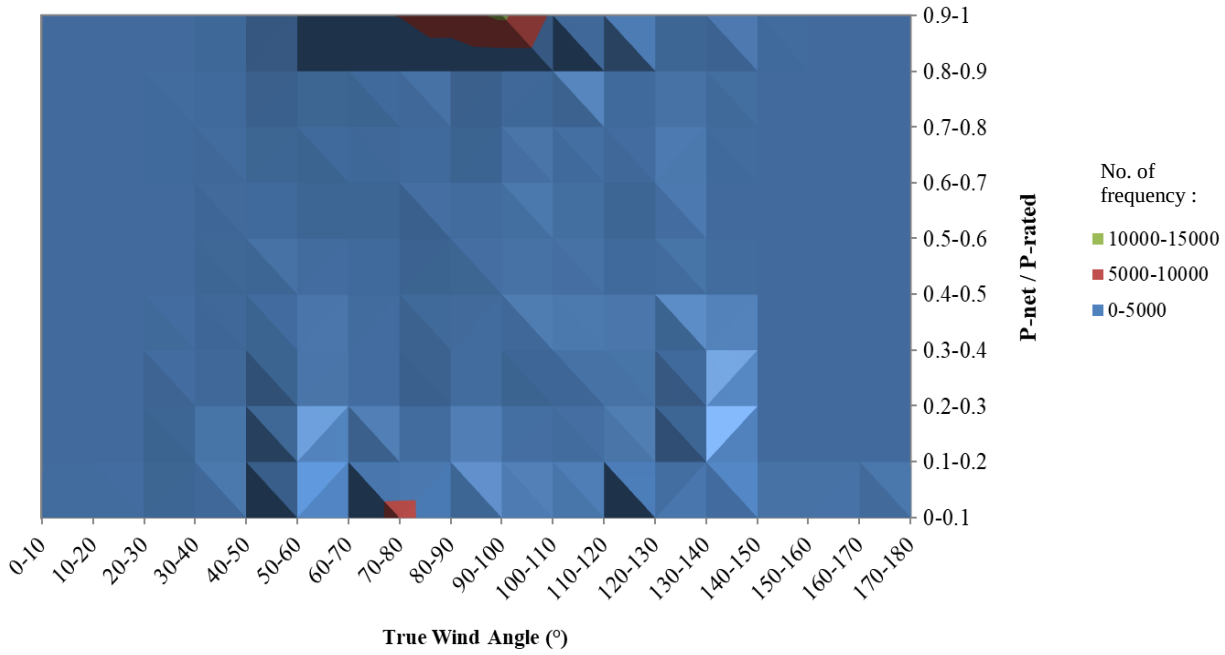

Figure 62 Frequency of true wind angle (°) and power production of the 1.6 MW energy ship at Ile de Sein

Figure 62 shows the frequency distribution of true wind angle and power production of the 1.6 MW energy ship deployed at Ile de Sein. As expected, one can see that the optimized routes correspond to routes for which the energy ship sails close to 90° true wind angle (beam reach).

4.4.6. Comparison with a stationary offshore wind turbine

In this section, the capacity factor of the 1.6 MW energy ship at Ile de Sein is compared to that of a stationary offshore wind turbine that would be deployed in same area. The capacity factor of the offshore wind turbine is obtained using the same methodology and wind data as presented in the Saint-Pierre-et-Miquelon case study.

Nine locations are considered for the deployment of the floating offshore wind farm (indicated by the boxes in Figure 64). The wind turbine hub height is assumed to be 90 meters. Its rated power is 1.6 MW. Figure 63 shows the wind distribution and power curve of the floating wind turbine studied at Ile de Sein. The wind distribution was obtained from MERRA-2 weather data [70].

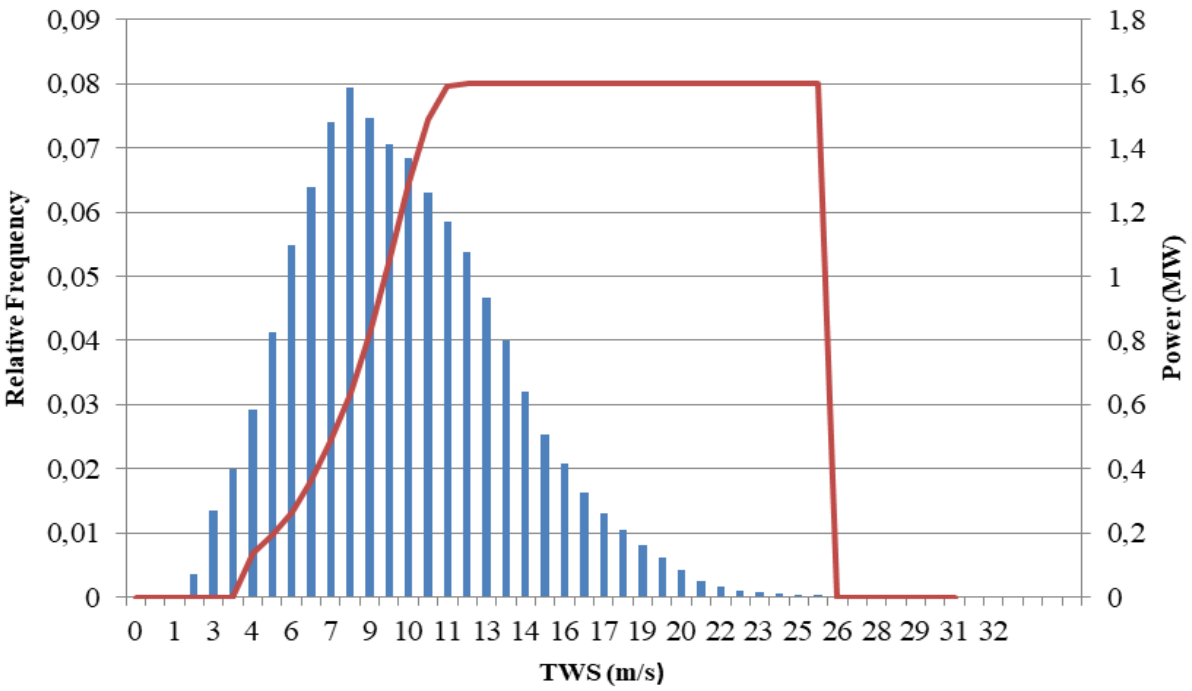

Figure 63 Wind distribution and power curve for the 1.6MW floating wind turbines over the three years of 2015, 2016 and 2017 in Ile de Sein
(Mean TWS = 9.81 m/s; Standard deviation = 3.96)

Table 25 shows the capacity factor of the offshore wind farm for the three years (2015, 2016 & 2017) and the average over the three years. The average capacity factor over the area reaches 63%. In addition, each wind turbine achieves a capacity factor over 60% except wind turbine #07 that achieves a capacity factor of 59%. It can be observed that the capacity factor decreases with approaching Ile de Sein. In comparison to Saint-Pierre-et-Miquelon, the average capacity factor is similar (62.7% in Ile de Sein vs 63.0% in Saint-Pierre-et-Miquelon). However, for the energy ship, the capacity factor is significantly smaller in Ile de Sein (49%) than in Saint-Pierre-et-Miquelon (53%). It shows that the capacity factor of an energy ship cannot be directly estimated from a wind turbine's capacity factor. Weather-routing appears to be necessary.

Table 25 Capacity factor for 1.6 MW floating offshore wind turbines in Ile de Sein for 3 years (2015, 2016 & 2017)

	Latitude (N)	Longitude (W)	2015	2016	2017	AVERAGE
FWT01	49.0 °	6.0°	66.6%	60.8%	61.4%	62.9%
FWT02	49.0 °	8.0°	68.1%	63.0%	63.0%	64.7%
FWT03	49.0 °	10.0°	68.9%	65.2%	64.7%	66.3%
FWT04	48.0 °	6.0°	64.5%	58.4%	58.4%	60.4%
FWT05	48.0 °	8.0°	66.7%	61.3%	60.3%	62.8%
FWT06	48.0 °	10.0°	67.9%	63.0%	62.0%	64.3%
FWT07	47.0 °	6.0°	62.3%	56.8%	56.6%	58.6%
FWT08	47.0 °	8.0°	65.5%	60.0%	59.0%	61.5%
FWT09	47.0 °	10.0°	66.9%	61.8%	60.6%	63.1%
						62.7%

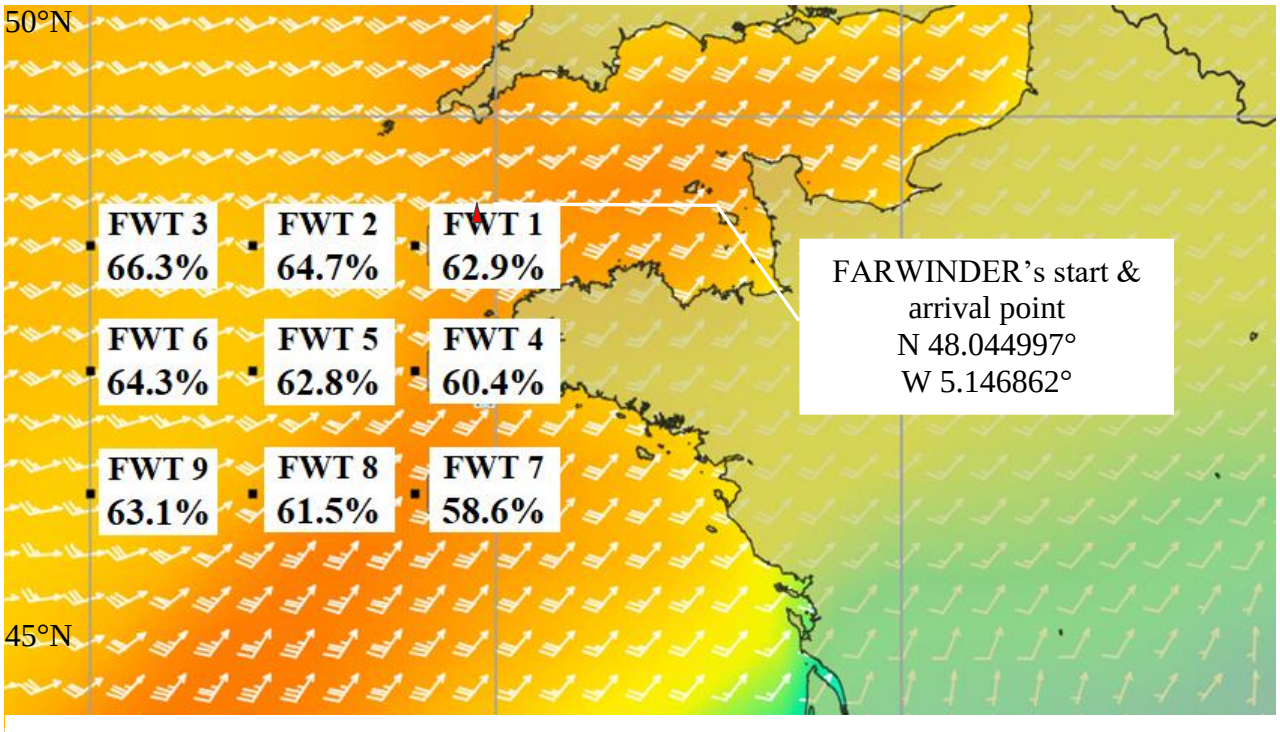

Figure 64 Tested locations for the 1.6 MW floating wind turbines and average capacity factor over the three years of 2015, 2016 and 2017 in Ile de Sein

4.5. Conclusions

In this chapter, we investigated the capacity factor of an energy ship that would be deployed near shore in Saint-Pierre-et-Miquelon and Ile de Sein. The capacity factor of the energy ship is optimized using weather-routing.

We found that energy ships could have achieved an average capacity factor of 53% at Saint-Pierre-et-Miquelon and 49% at Ile de Sein for the three years of 2015, 2016 and 2017. It is smaller than the result of weather routing in the far offshore, which can be explained by lower wind speeds. Indeed, Table 26 shows that the average true wind speed over 3 years at North Atlantic ocean is 12% greater than the average true wind speed in Saint-Pierre-et-Miquelon and Ile de Sein.

Table 26 Annual average true wind speed and route options at three deployment locations for energy ship

	Saint-Pierre-et-Miquelon		Ile de Sein		North Atlantic Ocean	
	TWS (m/s)	No. Routes	TWS (m/s)	No. Routes	TWS (m/s)	No. Routes
2015	9.58	206	10.23	196	11.42	253
2016	9.75	204	9.71	175	11.49	264
2017	9.78	211	9.68	191	10.89	248
Average of 3 years	9.70	207	9.87	187	11.27	255

A sensitivity study of the effect of the optimization parameters has been performed. Thus, the best numerical parameter is 8° search step angle and two waypoints. The option of doubling the waypoints after the first optimization can improve the results. However, it was not activated because the improvement is small in comparison to the increase in simulation time.

The sensitivity of rated power on the capacity factor and energy produced, three years was also analyzed. The results of capacity factor, filling ratio and total annual energy production for 1 MW, 1.3 MW and 1.6 MW energy ship deployed at Saint-Pierre-et-Miquelon and Ile de Sein were presented. It is found that when the rated power increases, the optimal capacity factors decreases. In contrast, the produced energy increases with the increment of the rated power of the energy ship.

The sensitivity to storage capacity and unloading time effect on the capacity factor was also investigated. The results were also found to be sensitive to these parameters. Surprisingly, in Saint-Pierre-et-Miquelon, the shortest batteries storage capacity was found to give the best capacity factors. This indicates that the optimization method which is currently implemented in QtVlm converges to a local optimum and not the global optimum.

For the statistical analysis of the energy production, we found that the pattern and energy production trends were the same at both deployment locations, Saint-Pierre-et-Miquelon and Ile de Sein. It is shown that the energy ship produced maximum power for all storage capacity configurations at most of the delivery time. However, there is also a relatively high route frequency, which is close to zero energy production compared to other energy production classes. This result can be explained by weaker wind or no wind available at a particular time, especially in the Summertime.

Comparisons of the energy ship's capacity factor and stationary offshore wind turbines deployed at same area were performed. The average capacity factor of offshore wind turbines in both Saint-Pierre-et-Miquelon and Ile de Sein is 63%. It is 20% greater than that of energy ships.

CHAPTER 5

CONCLUSION AND PERSPECTIVES

This chapter will conclude the thesis by summarizing the main results and then presenting some perspectives of future research to complete and improve this work.

5.1. Conclusion

This thesis aimed at addressing the knowledge gap for the capacity factor of weather-routed energy ships. The four objectives of the thesis are recalled here:

1. Investigate the annual average capacity factor for a given energy ship design deployed in the North Atlantic Ocean; and compare it to stationary floating wind turbines.
2. Investigate the annual average capacity factor for a given energy ship design deployed in the nearshore; and compare it to stationary floating wind turbines.
3. Assess the sensitivity of the capacity factor to the ship characteristics: onboard storage capacity, energy unloading time, and velocity and power production polars.
4. Assess the sensitivity of the capacity factor to the parameters of the weather routing algorithm: number of initial optimization waypoints and search step angle.

Objective 1 was addressed in chapters 2 and 3. A method has been developed to optimize the capacity factor of energy ships using a modified version of the weather-routing software qtVlm. It was used to analyze and compare the capacity factors of energy ships to stationary offshore wind turbines that would be deployed far-offshore in the North Atlantic Ocean. We found that 1.6 MW energy ships that would have been deployed there during the years of 2015, 2016 and 2017 could have achieved capacity factors over 80%. This very high capacity factor is achieved thanks to weather-routing and also because the wind resource is very high in the North Atlantic Ocean. Indeed, we confirmed in chapter 2 previous results, which indicate that the capacity factor of stationary floating offshore wind farms deployed there could exceed 69%.

Objective 2 was addressed in chapter 4, in which we investigated the capacity factor of a 1.6 MW energy ship that would be deployed near shore in Saint-Pierre-et-Miquelon (French

archipelago) and Ile de Sein (French island). We found that energy ships could have achieved an average capacity factor of 53% at Saint-Pierre-et-Miquelon and 49% at Ile de Sein for the three years of 2015, 2016 and 2017. In comparison, the capacity factor of a floating wind turbine that would be deployed in the same areas is over 60%. The variation in capacity factor between the two systems is mainly due to the height of the wind turbine which allows access to greater wind speeds.

Objectives 3 and 4 were addressed in both chapters 3 and 4. The effect of the numerical parameters of the weather routing optimization on weather-routing has been studied, and it was determined that the best numerical parameters are 2 initial waypoints for a deployment nearshore 6 and 8° for the search step angle. For an energy ship deployed in the North Atlantic ocean, it was found that the capacity factor and energy production is sensitive to the storage capacity, unloading time configuration and the rated power of the energy ship. It was observed that as the energy ship's rated power increases, the capacity factor and filling ratio significantly decrease. In contrast, the energy produced increases with increasing rated power. In the nearshore, it was observed that the capacity factor decreases much more rapidly with increasing rated power than in the far offshore. The sensitivity to storage capacity and unloading time was also investigated for the energy ship deployed at the near shore. Surprisingly, in Saint-Pierre-et-Miquelon, the shortest batteries storage capacity gave the best capacity factors. In contrast, in Ile de Sein, the best capacity factor would be obtained with the most prolonged batteries storage capacity. Overall, several results of the sensitivity studies indicate that the optimization method currently implemented in QtVlm conclusively converges to a local optimum, not a global optimum.

5.2. Future work

In order to fill the extensive knowledge gap for the capacity factor of weather-routed energy ships, there are still the following aspects to be studied in the future.

First, this thesis has provided the foundation of a method for the performance assessment of a weather-routed energy ship. However, the energy ship capacity factor investigation does not include the effect of sea conditions, turbine reliability, biofouling, and hazard avoidance. It is critical to consider these dynamic elements for real-world production. Thus, further sensitivity studies considering the dynamic elements of energy ships' performance are needed for future work.

Second, the optimized capacity factors of the energy ship obtained with different storage capacities were somewhat surprising. We may have expected that greater storage capacity would lead to a more significant number of weather-routing options and thus a better capacity factor. Therefore, this dubiety the capability of the optimization method currently implemented in qtVlm to converge to the global optimum. Improved optimization methods should be developed.

Third, the weather-routing is highly dependent on weather data. In this thesis, MERRA2 datasets used in Renewable Ninja and ERA-INTERIM datasets provided by ECMWF were compared. In future work, other updated and quality-assured wind datasets, i.e., the ERA5 dataset from ECMWF, should be used in future weather-routing optimization of energy ships capacity factors.

REFERENCES

[1] Equinor (2019) 2019 Annual report and Form 20-F. Accessible online at https://www.equinor.com/content/dam/statoil/documents/annual-reports/2019/equinor-2019-annual-report-and-form-20f.pdf

[2] IEA (2021), Global Energy Review 2021, IEA, Paris https://www.iea.org/reports/global-energy-review-2021

[3] IRENA (2019), Future of wind: Deployment, investment, technology, grid integration and socio-economic aspects (A Global Energy Transformation paper), International Renewable Energy Agency, Abu Dhabi.

[4] Capps, Scott & Zender, Charles. (2009). Global ocean wind power sensitivity to surface layer stability. Geophys. Res. Lett. 36. 10.1029/2008GL037063.

[5] Archer, Cristina & Jacobson, Mark. (2005). Evaluation of global wind power. Journal of Geophysical Research. 110. 10.1029/2004JD005462.

[6] A Possner and K Caldeira (2017) Geophysical potential for wind energy over the open oceans. Proceedings of the National Academy of Sciences of the United States of America 114(43) pp 11338-43

[7] Capps, Scott & Zender, Charles. (2010). Estimated global ocean wind power potential from QuikSCAT observations, accounting for turbine characteristics and siting. Journal of Geophysical Research. 115.

[8] France Energie Eolienne (2019) 2019 Wind Obsevatory: Analysis of the French wind power industry: market, jobs and challenges. Accessible online at https://fee.asso.fr/wp-content/uploads/2019/10/2019-wind-observatory-final.pdf

[9] Wind Europe (2020). Offshore wind energy in Europe: Key trends and statistics 2019. Accesible online at https://windeurope.org/wp-content/uploads/files/about-wind/statistics/WindEurope-Annual-Offshore-Statistics-2019.pdf

[10] Musial, Walt, Heimiller, Donna, Beiter, Philipp, Scott, George, & Draxl, Caroline. (2016) Offshore Wind Energy Resource Assessment for the United States. United States. https://doi.org/10.2172/1324533

[11] Shoaib, Muhammad & Siddiqui, I. & Khan, Shamim & Alhems, Luai. (2019). Assessment of wind energy potential using wind energy conversion system. Journal of Cleaner Production. 216. 10.1016/j.jclepro.2019.01.128.

[12] Dupont, Elise & Koppelaar, Rembrandt & Jeanmart, Hervé. (2017). Global available wind energy with physical and energy return on investment constraints. Applied Energy. 209. 10.1016/j.apenergy.2017.09.085.

[13] Abd Jamil, R, Gilloteaux, J, Lelong, P, & Babarit, A. "Investigation of the Capacity Factor of Weather-Routed Energy Ships Deployed in the Near-Shore." *Proceedings of the ASME 2021 3rd International Offshore Wind Technical Conference*. *ASME 2021 3rd International Offshore Wind Technical Conference*. Virtual, Online. February 16–17, 2021. V001T01A003. ASME. https://doi.org/10.1115/IOWTC2021-3545

[14] Aaron Smith, Tyler Stehly, and Walter Musial (2015) 2014–2015 Offshore Wind Technologies Market Report.Technical Report NREL/TP-5000-64283

[15] Umoh, Kubiat & Lemon, Mark. (2020). Drivers for and Barriers to the Take up of Floating Offshore Wind Technology: A Comparison of Scotland and South Africa. Energies. 13. 5618. 10.3390/en13215618.

[16] Alexandra Cosseron, Udaya Bhaskar Gunturu, C. Adam Schlosser,(2013) "Characterization of the Wind Power Resource in Europe and its Intermittency", Energy Procedia,Vol.40, Pages 58-66, ISSN 1876-6102,(https://doi.org/10.1016/j.egypro.2013.08.008.)

[17] Abd-Jamil, R., Chaigneau, A., Gilloteaux, J-C., Lelong, P., Babarit, (2019) A. Comparison of the capacity factor of stationary wind turbines and weather-routed energy ships in the far-offshore. In Journal of Physics: Conference series, 1356, 2019

[18] McLaurin, D, Aston, A, & Brand, J. (2021) "Prevention of Offshore Wind Power Cable Incidents by Employing Offshore Oil/Gas Common Practices." Proceedings of the ASME 2021 3rd International Offshore Wind Technical Conference. ASME 2021 3rd International Offshore Wind Technical Conference. Virtual, Online. February 16–17, 2021. V001T02A002. ASME. https://doi.org/10.1115/IOWTC2021-3524

[19] H Hagiwara (1989) Weather routing of (sail-assisted) motor vessels PhD Thesis of Delft University of Technology

[20] Kim J and Park C (2010) Wind power generation with a parawing on ships, a proposal Energy, Elsevier 35(3) 1425-32

[21] JC Gilloteaux and A Babarit (2017) Preliminary design of a wind driven vessel dedicated to hydrogen production. 6th International Conference on Ocean, Offshore and Artic Engineering (OMAE2017) June 2017 Trondheim, Norway

[22] Aurélien Babarit, Gaël Clodic, Simon Delvoye, Jean-Christophe Gilloteaux, (2020) Exploitation of the far-offshore wind energy resource by fleets of energy ships, Part A, Energy ship design and performance. Wind Energy Science. 5. 839-853. 10.5194/wes-5-839-2020.

[23] G. Clodic, A. Babarit, J-C. Gilloteaux, (2018) Wind propulsion options for energy ships, In. Proc. Of the 1st International Offshore Wind Technical Conference (IOWTC), San Francisco, California,

[24] Loi n° 2015-992 du 17 aout 2015 Relative à la transition énergétique pour la croissance verte. Journal officiel de la République Française, 18 aout 2015

[25] C Mone, M Hand, M Bolinger, J Rand, D Heimiller and J Ho (2015) Cost of wind energy review. Technical report NREL/TP-6A20-66861 May 2017

[26] A Babarit, JC Gilloteaux, G Clodic, M Duchet, A Simoneau and M F Platzer (2018) Techno-economic feasibility of fleets of far offshore hydrogen-producing wind energy converters. International Journal of Hydrogen Energy 43(15) pp 7266-89

[27] Manual of qtVlm version 5.8.3 downloaded at http://download.meltemus.com/qtvlm/qtVlm_documentation_en.pdf

[28] L Walther, A Rizvanolli, M Wendebourg and C Jahn (2016) Modeling and optimization algorithms in ship weather routing International Journal of e-Navigation and Maritime Economy 4 pp 31-45

[29] M F Platzer, Sarigul-Klijn, J Young, M A Ashraf and J C S Lai (2014) Renewable hydrogen production using sailing ships ASME Journal of Energy Resources Technology 136 / 021203-1

[30] Enercon (2013) Enercon e-ship 1: A wind-hybrid commercial cargo ship Presentation at 4th Conference on Ship efficiency Hamburg, Germany

[31] Det Norske Veritas (DNV) (2010) Recommended practice DNV-RP-C205; Environmental conditions and environmental loads downloaded at http://www.dnv.com

[32] R.E. Salomon. (1982) Process of converting wind energy to elemental hydrogen and apparatus therefor, Patent US4335093A Salomon

[33] Ouchi K. and Henzie J. (2017) Hydrogen generation sailing ship, conceptual design and feasibility study Proceeding of IEEE OCEAN 2017 conference, Aberdeen, UK.

[34] GIZARA, Andrew R. (2007). Turbine-Integrated Hydrofoil (US7298056). United State Patent. https://patents.google.com/patent/US7298056/no

[35] Meller M.: Wind-power linear motion hydrogen production systems. U.S. Patent 7,146,918 B2, 2006)

[36] Diyoke, C. (2019) A new approximate capacity factor method for matching wind turbines to a site: case study of Humber region, UK. Int J Energy Environ Eng 10, 451–462. https://doi.org/10.1007/s40095-019-00320-5

[37] C.L. Archer, M.Z. Jacobson, (2015) Evaluation of global wind power, J. Geophys. Res.:Atmos. 110 (D12), https://doi.org/10.1029/2004JD005462.

[38] GWEC (2021) Global wind report, Global Wind Energy Council, accessible online at https://gwec.net/global-wind-report-2021/

[39] Chidiebere Diyoke, (2019), A new approximate capacity factor method for matching wind turbines to a site: case study of Humber region, UK

[40] Alyssa Pek (2021) GWEC releases Global Wind Turbine Supplier Ranking for 2020, GWEC, Brussels, accessible online at https://gwec.net/gwec-releases-global-wind-turbine-supplier-ranking-for-2020/

[41] Giles Hundleby, Kate Freeman (2017) Unleashing Europe's offshore wind potential: A new resource assessment, Wind Europe.org

[42] GWEC (2019) Global wind report, Global Wind Energy Council, accessible online at https://gwec.net/global-wind-report-2019/

[43] Wind Europe (2020) Wind energy in Europe in 2019 - Trends and statistics accessible online at https://windeurope.org/intelligence-platform/product/wind-energy-in-europe-in-2019-trends-and-statistics/#

[44] Wind Europe (2021) Wind energy in Europe: 2020 Statistics and the outlook for 2021-2025 accessible online at https://windeurope.org/intelligence-platform/product/wind-energy-in-europe-in-2020-trends-and-statistics/

[45] Şahin, Ahmet. (2004). Progress and recent trends in wind energy. Progress in Energy and Combustion Science. 30. 501-543. 10.1016/j.pecs.2004.04.001.)

[46] Yogesh Kumar, Jordan Ringenberg, Soma Shekara Depuru, Vijay K.Devabhaktuni, Jin Woo Lee, Efstratios Nikolaidis, Brett Andersen, Abdollah Afjeh (2015). Wind energy: Trends and enabling technologies. Renewable and Sustainable Energy Reviews. 53. 209–224. 10.1016/j.rser.2015.07.200.

[47] Lennie, Matthew & Pechlivanoglou, Georgios & Marten, David & Nayeri, Christian & Paschereit, Christian. (2015). A Review of Wind Turbine Polar Data and its Effect on Fatigue Loads Simulation Accuracy. 10.1115/GT2015-43249.

[48] Juan Pablo Sanchez De Lara Garcia (2013) Wind turbine database: Modelling and analysis with focus on upscaling, Master's thesis Chalmers University Of Technology, Goteborg, Sweden

[49] Dong, Wenbin & Xing, Yihan & Moan, Torgeir. (2012). Time Domain Modeling and Analysis of Dynamic Gear Contact Force in a Wind Turbine Gearbox with Respect to Fatigue Assessment. Energies. 5. 10.3390/en5114350.

[50] Paynter, R.J.H., Lipman, N.H., Foster, J.E., 1991. The potential of hydrogen and electricity production from wind energy. Energy Research Unit, Rutherford Appleton Laboratory, September

[51] Abed, K.A. & El-Mallah, A.A., (1997) "Capacity factor of wind turbines," Energy, Elsevier, vol. 22(5), pages 487-491. https://ideas.repec.org/a/eee/energy/v22y1997i5p487-491.html

[52] Boccard, Nicolas. (2009). Capacity Factor of Wind Power: Realized Values vs. Estimates. SSRN Electronic Journal. 10.2139/ssrn.1285435.

[53] BWEA. (2006) Submission to energy review. Technical report, BritishWind Energy Association.

[54] EWEA. (2008) Wind energy scenarios up to 2030. Technical report, European Wind Energy Association, 3

[55] IRENA (2021), Renewable energy statistics 2021, International Renewable Energy Agency, Abu Dhabi.

[56] Newman, Nicholas. (2018). Wind-Power in Europe. 10.13140/RG.2.2.29979.52003.

[57] IRENA (2020), Renewable power generation cost in 2019, International Renewable Energy Agency, Abu Dhabi.

[58] Dilara Gulcin Caglayan, David Severin Ryberg, Heidi Heinrichs, Jochen Linßen, Detlef Stolten, Martin Robinius, (2019)The techno-economic potential of offshore wind energy with

optimized future turbine designs in Europe, Applied Energy, Volume 255, 113794,ISSN 0306-2619, https://doi.org/10.1016/j.apenergy.2019.113794.

[59] Bailey, Helen & Brookes, Kate & Thompson, Paul. (2014). Assessing Environmental Impacts of Offshore Wind Farms: Lessons Learned and Recommendations for the Future. Aquatic biosystems. 10. 8. 10.1186/2046-9063-10-8.

[60] Ackermann, Thomas & Leutz, Ralf & Hobohm, J.. (2001). World-wide offshore wind potential and European projects. 4 - 9 vol.1. 10.1109/PESS.2001.969970.

[61] Van der Valk, Paul. (2014). Coupled Simulations of Wind Turbines and Offshore Support Structures: Strategies based on the Dynamic Substructuring Paradigm. 10.4233/uuid:ac619319-9eae-443d-8b94-d0246f80ffdb.

[62] European Wind Energy Association. (2013) The European offshore wind industry - key trends and statistics 2013. Technical report, EWEA

[63] Byrne, Byron & Houlsby, Guy. (2004). Foundations for offshore wind turbines. Philosophical transactions. Series A, Mathematical, physical, and engineering sciences. 361. 2909-30. 10.1098/rsta.2003.1286.

[64] Sánchez, & López-Gutiérrez, & Negro, Vicente & Esteban, M. Dolores. (2019). Foundations in Offshore Wind Farms: Evolution, Characteristics and Range of Use. Analysis of Main Dimensional Parameters in Monopile Foundations. Journal of Marine Science and Engineering. 7. 441. 10.3390/jmse7120441.

[65] IEA (2019), Offshore wind outlook 2019, IEA, Paris accessible online at https://iea.blob.core.windows.net/assets/495ab264-4ddf-4b68-b9c0-514295ff40a7/Offshore_Wind_Outlook_2019.pdf

[66] H. Stiesdal (2009). Hywind: The world's first floating MW-scale wind turbine. Wind Directions, pages 52–53, accessible online at https://www.evwind.es/2009/12/28/hywind-the-world%C2%92s-first-floating-mw-scale-wind-turbine-by-henrik-stiesdal/3092

[67] IRENA (2018), "Offshore innovation widens renewable energy options: Opportunities, challenges and the vital role of international co-operation to spur the global energy transformation" (Brief to G7 policy makers), International Renewable Energy Agency, Abu Dhabi.

[68] Equinor (2021) Hywind Scotland remains the UK's best performing offshore wind farm. Accessible online at https://www.equinor.com/en/news/20210323-hywind-scotland-uk-best-performing-offshore-wind-farm.html

[69] IEEFA (2019) Equinor to build world's largest floating offshore wind project near the Canary Islands accessible online at https://ieefa.org/equinor-to-build-worlds-largest-floating-offshore-wind-project-near-the-canary-islands/

[70] European Centre for Medium-Range Weather Forecasts (ECMWF) reanalysis dataset accessible online at https://apps.ecmwf.int/datasets/data/interim-full-daily/levtype=sfc/

[71] Raphael Alwan , Aurelien Babarit , Thomas Choisnet , Jean-Christophe Gilloteaux (2019) Preliminary study of sailing wind turbines for the harvesting of the far-offshore wind energy resource, EAWE PhD Seminar 2019, Nantes, sciencesconf.org:eawephd2019:282860

[72] Bowditch, N., (2002). The American Practical Navigator: An epitome of navigation. National Imagery and Mapping Agency, Bethesda, Marland, USA. Acces from https://thenauticalalmanac.com/Bowditch.pdf

[73] Wang, H., (2018). Voyage Optimization Algorithms for Ship Safety and Energy-Efficiency. Licentiate Thesis. Chalmers University of Technology, Gothenburg, Sweden.

[74] Wang, Helong & Mao, Wengang & Eriksson, Leif. (2019). A Three-Dimensional Dijkstra's algorithm for multi-objective ship voyage optimization. Ocean Engineering. 186. 106131. 10.1016/j.oceaneng.2019.106131

[75] Marie, S., Courteille, E., (2009). Multi-objective optimisation of motor vessel route. TransNav Int. J. Mar. Navigation Saf. Sea Trans. 3, 133–14.

[76] Bijlsma, S.J., (1975). On Minimal-Time Ship Routing. Ph.D. thesis. Royal Netherlands Meteorological Institute, Delft University of Technology, Delft.

[77] DNVGL, (2015). Energy Management Study 2015 (Høvik, Norway). www.dnvgl.com.

[78] Hinnenthal, J., (2008). Robust Pareto Optimum Routing of Ships Utilizing Deterministic and Ensemble Weather Forecasts. PhD thesis. Technischen Universitat Berlin, Berlin, Germany.

[79] https://www.predictwind.com/

[80] https://www.adrena-software.com/en/

[81] https://mytimezero.com/

[82] https://fastseas.com/

[83] https://www.meltemus.com/index.php/en/

[84] Roh, Myung-Il. (2013). Determination of an economical shipping route considering the effects of sea state for lower fuel consumption. International Journal of Naval Architecture and Ocean Engineering. 5. 10.3744/JNAOE.2013.5.2.246.

[85] Tom Russel (2021) Hywind Scotland breaks capacity factor record. Equinor. Accessible online at https://www.4coffshore.com/news/hywind-scotland-breaks-capacity-factor-record-nid21202.html

[86] European Centre for Medium-Range Weather Forecasts (ECMWF) reanalysis dataset accessible online at https://apps.JCecmwf.int/datasets/data/interim-full-daily/levtype=sfc/

[87] Hans Hersbach, Bill Bell, Paul Berrisford, András Horányi, Joaquín Muñoz Sabater, Julien Nicolas, Raluca Radu, Dinand Schepers, Adrian Simmons, Cornel Soci, Dick Dee (2019) Global reanalysis: Goodbye ERA-Interim, hello ERA5, ECMWF Newsletter (No.159) accessible online at https://www.ecmwf.int/en/newsletter/159/meteorology/global-reanalysis-goodbye-era-interim-hello-era5

[88] Szlapczynska, Joanna & Smierzchalski, Roman. (2007). Adopted isochrone method improving ship safety in weather routing with evolutionary approach. International Journal of Reliability, Quality and Safety Engineering - IJRQSE. 14. 10.1142/S0218539307002842.

[89] Insee, (2021), Comparateur de territoire: Commune d'ile-de-sein (29083), detailed figures published on 21/04/2021, accesible online at https://www.insee.fr/fr/statistiques/1405599?geo=COM-29083

[90] Collectivité territoriale Saint-Pierre-et-Miquelon, (2018) Délibération n°136/2018: Programmation pluriannuelle de l'energie pour l'archipel de Saint-Pierre et Miquelon accesible online at https://www.jo-spm.fr/doc_jo/DELIB2018-0136.pdf

[91] Iain Staffell, Stefan Pfenninger (2016) Using bias-corrected reanalysis to simulate current and future wind power output, Energy, Volume 114, p.p 1224-1239, ISSN 0360-5442, https://doi.org/10.1016/j.energy.2016.08.068.

[92] Ramon, Jaume & Lledo, Llorenç & Torralba, Verónica & Soret, Albert & Doblas-Reyes, Francisco. (2019). What global reanalysis best represents near surface winds?. Quarterly Journal of the Royal Meteorological Society. 10.1002/qj.3616.

[93] Kabir Sadeghi and Hudaverdi Tozan (2018) Tension leg platforms: An overview of planning, design, construction and installation, Academic Research International, Volume 9 (2), p.p 55-65, ISSN 2223-9944.

[94] Blue H engineering (N/A) The Blue H historical technology development, accessible online at http://www.bluehengineering.com/historical-development.html.

[95] Sohoni, Vaishali & Gupta, S. & Nema, Rajesh. (2016). A Critical Review on Wind Turbine Power Curve Modelling Techniques and Their Applications in Wind Based Energy Systems. Journal of Energy. 2016. 1-18. 10.1155/2016/8519785.

APPENDIX 1

QTVLM SETTING AND CONFIGURATIONS

1.1.Route optimization using QtVlm

The multi-route optimization result is displayed in a Routes Comparator, which can be exported in CSV format. It contains various information and data regarding each route that has been optimized for a predetermined period (in this study is a period of one year). The important information and data displayed in the route comparator for this study is the start date and time and estimate time of arrival (ETA) of each route, sailed duration, sailed distance, an average of boat speed, average true wind speed (TWS), capacity factor, filling ratio and energy produced for one complete optimized route (see Figure A1- 1).

Other than route comparator, route logs displayed the data of true wind speed (TWS), true wind direction (TWD), true wind angle (TWA), apparent wind speed (AWS), apparent wind angle (AWA), capacity factor, filling ratio, and energy produced for specified time interval. The interval time can be specified with minimum of 5 minutes and the logs can be exported in CSV format.

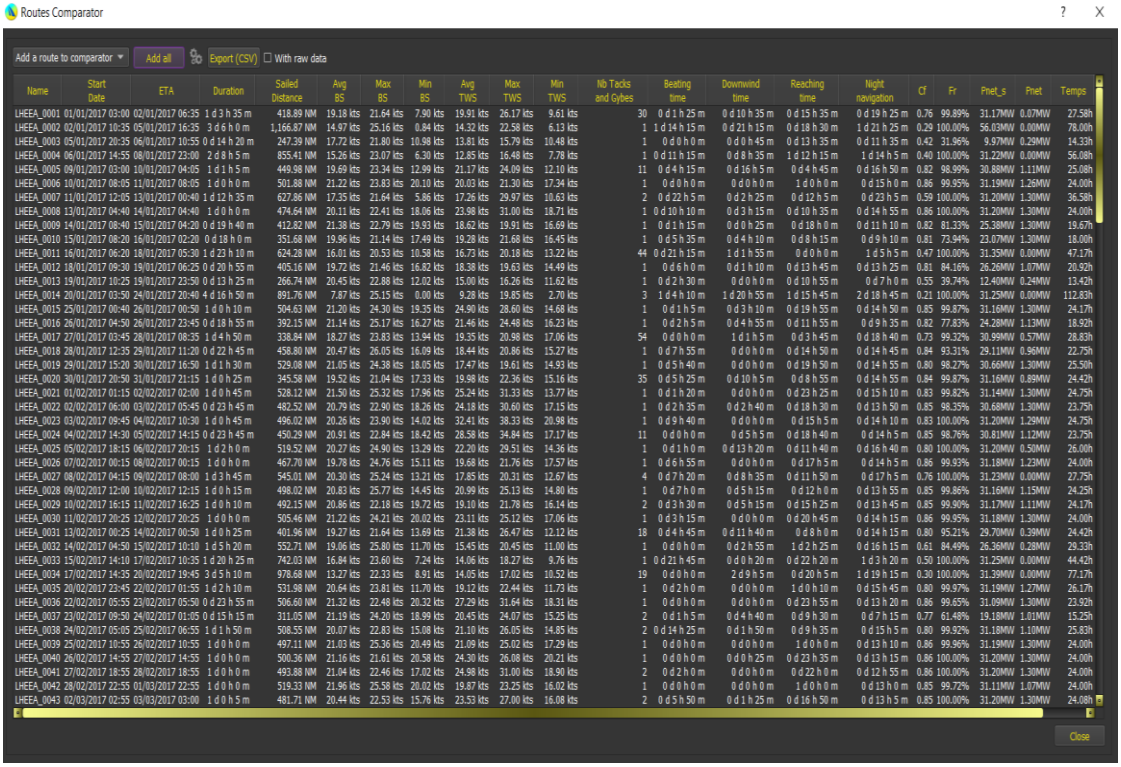

Figure A1- 1 Route comparator display the result of the multi-routes optimization

QtVlm menu has a configuration function, with all qtVlm settings. In configuration function, sub-function Routes (‘General’ configuration), the numerical parameter of initial search step angle used in the initial optimization process can be determined (see Figure A1- 2). The search step angle is used as a first distance to initialize the first step of the simplex and to increase the search range. It is not a bearing but a distance where one minute latitude is equal to one NM. It has nothing to do with the boat position or boat heading. It represents how far away from a POI the simplex will initially look when optimizing the capacity factor over the route. The standard public version of QtVlm does not have this field, and instead compute the optimal value based on the neighboring points.

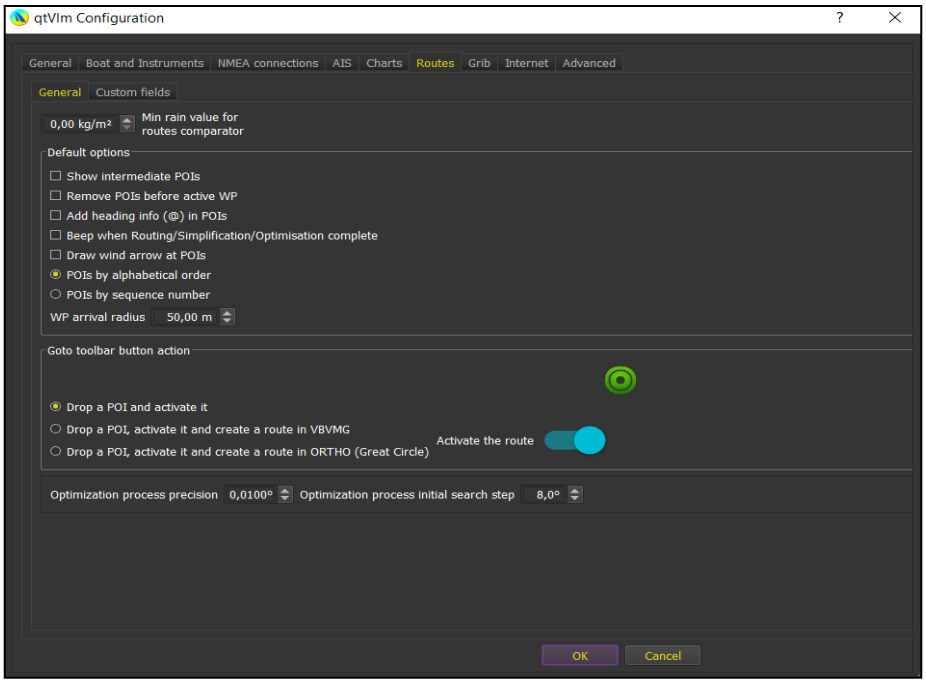

Figure A1- 2 QtVlm weather routing optimization configurations (General configurations)

The performance of the energy ship is characterized by polar plots for its speed and power production and this polar is use as an input for the energy ship capacity factor optimization.

In sub-function Routes ('Custom fields' configuration), the optimization criterion and its target value can be determined, and the polar of the energy ship's power production can be loaded (see Figure A1- 3). Meanwhile, the energy ship's velocity polar can be loaded into the boat menu which has the configuration functions for all boat's setting. The efficiency of upwind and downwind can also be determined in the boat setting field (see Figure A1- 4).

In the 'special LHEEA route' settings, the parameter used for the energy ship's capacity factor optimization, such as the numerical parameter (initial optimization waypoints), initial route target filling ratio and energy ship's sailing capability (energy ship power rating, storage capacity and unloading time) can be determined. The option to double the number of waypoints after the first optimization can also be selected in this 'special LHEEA route' settings (see Figure A1- 3).

The boundary of the sailing area also can be specified in this section by specifying the minimum and maximum latitude and longitude. But the energy ship's

weather routed optimization in this study is not bounded by sailing area and this option is not taken into consideration.

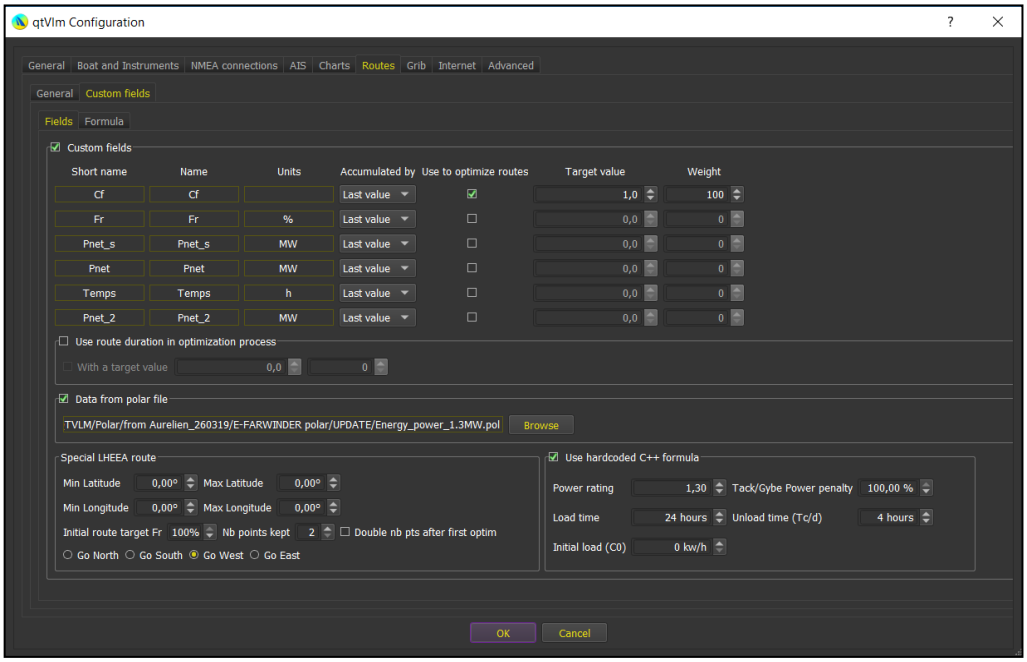

Figure A1- 3 ‘Special LHEEA route’ setting in QtVlm weather routing optimization configurations (Custom fields configuration)

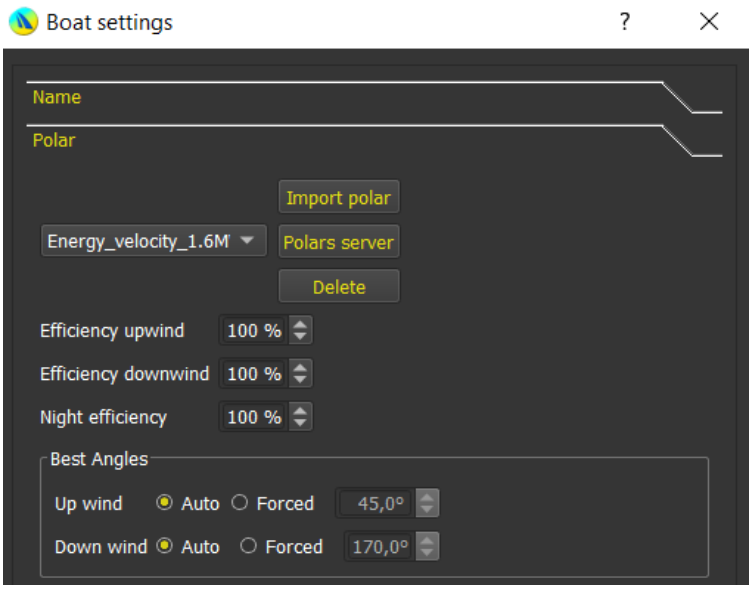

Figure A1- 4 Boat setting in QtVlm

In general, QtVlm can open or download a wide number of grib types (grib 1 or grib 2) [75]. Various types of download are available. QtVlm menu manages gribs (see Figure A1- 5). Three slots are available, where gribs can be loaded from different sources, containing different data or resolutions. It is also possible to merge gribs, for

instance to build a single grib containing Winds, Currents and Waves or merge gribs for few months or annual data. In this study, only winds grib for annual winds data are loaded into the slot.

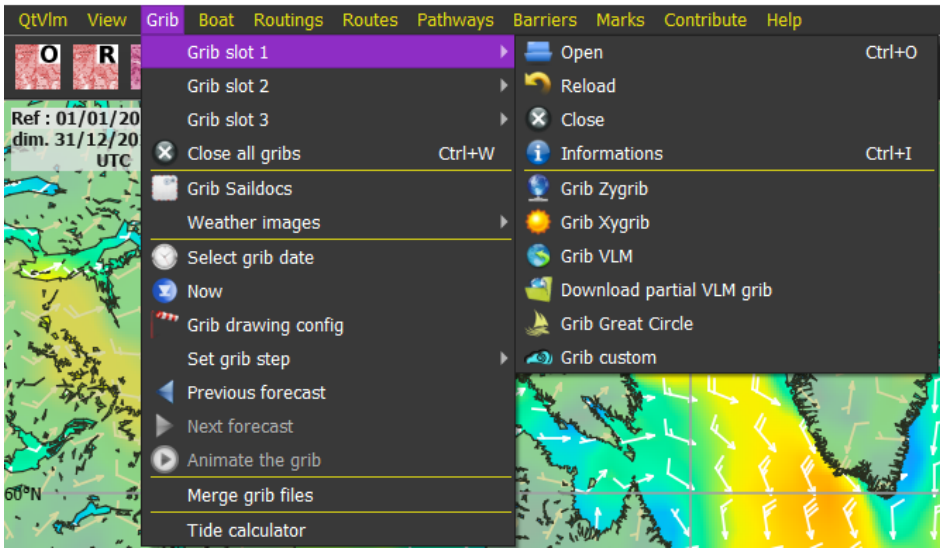

Figure A1- 5 Grib slot to enable QtVlm viewing grib files (weather data files)

Routes menu manages routes where the creation, deletion, edition, import, export, and comparing route can be made (see Figure A1- 6). For the custom built QtVlm batch-mode version used in this study, the optimization period and the unloading time can be defined here. The unloading time is the time required to unload the stored energy onboard the energy ship to the storage onshore.

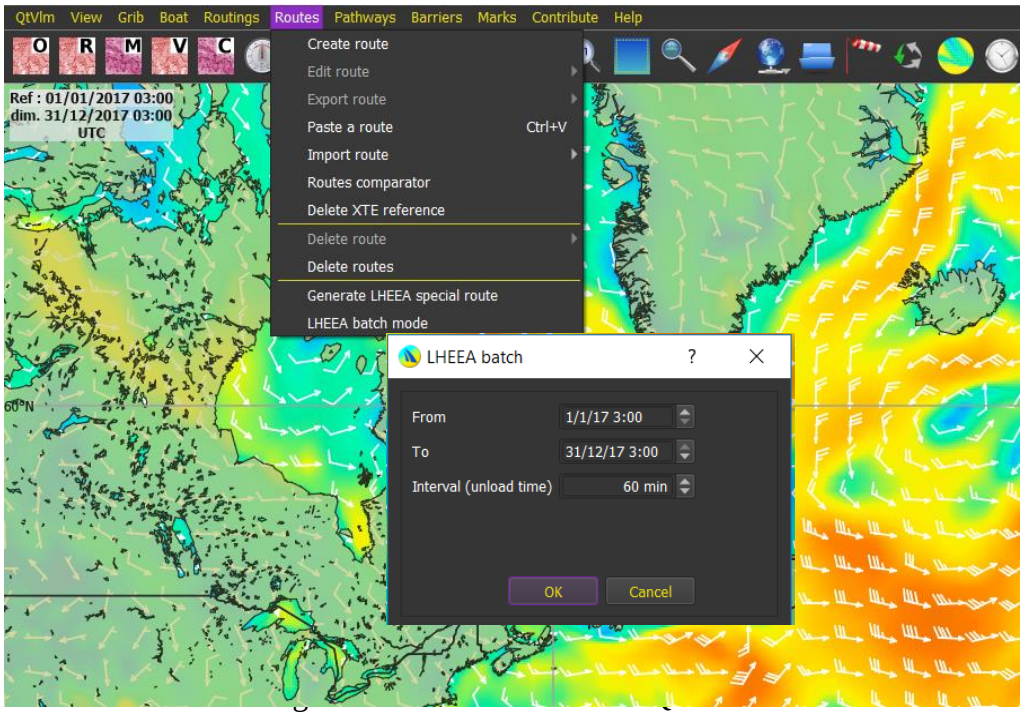
QtVlm View Grib Boat Routings Routes Pathways Barriers Marks Contribute Help
Create route
Edit route
Export route
Paste a route Ctrl+V
Import route
Routes comparator
Delete XTE reference
Delete route
Delete routes
Generate LHEEA special route
LHEEA batch mode
Ref : 01/01/2017 03:00
dim. 31/12/2017 03:00
UTC
60°N
LHEEA batch
From 1/1/17 3:00
To 31/12/17 3:00
Interval (unload time) 60 min
OK
Cancel

APPENDIX 2

SENSITIVITY STUDIES TO OPTIMIZATION PARAMETERS

It is essential to conduct an in-depth study of all the optimization parameters. Therefore, in this chapter, sensitivity studies have been performed to investigate the sensitivity of the optimized capacity factor of the energy ship in response to the two main parameters, the energy ship's sailing capability and numerical optimization parameter. This chapter consists of two parts of sensitivity analysis. The first part is the numerical optimization parameters as a function of the number of initial optimization waypoints and search step angle. In this part also present the analysis of effect of using double waypoint after first optimization option in QtVlm (presented in Chapter 1). The second part is the sensitivity of the energy ship's sailing capability as a function of the storage capacity aboard and unloads time and different rated power of the energy ship. This chapter presents the sensitivity analysis results compare and defines the best and optimal parameter to obtain the optimal capacity factor of an energy ship. It is shown that the optimization with optimal parameters input makes it possible to significantly increase the optimized capacity factor obtained by the energy ship proposed in this thesis.

2.1.Sensivity to numerical parameters

2.1.1. Data and input parameters

The energy ship capacity factor optimization results may also depend on the numerical optimization parameters as a function of the initial optimization search step angle and initial optimization waypoints.

This sensitivity study involved 1.6MW and 1.3MW rated energy ship both respectively deployed at Saint-Pierre-et-Miquelon and Ile de Sein. Except for a single case of a 1.6MW energy ship in Saint-Pierre-et-Miquelon which extended the analysis

to 36 waypoints and 16°, 32° and 64°, subsequent analysis for the other cases, each numerical optimization parameter as a function of search steps angle and initial optimization waypoints assessed for 6 clustered search steps angle ranging from 0.5° to 8°; and 6 clustered initial optimization waypoints ranging from 2 waypoints to 18 waypoints. Each search steps angle is set to 0.5°, 1°, 2°, 4°, 6°, and 8° are individually compared to each corresponding optimization search step angle that is set to 2, 4, 6, 12 and 18 waypoints.

In this sensitivity analysis, the default setting for the energy ship's sailing capability parameter as a function of the storage capacity aboard and unload time is fixed at 24 hours storage capacity and 4 hours unload time.

The sensitivity was measured by the average optimized capacity factor, using qtVlm weather routing software for three years of wind data, 2015, 2016 and 2017 presented in Chapter 2. The optimized capacity factor obtained for each year is then the average capacity factor over 3 years period is determined, presented and compared in the following section.

2.1.2. Sensitivity of initial optimization waypoints and search step angle

At the beginning of the sensitivity analysis, the analysis was started with 0.5° search step angle and 12 waypoints as the cluster of reference. Then, the value of search step angle were doubled up to 64° and assessed individually with 12 waypoints. Then the number of waypoints is decreased and increases accordingly and assessed individually to each search step angle to define the pattern of optimized capacity factor in response to the initial optimization waypoints and search step angle. Once the pattern has been identified the subsequent sensitivity analysis is limit to maximum of 18 numbers of waypoints and 8° search step angle.

Figure A2- 1 and Figure A2- 2 show the average capacity factor for the three years (2015, 2016 & 2017) for the sensitivity of search step angle and the initial number of optimization waypoints respectively at Saint-Pierre-et-Miquelon and Ile de Sein for 1.6MW energy ship.

In Figure A2- 1 one can see that for 2 initial optimization waypoints, as the search step angle increases, the average capacity factor also increases to a maximum of 52.8% at 8° search steps angle. However, this trend does not continue as the capacity

factor dropped to 52.5% when the search step angle reached at 16° search step angle. However, the absolute difference in capacity factor is slight, which is only 0.3%.

The maximum capacity factor for cluster of 4 initial optimization waypoints is 51.3% obtained by 32° search step angle, and 6 initial optimization waypoints are 50.1% obtained by 16° search step angle. For 12, 18 and 36 initial optimization waypoints, the capacity factor fluctuated as the search step angle increases. The maximum capacity factors respectively are 46.4%, 44.9% and 43.1%. However, these capacity factors are still cannot beat the best capacity factor obtained by 2 initial optimization waypoints and an 8° search step angle.

The decrement of average capacity factors can be seen as the initial optimization waypoints increase. The highest and best average capacity factor for the 1.6MW energy ship in Saint-Pierre-et-Miquelon was 52.8%, obtained by 2 initial optimization waypoints and 8° search step angle. These results were used to define the pattern of optimized capacity factor in response to different numerical parameters. It shown that the highest optimized capacity factor (52.8%) for 1.6MW energy ship at Saint-Pierre-et-Miquelon obtained by 2 initial optimization waypoints and 8° of optimization search step angle.

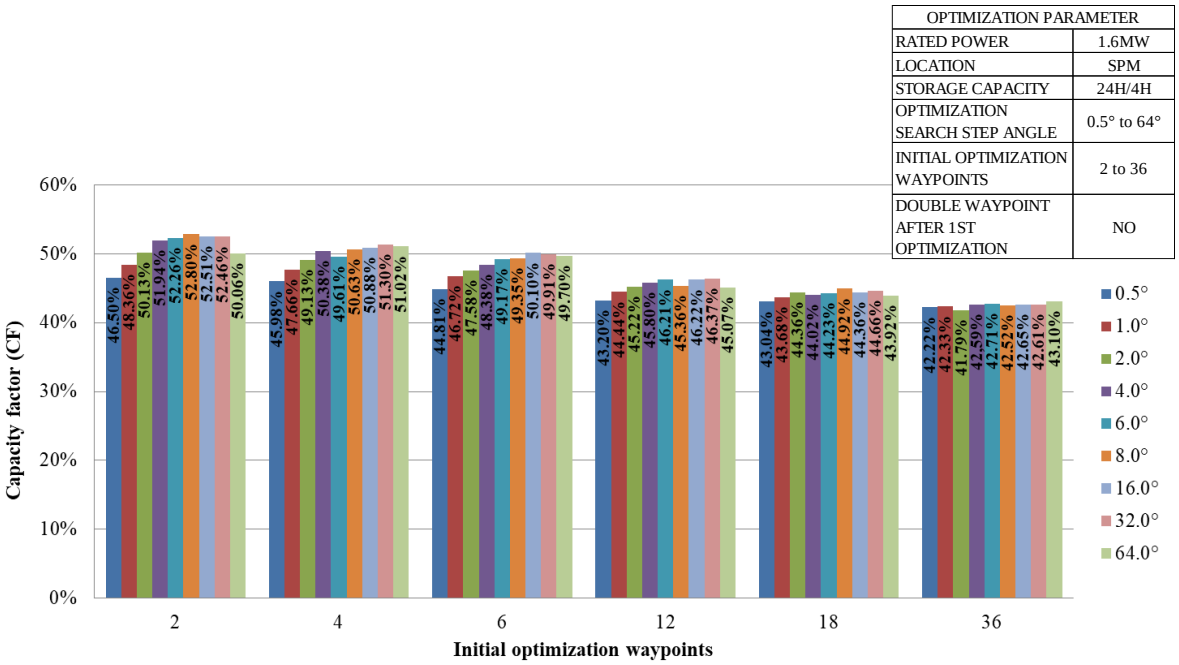

Figure A2- 1 Sensitivity study on weather routing optimization criteria. The results of the 6 clustered initial optimization waypoints and 9 clustered optimization search steps angle for 1.6MW energy ship in Saint-Pierre-et-Miquelon (average of 2015, 2016 & 2017) are presented. These results influence by 6 different initial waypoints of optimization that are set to 2, 4, 6, 12, 18 and 36; and 9 different optimization search steps.

Meanwhile, Figure A2- 2 shows the same information for 1.6MW energy ship deployed at Ile de Sein. The results show that the capacity factor also decrease as the initial optimization waypoints increase with the highest average capacity factor, 49.3%, obtained by 2 initial optimization waypoints and 6° search step angle. The optimized capacity factor reduced when the optimization search step angle increased to 8°. The maximum capacity factor for another cluster of 4, 6, 12 and 18 optimization waypoints respectively are 47.6%, 44.9%, 41.4% and 39.9%.

The best average capacity factor obtained in Ile de Sein (49.3%) for a 1.6MW energy ship was slightly lower than the best average capacity factor obtained in Saint-Pierre-et-Miquelon (52.8%) absolute difference of 3.5%. Overall, one can see that the optimized capacity factor obtained by two initial optimization waypoints is more sensitive than the 18 and 36 waypoints, where minimal changes in the optimized capacity factor obtained by those number of waypoints. One can also note that subsequent sensitivity analysis limits 18 numbers of waypoints and 8° search step angle. The limit is due to the identified pattern of optimized capacity factor obtained in sensitivity analysis for 1.6MW energy ship in Saint-Pierre-et-Miquelon.

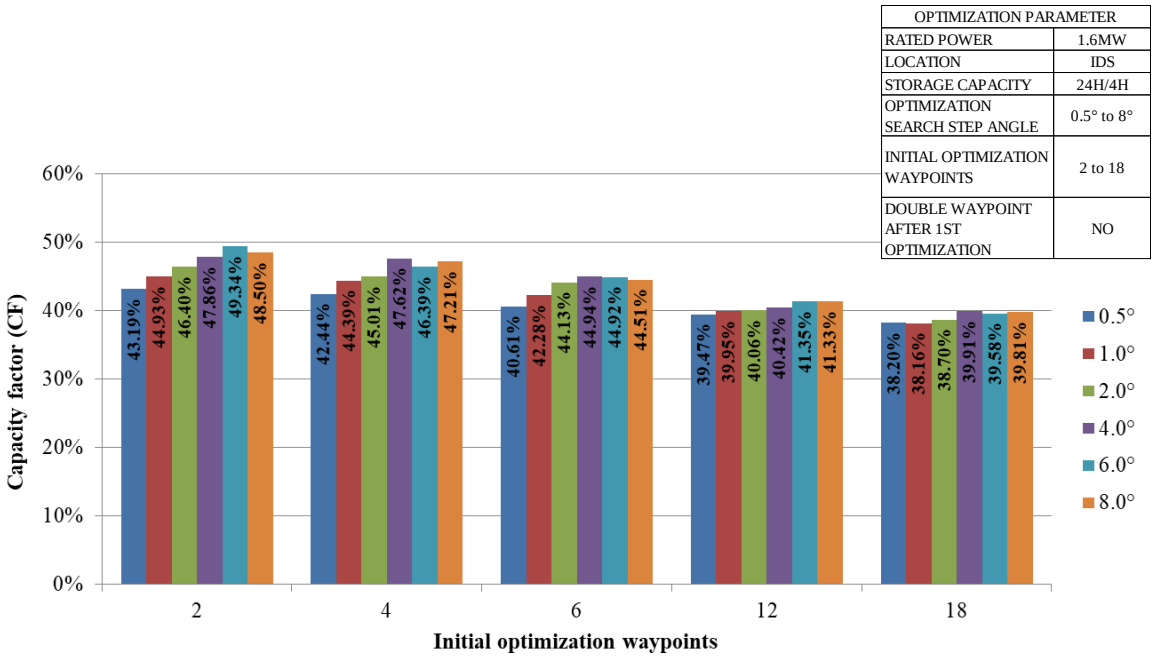

Figure A2- 2 Sensitivity study on weather routing optimization criteria. The results of the 5 clustered initial optimization waypoints and 6 clustered optimization search steps angle for 1.6MW energy ship in Ile de Sein (average of 2015, 2016 & 2017) are presented. These results influence by 5 different initial waypoints of optimization that are set to 2, 4, 6, 12, and 18; and 6 different initial optimization search steps.

Next, Figure A2- 3 and Figure A2- 4 show the average capacity factor for the three years (2015, 2016 & 2017) as a function of the search step angle and the initial number of optimization waypoints for 1.3MW energy ship deployed in Saint-Pierre-et-Miquelon and Ile de Sein.

In Figure A2- 3, the results show that for two initial optimization waypoints, as the search step angle increases, the average capacity factor also increases to a maximum of 55.6% at a 6° search steps angle. However, this trend does not continue as the capacity factor dropped to 55.1% when the search step angle reached an 8° search step angle.

The maximum capacity factor for another cluster of 4, 6 and 12 initial optimization waypoints are respectively 53.9%, 52.1%, 49.9% obtained by 8° search step angle. Meanwhile, for 18 initial optimization waypoints, the maximum capacity factor of 47.8% obtained by a 6° search step angle.

Similarly, with the results obtained for the sensitivity study for 1.6MW energy ship, the decrement of average capacity factors can be seen for 1.3MW energy ship as the initial optimization waypoints increase. The highest average capacity factor for the 1.3MW

energy ship in Saint-Pierre-et-Miquelon was 55.6%, obtained by two initial optimization waypoints and a 6° search step angle.

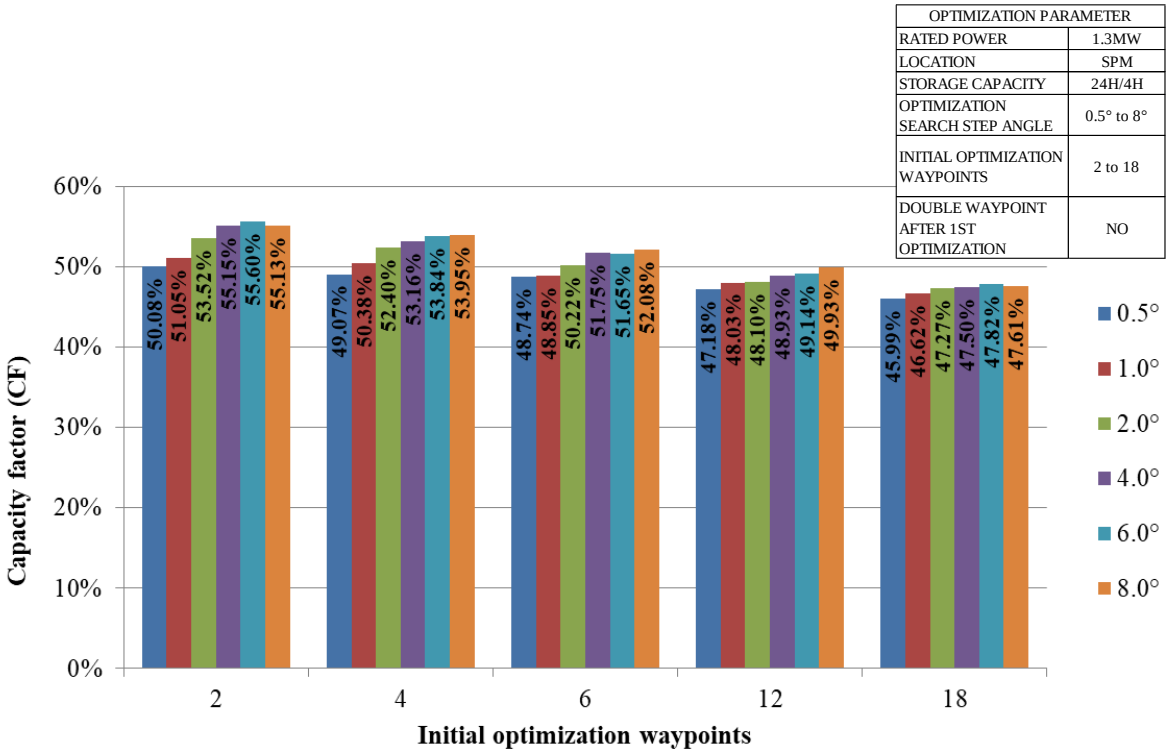

Figure A2- 3 Sensitivity study on weather routing optimization criteria. The results of the 5 clustered initial optimization waypoints and 6 clustered optimization search steps angle for 1.3MW energy ship in Saint-Pierre-et-Miquelon (average of 2015, 2016 &

In Figure A2- 4, shows the same information for 1.3MW energy ship in Ile de Sein. The results show that the capacity factor also decrease as the initial optimization waypoints increase with the highest average capacity factor, 51.1%, obtained by 2 initial optimization waypoints and 8° search step angle. The average capacity factor obtained in Ile de Sein slightly lower than average capacity factor obtained in Saint-Pierre-et-Miquelon (55.6%) with absolute different of 4.5%.

The maximum capacity factor for another cluster of 4, 6 and 12 initial optimization waypoints are respectively 49.7%, 47.2% and 43.9% obtained by 6° search step angle and for 18 obtained by 8° search step angle. Meanwhile, for 18 initial optimization waypoints, maximum capacity factor of 42.7% obtained by 4° search step angle.

The best average capacity factor obtained in Ile de Sein (51.1%) for 1.3MW energy ship slightly lower than the best average capacity factor obtained in Saint-Pierre-et-Miquelon (55.6%) with an absolute difference of 3.5%.

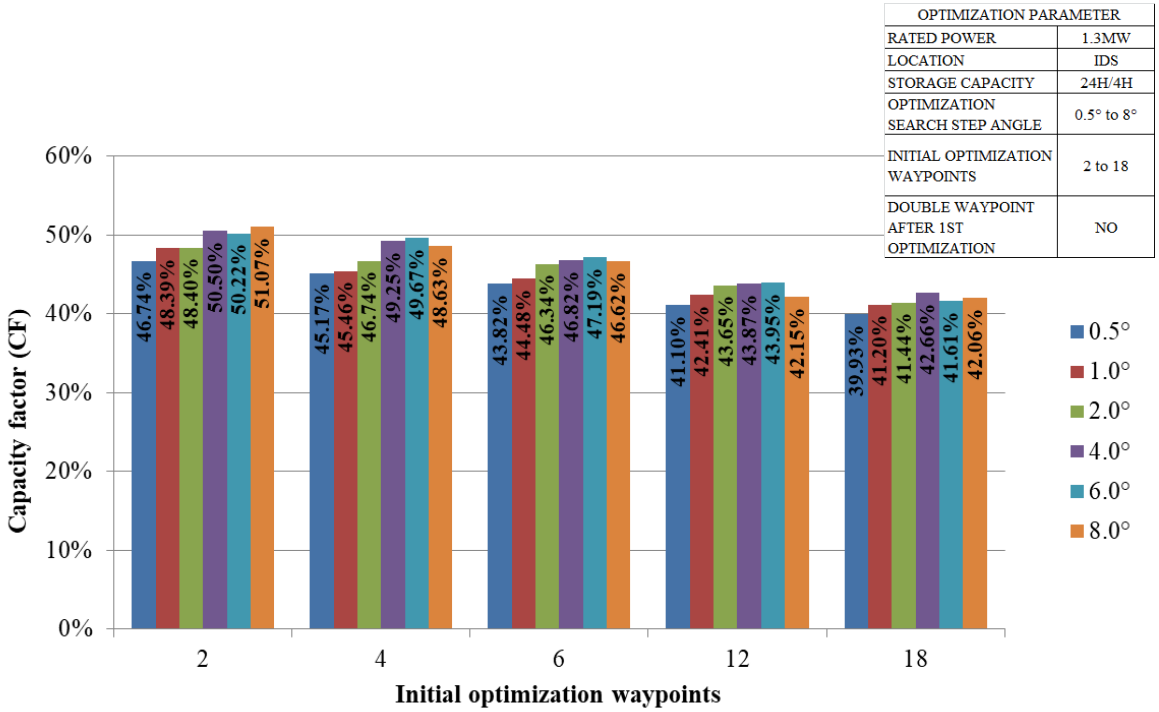

Figure A2- 4 Sensitivity study on weather routing optimization criteria. The results of the 5 clustered initial optimization waypoints and 6 clustered optimization search steps angle waypoints for 1.3MW energy ship in Ile de Sein (average of 2015, 2016 & 2017)

Table A2- 1 shows the summary of this sensitivity study production. The best average capacity factor over three years (2015, 2016 and 2017) for 1.3MW energy ship in Saint-Pierre-et-Miquelon (55.6%) and Ile de Sein (51.1%) are higher compared to the best average capacity factor for 1.6MW in the same deployment location, Saint-Pierre-et-Miquelon (52.8%) and Ile de Sein (49.3%). Best initial optimization waypoints obtained highest capacity factor is 2 initial waypoints. In other hand, the best optimization search step angle is between 6 and 8°. One would think more points initially in the route would be better, but that may be actually be counter-productive, because of the way the simplex works: it optimizes one point after another, so if the points n+1 and n-1 are too close the algorithm will not have enough space to work correctly. The Simplex algorithm used in QtVlm route's optimization process has been modified to use the custom fields accumulation parameters (see Figure 14) as a goal instead of best estimated time arrival.

This sensitivity analysis also shows that the optimal capacity factor is also significantly sensitive to the rated power of the energy ship. Thus, the sensitivity study of the energy ship's optimized capacity factor in response to the storage capacity and

unload time and the rated power have been analyzed and presented in Section 4.2 of this chapter.

Table A2- 1 Summary of optimal numerical parameter for 1.6MW and 1.3MW rated energy ship with storage capacity of 24 hours including 4 hours unload time.

Rated Power	Deployment Area	Best Initial optimization waypoints	Best optimization search step angle (°)	Best optimized capacity factor (%)
1.6MW	Saint-Pierre-et-Miquelon	2	8	52.8
	Ile de Sein	2	6	49.3
1.3MW	Saint-Pierre-et-Miquelon	2	6	55.6
	Ile de Sein	2	8	51.1

2.1.3. Sensitivity of double waypoints after first optimization

In QtVlm batchmode version presented in Chapter 2, there is an option to double the number of waypoints after the first optimization. This means the indicated waypoints at initial optimization process will be doubled after first optimization.

A sensitivity analysis using this parameter has been done and the capacity factor assessed for energy ship 1.6MW and 1.3MW with same numerical parameter of 24 hours storage capacity and 4 hours unload time; 8° search step angle and 4 initial number of waypoints. Even though a two number of initial waypoint is the best parameter obtained in the sensitivity analysis, but 2 waypoints are too small for the purpose of this analysis, thus a 4 waypoints parameter is used. Furthermore, the optimized capacity factor obtained by 4 waypoints is considerably high.

Table A2- 2 shows the results of the optimized capacity factor for a 1.6MW energy ship deployed at Saint-Pierre-et-Miquelon and Ile de Sein for the year 2015, 2016 and 2017 and the average optimized capacity factor for those three years. Table A2- 2 also shows a less than 1% difference between averaged optimized capacity factor with and without using the option of double the number of waypoints after the first optimization. It shows that the optimized CF remains 52% for 1.6MW in Saint-Pierre-Et-Miquelon and 48% in Ile de Sein. Meanwhile, for 1.3MW, optimized CF remains 55% in Saint-Pierre-Et-Miquelon and 50% in Ile de Sein. Even though the filling ratio

increased significantly to more than 98% by doubled the waypoints than without double the waypoint after the first optimization, the filling ratio remains high, which more than 92% achieved.

Therefore, the difference is negligible. Since considering double the number of waypoint after first optimization cause slightly higher simulation time, the option of double the number of waypoints after the first optimization is not taken into account for the remaining energy ship's weather routing optimization in this study.

Table A2- 2 Comparison of CF optimized with and without using the parameter double waypoint after first optimization

		1.6MW (Saint-Pierre-et-Miquelon) 24h storage capacity / 4h unload; 8° / 4WP (Starting time 03:00:00)		1.6MW (Ile de Sein) 24h storage capacity / 4h unload; 8° / 4WP (Starting time 03:00:00)		1.3MW (Saint-Pierre-et-Miquelon) 24h storage capacity / 4h unload; 8° / 4WP (Starting time 03:00:00)		1.3MW (Ile de Sein) 24h storage capacity / 4h unload; 8° / 4WP (Starting time 03:00:00)	
		FR	CF	FR	CF	FR	CF	FR	CF
DOUBLE WAYPOINT AFTER FIRST OPTIMIZATION	2015	98.07%	52.50%	98.63%	52.56%	99.53%	54.89%	98.46%	52.85%
	2016	98.20%	52.19%	96.98%	45.63%	98.34%	56.07%	97.49%	47.57%
	2017	97.87%	52.42%	98.65%	47.64%	98.02%	54.96%	98.80%	51.04%
	AVERAGE	98.05%	52.37%	98.09%	48.61%	98.63%	55.31%	98.25%	50.49%
WITHOUT DOUBLE WAYPOINT AFTER FIRST OPTIMIZATION	2015	92.48%	52.39%	93.53%	50.04%	94.30%	56.69%	95.28%	54.99%
	2016	93.39%	52.31%	93.54%	45.05%	93.85%	54.77%	93.70%	47.98%
	2017	92.59%	53.70%	94.94%	49.77%	93.63%	54.80%	95.20%	50.23%
	AVERAGE	92.82%	52.80%	94.00%	48.29%	93.93%	55.42%	94.73%	51.07%

2.2.Sensitivity study on the energy ship's sailing capability

2.2.1. Data and input parameters

In addition, the energy ship capacity factor optimization results may also depend on the physical parameters of the energy ship sailing capability as function on storage capacity and unload time and the rated power production the energy ship. The sensitivity studies in this section consist of two parts. First part investigating the sensitivity of storage capacity and unload time to the optimized capacity factor of the energy ship, and second part investigate the results of similar output in response to the different rated power of the energy ship.

This sensitivity also was measured by the optimized capacity factor of an energy ship. The method of optimization using qtVlm weather routing software and three years of wind data, 2015, 2016 and 2017 are as presented in Chapter 2.

For the first part, the sensitivity study assessed 4 clustered storage capacity and unload time; that are set to 6 hours storage capacity and 1 hour unload time; 12 hours storage capacity and 2 hour unload time; 24 hours storage capacity and 4 hour unload time; and 48 hours storage capacity and 8 hours unload time.

One may note that the unload time is also greater, but it does not change the theoretical maximum capacity factor, which is given by:

$$CF_{max} = \frac{N}{N + T_0}$$

Where we recall that N is the energy storage capacity in hours at rated power and T_0 is the unload time. The proportion of storage capacity and unload time for all 4 clustered configurations meet the theoretical maximum capacity (85.7%).

To perform the sensitivity on energy ship's sailing capability parameter, the parameter of storage capacity and unloading time and the rated power of the energy ship were taken into consideration. Few set of optimal numerical parameter as function to search steps angle and optimization search step angle defined in previous section were

chosen and set as the default setting. In this context, 3 set of search step angle and initial number of waypoints was chosen; they are 0.5° search step angle and 12 initial optimization waypoints, 8° search step angle and 2 initial optimization waypoint and 16° search step angle and 2 initial optimization waypoints. These numerical parameter clusters were chosen based on the referral cluster and the optimal cluster defined in the previous numerical parameter sensitivity study.

Note that all the tables shown the results for over the years 2015, 2016 and 2017 fixed for 4 different storage capacities and unload times.

2.2.2. Sensitivity of storage capacity and unload time

Table A2- 3 shows the results of the optimized capacity factor for the 1.6 MW energy ship in both Saint-Pierre-et-Miquelon and Ile de Sein for the year 2015, 2016 and 2017 and the average of 3 years. One can note that the numerical parameter is set to 0.5° search step angle and 12 initial optimization waypoints.

One can see that, in Saint-Pierre-et-Miquelon, the highest three years averaged optimized capacity factor of 49.8% obtained by the smallest storage capacity of 6 hours and 1 hour unload time. Then followed by 12 hours storage capacity and 2 hours unload time (47.3%), 24 hours storage capacity and 4 hours unload time (47.3%), then 48 hours storage capacity and 8 hours unload time (47.3%).

Meanwhile, in Ile de Sein, the highest three years averaged optimized capacity factor of 44.2% was also obtained by the smallest storage capacity of 6 hours and 1 hour unload time followed by 12 hours storage capacity and 2 hours unload time (43.3%), 24 hours storage capacity and 4 hours unload time (39.5%) then 48 hours storage capacity and 8 hours unload time (37.9%).

Once can see, the optimized capacity factor reduced as the storage capacity increased. However, the filling ratios for all storage capacity at both deployment locations remain higher, more than 98%.

Table A2- 3 Results for the optimization of the capacity factor (%) of the 1.6MW energy ship for optimization parameter 0.5° search step angle & 12 number of waypoints

		Saint-Pierre-et-Miquelon				Ile de Sein			
		Capacity factor (CF)		Filling ratio (FR)		Capacity factor (CF)		Filling ratio (FR)	
		0.5°; 12 WPs	Average over 3 years		Average over 3 years	0.5°; 12 WPs	Average over 3 years		Average over 3 years
6h storage capacity / 1h unload time	2015	51,79%	49,78%	99.44%	99.29%	48.09%	44.18%	99.22%	99.20%
	2016	49,83%		99.25%		42.24%		99.24%	
	2017	47,72%		99.19%		42.21%		99.15%	
12h storage capacity / 2h unload time	2015	46,36%	47.32%	99.30%	99.24%	46.05%	43.30%	99.38%	99.03%
	2016	48,28%		99.16%		41.55%		99.07%	
	2017	47,33%		99.27%		42.30%		98.65%	
24h storage capacity / 4h unload time	2015	41,78%	43.20%	99.49%	99.36%	41.55%	39.47%	98.9%	98.75%
	2016	43,58%		99.20%		37.35%		98.8%	
	2017	44,24%		99.38%		39.50%		98.5%	
48h storage capacity / 8h unload time	2015	41,86%	41.81%	99.41%	99.02%	39.94%	37.91%	98.52%	98.42%
	2016	40,81%		99.19%		37.63%		97.39%	
	2017	42,77%		98.45%		36.17%		99.36%	

Table A2- 4 shows the results of the optimized capacity factor for the 1.6 MW energy ship in both Saint-Pierre-et-Miquelon and Ile de Sein for the year 2015, 2016 and 2017 and the average of 3 years. One can note that the numerical parameter is set to an 8° search step angle and two initial optimization waypoints.

As presented in Table A2- 4, the optimized capacity factor obtained in Saint-Pierre-et-Miquelon shows that the highest three years averaged optimized capacity factor of 53.8% obtained by the smallest storage capacity of 6 hours and 1 hour unload time. Then followed by 12 hours storage capacity and 2 hours unload time (53.2%), 24 hours storage capacity and 4 hours unload time (52.8%), then 48 hours storage capacity and 8 hours unload time (50.9%).

Meanwhile, in Ile de Sein, the result shows fluctuated averaged optimized capacity factor. As might see, the highest optimized capacity factor, 50.2%, was obtained by 48 hours storage capacity and 8 hours unload time, followed by 12 hours storage capacity and 2 hours unload time (48.9%) and 24 hours storage capacity and 4 hours unload time. The smallest optimized capacity factor of 47.8% was obtained by the smallest storage capacity, 6 hours storage capacity and 1 hour unload time. The filling ratios for all storage capacity at both deployment locations remain considerably high, which are more than 92%.

Table A2- 4 Results for the optimization of the capacity factor (%) of the 1.6 MW energy ship for optimization parameter 8° search step angle & 2 number of waypoints

		Saint-Pierre-et-Miquelon				**Ile de Sein**			
		Capacity factor (CF)		Filling ratio (FR)		Capacity factor (CF)		Filling ratio (FR)	
		8°; 2 WPs	Average over 3 years		Average over 3 years	8°; 2 WPs	Average over 3 years		Average over 3 years
6h storage capacity / 1h unload time	2015	55.97%	53.76%	93.96%	94.45%	52.16%	47.78%	96.07%	95.59%
	2016	54.21%		94.00%		45.79%		94.84%	
	2017	51.10%		95.38%		45.40%		95.87%	
12h storage capacity / 2h unload time	2015	54.52%	53.16%	94.02%	94.49%	52.56%	48.94%	95.15%	95.33%
	2016	53.29%		94.73%		46.16%		94.92%	
	2017	51.68%		94.72%		48.10%		95.91%	
24h storage capacity / 4h unload time	2015	52.39%	52.80%	92.48%	92.82%	50.87%	48.50%	94.54%	94.36%
	2016	52.31%		93.39%		44.85%		93.61%	
	2017	53.70%		92.59%		49.77%		94.94%	
48h storage capacity / 8h unload time	2015	49.72%	50.97%	91.55%	91.12%	53.53%	50.20%	93.14%	92.56%
	2016	52.48%		93.06%		48.08%		92.43%	
	2017	50.70%		88.74%		49.00%		92.10%	

Table A2- 5 shows the results of the optimized capacity factor for the 1.6 MW energy ship in both Saint-Pierre-et-Miquelon and Ile de Sein for the year 2015, 2016 and 2017 and the average of 3 years. The numerical parameter is set to 16° search step angle and two initial optimization waypoints in this sensitivity analysis.

As shown, in Saint-Pierre-et-Miquelon, the highest three years averaged optimized capacity factor of 53.5% obtained by the smallest storage capacity of 6 hours and 1 hour unload time. Then followed by 12 hours storage capacity and 2 hours unload time (53.4%), 24 hours storage capacity and 4 hours unload time (52.5%), then 48 hours storage capacity and 8 hours unload time (50.2%).

Meanwhile, in Ile de Sein, the optimized capacity factor obtained using 16° search step angle, and two initial optimization waypoints show a fluctuated result. One can see that the optimized capacity factor obtained for 12 hours storage capacity and 2 hours unload time is 49% and 48 hours storage capacity and 8 hours unload is 49.9%. The optimized capacity factors are higher than 12 hours storage capacity and 2 hours unload time (47.5%) and 24 hours storage capacity and 4 hours unload time (47.9%). The highest three years averaged optimized capacity factor of 49.9% was obtained by the largest storage capacity of 48 hours and 8 hour unload time.

However, the filling ratios for all storage capacity at both deployment locations remain higher, which are more than 93%.

Table A2- 5 Results for the optimization of the capacity factor (%) of the 1.6 MW energy ship for optimization parameter 16° search step angle & 2 number of waypoints

		Saint-Pierre-et-Miquelon				**Ile de Sein**			
		Capacity factor (CF)		Filling ratio (FR)		Capacity factor (CF)		Filling ratio (FR)	
		16°; 2 WPs	Average over 3 years		Average over 3 years	16°; 2 WPs	Average over 3 years		Average over 3 years
6h storage capacity / 1h unload time	2015	55.98%	53.46%	93.89%	94.38%	51.54%	47.51%	96.28%	95.74%
	2016	53.73%		94.36%		45.21%		94.53%	
	2017	50.66%		94.88%		45.77%		96.41%	
12h storage capacity / 2h unload time	2015	55.07%	53.43%	93.23%	93.74%	53.05%	49.02%	95.82%	95.37%
	2016	53.03%		93.73%		45.85%		94.03%	
	2017	52.18%		94.25%		48.15%		96.27%	
24h storage capacity / 4h unload time	2015	52.92%	52.51%	93.07%	93.51%	50.93%	47.96%	95.08%	94.31%
	2016	52.90%		93.78%		44.54%		93.55%	
	2017	51.70%		93.69%		48.41%		94.31%	
48h storage capacity / 8h unload time	2015	49.18%	50.24%	94.22%	93.70%	52.96%	49.94%	92.95%	93.26%
	2016	50.92%		94.76%		46.97%		93.12%	
	2017	50.62%		92.13%		49.90%		93.71%	

Next, same with the sensitivity analysis done for the 1.6MW energy ship, the same sensitivity analysis was done for the 1.3MW energy ship. Table A2- 6 shows the optimized capacity factor results with a set numerical parameter of 0.5° search step angle and 12 initial optimization waypoints.

As shown in Table A2- 6, in Saint-Pierre-et-Miquelon, the highest three-year averaged optimized capacity factor of 52.6% was obtained by the smallest storage capacity of 6 hours and 1 hour unload time. And then followed by 12 hours storage capacity and 2 hours unload time (50.7%), 24 hours storage capacity and 4 hours unload time (47.2%), then 48 hours storage capacity and 8 hours unload time (45.4%).

Meanwhile, in Ile de Sein, the optimized capacity factor also shows a decreasing pattern as the storage capacity and unloads time increase. One can see that the optimized capacity factor obtained for 6 hours storage capacity and 1 hour unload time obtained the highest optimized capacity factor (46.6%). It then followed by 12 hours storage capacity and 2 hours unload time (45.2%) and 24 hours storage capacity and 4 hours unload time (41.1%). However, a small increment of the optimized capacity factor as the storage capacity increased to 48 hours storage capacity and 8 hours unload time (41.3%) which only marked a 0.2% difference with 24 hours storage capacity and 4 hours unload. The filling ratios for all storage capacity at both deployment locations remain higher which most are at 99%.

Table A2- 6 Results for the optimization of the capacity factor (%) of the 1.3 MW energy ship for optimization parameter 0.5° search step angle & 12 number of waypoints

		Saint-Pierre-et-Miquelon				**Ile de Sein**			
		Capacity factor (CF)		Filling ratio (FR)		Capacity factor (CF)		Filling ratio (FR)	
		0.5°; 12 WPs	Average over 3 years		Average over 3 years	0.5°; 12 WPs	Average over 3 years		Average over 3 years
6h storage capacity / 1h unload time	2015	55.12%	52.62%	99.40%	99.43%	50.39%	46.61%	99.41%	99.29%
	2016	52.55%		99.53%		44.38%		99.18%	
	2017	50.20%		99.35%		45.07%		99.29%	
12h storage capacity / 2h unload time	2015	51.83%	50.72%	99.29%	99.26%	47.54%	45.15%	99.57%	99.37%
	2016	50.45%		99.44%		42.76%		99.40%	
	2017	49.88%		99.06%		45.15%		99.15%	
24h storage capacity / 4h unload time	2015	45.81%	47.18%	99.22%	99.26%	43.76%	41.10%	98.89%	98.73%
	2016	47.40%		99.23%		38.76%		98.94%	
	2017	48.34%		99.34%		40.77%		98.35%	
48h storage capacity / 8h unload time	2015	44.83%	45.41%	99.24%	99.20%	45.52%	41.33%	99.80%	99.15%
	2016	43.75%		99.77%		40.28%		98.42%	
	2017	47.66%		98.60%		38.20%		99.22%	

Table A2- 7 shows the results of the optimized capacity factor for the 1.3 MW energy ship in both Saint-Pierre-et-Miquelon and Ile de Sein for the year 2015, 2016 and 2017 and the average of 3 years. The numerical parameter is set to an 8° search step angle and two initial optimization waypoints in this sensitivity analysis.

As shown, in Saint-Pierre-et-Miquelon, the highest three years averaged optimized capacity factor of 56.5% obtained by the smallest storage capacity of 6 hours and 1 hour unload time. It then followed by 12 hours storage capacity and 2 hours unload time (55.7%), 24 hours storage capacity and 4 hours unload time (55.1%), then 48 hours storage capacity and 8 hours unload time (54.6%). Overall at Saint-Pierre-et-Miquelon, the optimized capacity factor decrease as the storage capacity increases.

Contrary to Ile de Sein, the optimized capacity factor increases as storage capacity and unload time increase. The optimized capacity factor obtained for 48 hours and 8 hours unload time shows the highest value of 53% capacity factor. It then followed by 24 hours and 4 hours unload time (51.1%) and 12 hours and 2 hours unload time (51%). The lowest three-year averaged optimized capacity factor of 49.9% was obtained by the smallest storage capacity of 6 hours and 1 hour unload time.

However, as in the other sensitivity analysis cases, the filling ratios for all storage capacity at both deployment locations remain higher, which are more than 93%.

Table A2- 7 Results for the optimization of the capacity factor (%) of the 1.3 MW energy ship for optimization parameter 8° search step angle & 2 number of waypoints

		Saint-Pierre-et-Miquelon				**Ile de Sein**			
		Capacity factor (CF)		Filling ratio (FR)		Capacity factor (CF)		Filling ratio (FR)	
		8°; 2 WPs	Average over 3 years		Average over 3 years	8°; 2 WPs	Average over 3 years		Average over 3 years
6h storage capacity / 1h unload time	2015	59.07%	56.51%	94.36%	95.32%	54.01%	49.95%	96.25%	96.07%
	2016	57.16%		95.76%		47.36%		96.03%	
	2017	53.31%		95.84%		48.47%		95.92%	
12h storage capacity / 2h unload time	2015	58.15%	55.74%	93.52%	94.30%	54.68%	51.00%	96.04%	95.74%
	2016	55.41%		94.19%		47.86%		94.65%	
	2017	53.67%		95.19%		50.45%		96.52%	
24h storage capacity / 4h unload time	2015	55.81%	55.13%	94.30%	93.93%	54.99%	51.07%	95.28%	94.73%
	2016	54.77%		93.85%		47.98%		93.70%	
	2017	54.80%		93.63%		50.23%		95.20%	
48h storage capacity / 8h unload time	2015	56.18%	54.57%	93.76%	92.63%	56.29%	53.03%	94.29%	93.63%
	2016	54.92%		92.85%		50.81%		93.62%	
	2017	52.62%		91.28%		51.99%		92.99%	

Table A2- 8 shows the results of the optimized capacity factor for the 1.3 MW energy ship in both Saint-Pierre-et-Miquelon and Ile de Sein for the year 2015, 2016 and 2017 and the average of 3 years. The numerical parameter is set to 16° search step angle and two initial optimization waypoints in this sensitivity analysis.

As shown in Saint-Pierre-et-Miquelon, the optimized capacity factor obtained shown a decreasing pattern as the storage capacity and unload time increases. The optimized capacity factor obtained for 6 hours storage capacity and 1 hour unload time obtained the highest optimized capacity factor (56.3%), followed by 12 hours storage capacity and 2 hours unload time (56.1%) and 24 hours storage capacity and 4 hours unload time (55.1%). Even so, there is a small increment of 0.1% to the optimized capacity factor for the 48 hours storage capacity and 8 hours unload time (55.2%).

Unlike the capacity factor obtained in Saint-Pierre-et-Miquelon, the optimized capacity factors obtained in Ile de Sein fluctuated. One can see that the highest optimized capacity factor was acquired by the largest storage capacity of 48 hours and 8 hours unload time, with a value of 52.3%. The second highest optimized capacity factor obtained for 12 hours storage capacity and 2 hours unload time, 51.2% and followed by 24 hours storage capacity and 4 hours unload, 50.1%. The lowest three-year averaged optimized capacity factor of 49.9% was obtained by the smallest storage capacity of 6 hours and 1 hour unloads time. The filling ratios for all storage capacity at both deployment locations remain higher, which are more than 93%.

Overall, as one may have expected that greater storage capacity would lead to a greater number of weather-routing options and thus greater capacity factor. However, to that end, only four cases meet that expectation mentioned above which are used the numerical of 8° and 16° search step angle and two initial waypoints. All of them are 1.6MW and 1.3MW rated energy ship deployed at Ile de Sein. But, with the same parameter and rated power of the energy ship, the capacity factor decrease as the storage capacity increases.

In addition, in most cases, the optimized capacity factors for the energy ship were also decrease as the storage capacity increases. The result is rather surprising as one may note that the unload time is also greater as the storage capacity increases. But, it does not change the theoretical maximum capacity factor (85.7%), which is given by equation (8) explained in section 4.2.1.

Thus, the decreases in optimized capacity factor cannot be explained by the increasing batteries capacities and the unload time. Therefore, the question of why the capacity factor decreases with increasing batteries capacity remains open and will be addressed in future work.

On the other point of view, this sensitivity study shows that the “optimal” capacity factor and energy ship route is also highly sensitive to the physical optimization parameters and the deployment location. Thus, the optimization method is currently implemented in QtVlm converges to a local optimum and not the global optimum. Furthermore, in -depth studies need to be done to examine other factors that influence the increase and decrease of the optimized capacity factor of the energy ships.

Table A2- 8 Results for the optimization of the capacity factor (%) of the 1.3 MW energy ship for optimization parameter 16° search step angle & 2 number of waypoints

		Saint-Pierre-et-Miquelon				**Ile de Sein**			
		Capacity factor (CF)		Filling ratio (FR)		Capacity factor (CF)		Filling ratio (FR)	
		16°; 2 WPs	Average over 3 years		Average over 3 years	16°; 2 WPs	Average over 3 years		Average over 3 years
6h storage capacity / 1h unload time	2015	59.24%	56.32%	94.93%	95.58%	53.04%	49.87%	96.79%	96.19%
	2016	56.75%		95.73%		47.95%		95.34%	
	2017	52.98%		96.08%		48.63%		96.43%	
12h storage capacity / 2h unload time	2015	57.92%	56.07%	94.51%	94.40%	53.98%	51.18%	95.48%	95.32%
	2016	55.39%		94.31%		48.96%		94.69%	
	2017	54.90%		94.37%		50.60%		95.80%	
24h storage capacity / 4h unload time	2015	56.10%	55.12%	92.78%	93.47%	52.97%	50.58%	94.89%	94.50%
	2016	54.69%		93.51%		48.04%		93.29%	
	2017	54.57%		94.11%		50.72%		95.32%	
48h storage capacity / 8h unload time	2015	54.09%	55.23%	92.64%	93.08%	55.23%	52.34%	94.03%	93.66%
	2016	55.67%		93.19%		49.09%		93.68%	
	2017	55.94%		93.41%		52.71%		93.28%	

2.2.3. Sensitivity of rated power of energy ship (1MW, 1.3MW, 1.6MW and 1.9MW)

The resulting 3 years averaged capacity factor for the sensitivity of initial optimization waypoints and search step angle presented in Section 4.2.1, one can see that the best average capacity factor for 1.3MW energy ship in Saint-Pierre-et-Miquelon and Ile de Sein are higher compared to the best average capacity factor for 1.6MW in same deployment locations.

Therefore, in this section a sensitivity study has been performed to investigate the sensitivity of the optimized capacity factor in response to the rated power of the energy ship.

This sensitivity study involved four rated powers of energy ship, 1MW, 1.3MW, 1.6MW and 1.9MW. The output was also measured by the optimized capacity factor obtained by the energy ship. The optimization of the capacity factor for each rated power energy ship are using qtVlm weather routing software loaded with energy ship's speed and power production polar and three years of wind data as presented in Chapter 2. The performance of each rated energy ship is characterized by polar plots for its speed and power production.

For the optimization, the numerical optimization parameter as a function of the initial optimization waypoints and search steps angle are fixed to 2 initial optimization waypoints and 8° search steps angle. These numerical parameters are chosen based on the previous sensitivity study on the numerical optimization parameter which obtained the optimum value of optimized capacity factor for the energy ship. The sensitivity analysis also carried out for all storage capacity and unloading times of the energy ship analyzed in previous section.

Figure A2- **5** shows the average capacity factor for 1MW, 1.3MW, 1.6MW and 1.9MW energy ship in Saint-Pierre-et-Miquelon and Ile de Sein for 3 years (2015, 2016 & 2017). Overall, at both deployment locations, one can note that as the rated power increased, the optimized capacity factors obtained were significantly decreased.

The differences are classified through 4 cluster of rated energy ships equipped with storage capacities ranging from 6 hours storage capacity 1 hour unloading time, 12

hours storage capacity 2 hour unloading time, 24 hours storage capacity 4 hour unloading time and 48 hours storage capacity 8 hour unloading time.

Looking into the relationship between the optimized capacity factor with the increment of the storage capacity, for the energy ship deployed at the Saint-Pierre-et-Miquelon, the capacity factor slightly reduced with the increased storage capacity and unloading time. In contrast, the increment of capacity factor was parallel with the increments of storage capacity and unloading time for the energy ship deployed at the Ile de Sein.

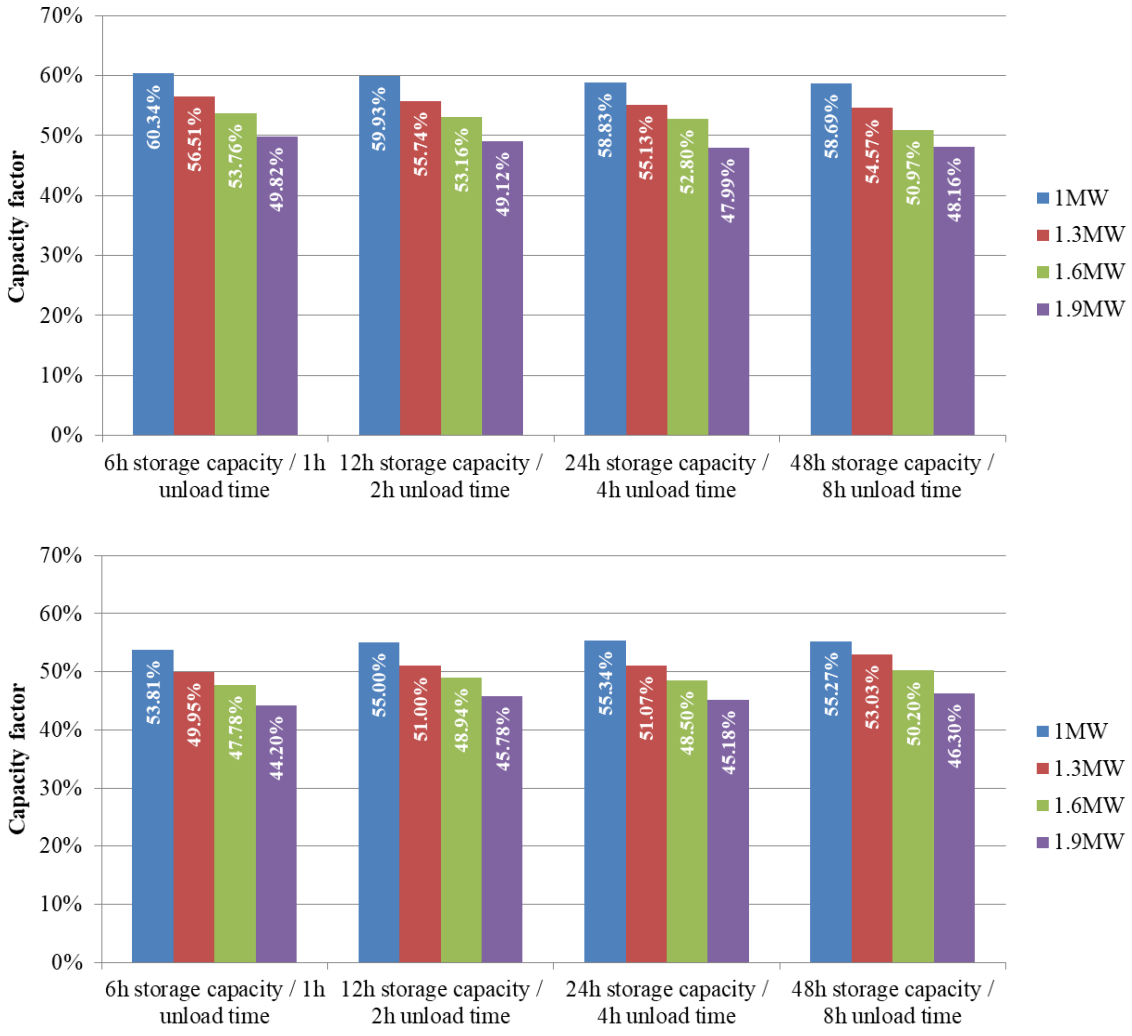

Figure A2- 5 Average capacity factor for 1MW, 1.3MW, 1.6MW and 1.9MW energy ship in (top) Saint-Pierre-et-Miquelon and (below) Ile de Sein for 3 years (2015, 2016 & 2017)

In Saint-Pierre-et-Miquelon, Table A2- 9 shows the highest optimized capacity factor is obtained by a 1MW energy ship equipped with 6 hours of storage capacity with an average of 3 years capacity factor of 60.3%. With same rated energy ship, a slight

decrease in average capacity factor of 59.9% were obtained by 12 hours storage capacity, and then followed by 58.8% by 24 hours storage capacity and 58.7% by 48 hours storage capacity.

For 1.3MW energy ship, it produced about 4% smaller amounts of average capacity factor from 1MW energy ship. The capacity factors can vary by 56.5% to 54.5% for all storage capacities of 6, 12, 24 and 48 hours storage capacity. Further reduction in capacity factor obtained for all storage capacity can be seen as the rated power increase to 1.6MW and 1.9MW. The capacity factor obtained for a 1.6MW energy ship was ranging from 53.8% to 51%. Meanwhile, the capacity factor obtained by 1.9MW energy ship was ranging from 50% to 48.2%.

Table A2- 10 and Table A2- 11 separately show the filling ratio and the energy production for 1MW, 1.3MW, 1.6MW and 1.9MW energy ship in Saint-Pierre-et-Miquelon for 2015, 2016 & 2017 and its average for the three years. The average filling ratio obtained by all rated energy ships equipped with all cluster storage capacity was high, ranging from 89% to 96%. In other hand, the energy ship capable to produce average energy ranging from 5271MW per hour to 8271MW per hour. One can see also, larger rated energy ship will produced more energy but the energy production will slightly reduce as the storage capacity increased. This event reflects with the reduction of the average capacity factor presented in Table A2- 9.

Table A2- 9 Capacity factor for 1MW, 1.3MW, 1.6MW and 1.9MW energy ship In Saint-Pierre-et-Miquelon for 3 years (2015, 2016 & 2017)

		SAINT-PIERRE-ET-MIQUELON							
		1MW		**1.3MW**		**1.6MW**		**1.9MW**	
		Capacity factor (CF)		Capacity factor (CF)		Capacity factor (CF)		Capacity factor (CF)	
		8°; 2 WPs	Average over 3 years	8°; 2 WPs	Average over 3 years	8°; 2 WPs	Average over 3 years	8°; 2 WPs	Average over 3 years
6h storage capacity / 1h unload time	2015	63.54%	60.34%	59.07%	56.51%	55.97%	53.76%	51.45%	49.82%
	2016	60.30%		57.16%		54.21%		49.84%	
	2017	57.19%		53.31%		51.10%		48.16%	
12h storage capacity / 2h unload time	2015	61.70%	59.93%	58.15%	55.74%	54.52%	53.16%	50.40%	49.12%
	2016	60.73%		55.41%		53.29%		48.94%	
	2017	57.37%		53.67%		51.68%		48.03%	
24h storage capacity / 4h unload time	2015	59.94%	58.83%	55.81%	55.13%	52.39%	52.80%	48.91%	47.99%
	2016	59.08%		54.77%		52.31%		47.53%	
	2017	57.46%		54.80%		53.70%		47.54%	
48h storage capacity / 8h unload time	2015	58.05%	58.69%	56.18%	54.57%	49.72%	50.97%	48.63%	48.16%
	2016	59.37%		54.92%		52.48%		46.95%	
	2017	58.66%		52.62%		50.70%		48.89%	

Table A2- 10 Filling ratio for 1 MW, 1.3 MW, 1.6 MW and 1.9 MW energy ship in Saint Pierre et Miquelon for 3 years (2015, 2016 & 2017)

		SAINT-PIERRE-ET-MIQUELON							
		1MW		**1.3MW**		**1.6MW**		**1.9MW**	
		Filling ratio (FR)		Filling ratio (FR)		Filling ratio (FR)		Filling ratio (FR)	
		8°; 2 WPs	Average over 3 years	8°; 2 WPs	Average over 3 years	8°; 2 WPs	Average over 3 years	8°; 2 WPs	Average over 3 years
6h storage capacity / 1h unload time	2015	95.92%	96.24%	94.36%	95.32%	93.96%	94.45%	92.01%	92.28%
	2016	96.02%		95.76%		94.00%		92.29%	
	2017	96.78%		95.84%		95.38%		92.53%	
12h storage capacity / 2h unload time	2015	94.82%	95.03%	93.52%	94.30%	94.02%	94.49%	90.84%	90.89%
	2016	95.31%		94.19%		94.73%		90.14%	
	2017	94.96%		95.19%		94.72%		91.68%	
24h storage capacity / 4h unload time	2015	94.38%	94.66%	94.30%	93.93%	92.48%	92.82%	88.61%	89.24%
	2016	94.54%		93.85%		93.39%		89.08%	
	2017	95.06%		93.63%		92.59%		90.02%	
48h storage capacity / 8h unload time	2015	94.18%	93.55%	93.76%	92.63%	91.55%	91.12%	90.43%	91.45%
	2016	92.70%		92.85%		93.06%		92.14%	
	2017	93.76%		91.28%		88.74%		91.77%	

Table A2- 11 Energy production for 1 MW, 1.3 MW, 1.6 MW and 1.9 MW energy ship in Saint Pierre et Miquelon for 3 years (2015, 2016 & 2017)

		SAINT-PIERRE-ET-MIQUELON							
		1MW		**1.3MW**		**1.6MW**		**1.9MW**	
		Energy Produced (MWh)		Energy Produced (MWh)		Energy Produced (MWh)		Energy Produced (MWh)	
		8°; 2 WPs	Average over 3 years	8°; 2 WPs	Average over 3 years	8°; 2 WPs	Average over 3 years	8°; 2 WPs	Average over 3 years
6h storage capacity / 1h unload time	2015	5540.40	5271.35	6698.67	6418.91	7808.28	7513.39	8528.06	8271.19
	2016	5278.93		6504.34		7593.11		8291.47	
	2017	4994.72		6053.73		7138.79		7994.03	
12h storage capacity / 2h unload time	2015	5378.78	5234.70	6602.15	6335.41	7620.28	7432.68	8353.49	8156.82
	2016	5315.07		6310.42		7454.48		8145.28	
	2017	5010.26		6093.66		7223.27		7971.70	
24h storage capacity / 4h unload time	2015	5233.43	5142.74	6328.34	6263.42	7311.22	7378.73	8117.98	7974.41
	2016	5174.75		6237.78		7317.95		7913.40	
	2017	5020.05		6224.14		7507.00		7891.85	
48h storage capacity / 8h unload time	2015	5058.90	5129.98	6380.05	6206.05	6955.43	7021.69	8074.31	8005.04
	2016	5203.70		6258.66		7360.10		7819.52	
	2017	5127.34		5979.44		6749.54		8121.27	

In the other deployment location, Ile de Sein, on the whole, Table A2- 12 shows that in each storage capacity and unloading time, the capacity factor obtained was reduced as the rated power of the energy ship increased. In decreasing order, the highest average capacity factor of 55.3% was obtained in Ile de Sein by a 1MW energy ship equipped with a storage capacity of 24 and 48 hours. The differences between the average capacity factor obtained by the 48 hours storage capacity are minimal, which 0.07% lower compared to 24 hours storage capacity, 55% capacity factor obtained for energy ship equipped with 12 hours storage capacity and 53.8% capacity factor for 6 hours storage capacity.

Meanwhile, for 1.3MW energy ship deployed in Ile de Sein, the energy ship produced also about 4% smaller amounts of average capacity factor from 1MW energy ship, this difference are exactly same compared with average capacity factor obtained in Saint-Pierre-et-Miquelon. The capacity factors can vary by 49.9% to 53% for all storage capacities of 6, 12, 24 and 48 hours storage capacity.

Further reduction is also can be seen in average capacity factor obtained by all storage capacities as the rated power increase to 1.6MW and 1.9MW. The average capacity factor obtained for a 1.6MW energy ship was ranging from 47.8% to 50.2%. Meanwhile, the average capacity factor obtained by 1.9MW energy ship was ranging from 44.2% to 46.3%.

Table A2- 13 and Table A2- 14 separately show the filling ratio and the energy production for 1MW, 1.3MW, 1.6MW and 1.9MW energy ship in Ile de Sein for 2015, 2016 & 2017 and its average for the three years. The average filling ratio obtained by all rated energy ships equipped with all cluster storage capacity was also high compared with the filing ratio obtained by energy ship deployed in Saint-Pierre-et-Miquelon, ranging from 89% to 96%. Additionally, the energy ship can produce average energy ranging from 4705MW per hour to 7343MW per hour. These amounts of energy production by the energy ships produced in Ile de Sein were slightly lower comparing to the energy production in Saint-Pierre-et-Miquelon. One can see also that, larger rated energy ship will produce more energy, but contrary with case in Saint-Pierre-et-Miquelon, the energy production were also grow bigger concurrent with the storage capacity and unloading time. This event also reflects the expansion of the average capacity factor presented in Table A2- 12.

Table A2- 12 Capacity factor for 1 MW, 1.3 MW, 1.6 MW and 1.9 MW energy ship in Ile de Sein for 3 years (2015, 2016 & 2017)

		ILE DE SEIN							
		1MW		**1.3MW**		**1.6MW**		**1.9MW**	
		Capacity factor (CF)		Capacity factor (CF)		Capacity factor (CF)		Capacity factor (CF)	
		8°; 2 WPs	Average over 3 years	8°; 2 WPs	Average over 3 years	8°; 2 WPs	Average over 3 years	8°; 2 WPs	Average over 3 years
6h storage capacity / 1h unload time	2015	57.60%	53.81%	54.01%	49.95%	52.16%	47.78%	48.02%	44.20%
	2016	50.96%		47.36%		45.79%		42.04%	
	2017	52.87%		48.47%		45.40%		42.54%	
12h storage capacity / 2h unload time	2015	58.36%	55.00%	54.68%	51.00%	52.56%	48.94%	50.40%	45.78%
	2016	52.48%		47.86%		46.16%		42.42%	
	2017	54.15%		50.45%		48.10%		44.52%	
24h storage capacity / 4h unload time	2015	59.49%	55.34%	54.99%	51.07%	50.87%	48.50%	47.85%	45.18%
	2016	51.61%		47.98%		44.85%		41.57%	
	2017	54.93%		50.23%		49.77%		46.12%	
48h storage capacity / 8h unload time	2015	58.38%	55.27%	56.29%	53.03%	53.53%	50.20%	48.84%	46.30%
	2016	52.99%		50.81%		48.08%		45.38%	
	2017	54.44%		51.99%		49.00%		44.67%	

Table A2- 13 Filling ratio for 1 MW, 1.3 MW, 1.6 MW and 1.9 MW energy ship in Ile de Sein for 3 years (2015, 2016 & 2017)

		ILE DE SEIN							
		1MW		**1.3MW**		**1.6MW**		**1.9MW**	
		Filling ratio (FR)		Filling ratio (FR)		Filling ratio (FR)		Filling ratio (FR)	
		8°; 2 WPs	Average over 3 years	8°; 2 WPs	Average over 3 years	8°; 2 WPs	Average over 3 years	8°; 2 WPs	Average over 3 years
6h storage capacity / 1h unload time	2015	96.99%	96.54%	96.25%	96.07%	96.07%	95.59%	95.22%	94.29%
	2016	95.78%		96.03%		94.84%		92.60%	
	2017	96.85%		95.92%		95.87%		95.06%	
12h storage capacity / 2h unload time	2015	95.75%	95.74%	96.04%	95.74%	95.15%	95.33%	94.49%	93.77%
	2016	95.21%		94.65%		94.92%		92.62%	
	2017	96.26%		96.52%		95.91%		94.19%	
24h storage capacity / 4h unload time	2015	95.33%	94.63%	95.28%	94.73%	94.54%	94.36%	94.54%	92.98%
	2016	93.20%		93.70%		93.61%		93.17%	
	2017	95.36%		95.20%		94.94%		91.23%	
48h storage capacity / 8h unload time	2015	93.18%	94.42%	94.29%	93.63%	93.14%	92.56%	91.80%	89.84%
	2016	94.79%		93.62%		92.43%		88.29%	
	2017	95.28%		92.99%		92.10%		89.43%	

Table A2- 14 Energy production for 1 MW, 1.3 MW, 1.6 MW and 1.9 MW energy ship in Ile de Sein for 3 years (2015, 2016 & 2017)

		ILE DE SEIN							
		1MW		**1.3MW**		**1.6MW**		**1.9MW**	
		Energy Produced (MWh)		Energy Produced (MWh)		Energy Produced (MWh)		Energy Produced (MWh)	
		8°; 2 WPs	Average over 3 years	8°; 2 WPs	Average over 3 years	8°; 2 WPs	Average over 3 years	8°; 2 WPs	Average over 3 years
6h storage capacity / 1h unload time	2015	5031.44	4704.57	6134.21	5677.46	7291.28	6670.25	7971.64	7343.31
	2016	4463.96		5393.17		6374.22		6996.50	
	2017	4618.31		5504.99		6345.26		7061.79	
12h storage capacity / 2h unload time	2015	5099.12	4809.38	6209.07	5797.06	7346.57	6847.07	8366.94	7605.90
	2016	4597.67		5451.36		6471.27		7060.50	
	2017	4731.36		5730.74		6723.37		7390.26	
24h storage capacity / 4h unload time	2015	5198.18	4835.71	6246.38	5806.17	7110.62	6786.01	7944.41	7507.98
	2016	4522.51		5465.55		6287.91		6921.95	
	2017	4786.45		5706.59		6959.51		7657.57	
48h storage capacity / 8h unload time	2015	5103.53	4835.65	6358.63	6019.26	7441.51	7013.52	8111.99	7697.23
	2016	4644.52		5790.10		6744.09		7558.81	
	2017	4758.90		5909.04		6854.96		7420.89	

Titre : Optimisation du facteur de capacité des voilier hydro-éolien pour la conversion de l'énergie éolienne en mer en utilisant le routage météo

Mots clés : Énergie éolienne en mer, Voilier hydro-éolien, Facteur de capacité, Routage météorologique, Optimisation

Résumé : Le navire à énergie est un concept relativement nouveau pour la récolte d'énergie éolienne offshore. Il s'agit d'un navire propulsé par le vent qui produit de l'électricité à l'aide de turbines hydrauliques fixées sous sa coque. Étant donné que le navire énergétique n'est pas connecté au réseau, l'énergie générée est stockée à bord (par exemple, à l'aide de batteries ou par conversion en hydrogène à l'aide d'un électrolyseur).
Un avantage clé du navire énergétique est qu'il est mobile. Par conséquent, sa trajectoire peut être optimisée à l'aide d'un routage météorologique afin de maximiser la production d'énergie, ce qui est l'objet de cette thèse.
L'analyse de la thèse est basée sur des simulations numériques. Le logiciel de routage météo est une version modifiée de QtVlm dans laquelle l'objectif d'optimisation a été remplacé par la maximisation de la production d'énergie. Le vaisseau énergétique est modélisé dans le logiciel par une polaire de vitesse et une polaire de production d'énergie. Les données de vent sont basées sur le jeu de données de vent ECMWF ERA-5.
Le concept de navire à énergie est particulièrement bien adapté à la récolte de la conversion d'énergie éolienne dans le lointain au large. Par conséquent, le facteur de capacité des navires à énergie déployés dans l'océan Atlantique Nord est d'abord étudié.
Les résultats montrent qu'un facteur de capacité de 70 % peut être atteint (moyenne annuelle). Elle est similaire à celle des parcs éoliens offshore flottants qui seraient déployés dans la même zone.
Les navires à énergie peuvent également être utilisés pour l'alimentation électrique des îles et des communautés côtières. Par conséquent, le facteur de capacité des navires à énergie déployés à proximité du littoral est également étudié. Deux études de cas sont envisagées : l'île de « l'Ile de Sein » et l'archipel de « Saint-Pierre-et-Miquelon ». Les résultats montrent que le facteur de capacité est de l'ordre de 50 %. Dans ce cas, elle serait de 10 à 20 % inférieure à celle des parcs éoliens offshore.
L'optimisation du routage météo dépend de paramètres physiques (par exemple, capacité de stockage, puissance nominale) et numériques. Des analyses de sensibilité sont effectuées afin de comprendre leur effet sur la production d'énergie. Les résultats montrent que l'algorithme d'optimisation dans QtVlm tend à converger vers les maxima locaux. Par conséquent, les travaux futurs devraient être orientés vers le développement de meilleures méthodes d'optimisation.

Title : Optimization of the capacity factor of energy ships for far-offshore wind energy conversion using weather-routing

Keywords : Offshore wind energy, Energy ship, Capacity factor, Weather-routing, Optimization

Abstract : The energy ship is a relatively new concept for offshore wind energy harvesting. It consists of a wind-propelled ship that generates electricity using water turbines attached underneath its hull. Since the energy ship is not grid-connected, the generated energy is stored aboard (for instance, using batteries or through conversion to hydrogen using an electrolyzer).
A key advantage of the energy ship is that it is mobile. Therefore, its trajectory can be optimized using weather-routing in order to maximize energy production, which is the focus of this thesis.
The analysis in the thesis is based on numerical simulations. The weather-routing software is a modified version of QtVlm in which the optimization objective has been replaced by the maximization of the energy production. The energy ship is modelled in the software by a velocity polar and a power production polar. The wind data is based on the ECMWF ERA-5 wind dataset.
The energy ship concept is particularly well-suited for the harvesting of the wind energy conversion in the far-offshore. Therefore, the capacity factor of energy ships deployed in the North-Atlantic Ocean is investigated first.
Results show that a capacity factor of 70% can be achieved (annual average). It is similar to that of floating offshore wind farms which would be deployed in the same area.
Energy ships may also be used for the power supply of islands and coastal communities. Therefore, the capacity factor of energy ships deployed nearshore is also investigated. Two case studies are considered: the island of “Ile de Sein” and the “Saint-Pierre-et-Miquelon” archipelagos. Results show that the capacity factor is in the order of 50%. In this case, it would be 10 to 20% smaller than that of offshore wind farms.
The weather-routing optimization depends on physical (e.g. storage capacity, rated power) and numerical parameters. Sensitivity analyses are performed in order to understand their effect on energy production. Results show that the optimization algorithm in QtVlm tends to converge to local maxima. Therefore, future work should be directed towards the development of better optimization methods.